

Faria

# New Bacterial Cellulose Nanocomposites Prepared by *In Situ* Radical Polymerization of Methacrylate Monomers

MASTER DISSERTATION

**Marisa Camacho Gonçalves Faria**

MASTER IN APPLIED BIOCHEMISTRY



UNIVERSIDADE da MADEIRA

*A Nossa Universidade*

[www.uma.pt](http://www.uma.pt)

September | 2015

New  
-R

T/H  
574  
FAR NW  
+ PD-R

UNIVERSIDADE DA MADEIRA  
BIBLIOTECA

**New Bacterial Cellulose  
Nanocomposites Prepared  
by *In Situ* Radical Polymerization  
of Methacrylate Monomers**

MASTER DISSERTATION

**Marisa Camacho Gonçalves Faria**

MASTER IN APPLIED BIOCHEMISTRY

SUPERVISOR

Nereida Maria Abano Cordeiro

CO-SUPERVISOR

Carmen Sofia da Rocha Freire Barros

# **NEW BACTERIAL CELLULOSE NANOCOMPOSITES PREPARED BY *IN SITU* RADICAL POLYMERIZATION OF METHACRYLATE MONOMERS**

Tese apresentada à Universidade da Madeira com vista à  
obtenção do grau de Mestre em Bioquímica Aplicada

Marisa Camacho Gonçalves Faria

Sob a orientação de:

Professora Doutora Nereida Maria Abano Cordeiro

Professora Doutora Carmen Sofia da Rocha Freire Barros

Faculdade de Ciências Exatas e da Engenharia

Universidade da Madeira

Funchal – Portugal

Departamento de Química e CICECO

Universidade de Aveiro

Aveiro, Portugal

**2015**



## ACKNOWLEDGEMENTS

I would like to acknowledge every one that contribute in any way to the performance of my master thesis, either at professional or/and motivational/personal level and made possible their execution.

To my supervisor Prof. Dr. Nereida Cordeiro, for her constant support, guidance, encouragement, patience and constructive critics which help me during my project and be indispensable for the accomplishment of my project.

To my co-supervisor Prof. Dr. Carmen Freire for the support and all help in recommending and understanding through my master thesis. To Dr. Armando Silvestre for all the support and collaboration given in my project.

To University of Madeira for providing the facilities to carry out this project.

To Dr. Carla Vilela (University of Aveiro, Portugal), for performing the Infrared Spectroscopy, NMR, X-ray diffraction, Scanning Electron Microscopy, Thermogravimetric Analysis and Dynamic Mechanical Analysis and all support in data collection.

To Dr. Faranak Mohammadkazemi (Shahid Beheshti University, Iran) for running the elemental chemical composition analyses.

To the laboratory technicians Paula Andrade and Paula Vieira, for availability and support in the reagents and laboratory during my project.

To my colleagues and friends, Dina Maciel, Igor Fernandes, Micael Leça, Tomásia Fernandes, Roberto Aguiar, Nuno Nunes, Emanuel Gouveia, Gabriel Freitas, Carla Alves, Rogério Correia, José Rodrigues, Marisela Santos, Francisco Maciel, and Dr. Gabriel Leça for all the motivation and help with their good dispositions and willingness through this years.

To my family, Mom, Isabel, my sister, Elisabete, my brother, Roberto and João, and my nephew, Afonso, for all support, encouragement and love all the time which help me to continue and supporting me to go through.

Last but not the least, to my boyfriend, Ricardo Pascoal, for his endless support, tireless patience and lovely sense of humor encouraging me all the time. Love you!





## LIST OF PUBLICATIONS

Cordeiro, N., Ashori, A., Hamzeh, Y. & Faria, M. (2013) Effects of hot water pre-extraction on surface properties of bagasse soda pulp. *Materials Science and Engineering C*, 33, 613–617

Ashori, A., Cordeiro, N., Faria, M. & Hamzeh, Y. (2013) Effect of chitosan and cationic starch on the surface chemistry properties of bagasse paper. *International Journal of Biological Macromolecules*, 58, 343–348

Cordeiro, N., Faria M., Abraham, E. & Pothan, L. A. (2013) Assessment of the changes in the cellulosic surface of micro and nano banana fibres due to saponin treatment. *Carbohydrate Polymers* 98, 1065–1071

Cordeiro, N., Freitas, N., Faria, M. & Gouveia, M. (2013) *Ipomoea batatas* (L.) Lam.: A Rich Source of Lipophilic Phytochemicals. *J. Agric. Food Chem*, 61, 12380–12384

Deepa, B., Abraham, E., Cordeiro, N., Mozetic, M., Mathew, A. P., Oksman, K., Faria, M., Thomas, S. & Pothan, L. A. (2015) Utilization of various lignocellulosic biomass for the production of nanocellulose: a comparative study. *Cellulose* 22, 1075–1090

Castro, C., Cordeiro, N., Faria, M., Zuluaga, R., Putaux, J.L., Filpponen, I., Velez, L., Rojas, O.J. & Gañán, P. (2015) *In situ* glyoxalization during biosynthesis of bacterial cellulose. *Carbohydrate Polymers* 126 (2015) 32–39

Mohammadkazemi, F., Faria, M., Cordeiro, N. *In situ* biosynthesis of bacterial nanocellulose- CaCO<sub>3</sub> hybrid composite: one step process. 2015 (Submitted)

## LECTURE

Moares, A.G.O., Faria, M., Silva, F.W., Cordeiro, N. & Amico, S.C. (2013) Efeito de tratamentos químicos nas propriedades de superfície de fibras de carbono via cromatografia gasosa inversa. 12° Congresso Brasileiro de Polímeros (12°CBPol) Brasil

## ABSTRACT

Bacterial cellulose/polymethacrylate nanocomposites have received attention in numerous areas of study and in a variety of applications. The attractive properties of methacrylate polymers and bacterial cellulose, BC, allow the synthesis of new nanocomposites with distinct characteristics. In this study, BC/poly(glycidylmethacrylate) (BC/PGMA) and BC/poly(ethyleneglycol)methacrylate (BC/PPEGMA) nanocomposites were prepared through *in situ* free radical polymerization of GMA and PEGMA, respectively. Ammonium persulphate (APS) was used as an initiator and *N,N'*-methylenebisacrilamide (MBA) was used as a crosslinker in BC/PGMA. Chemical composition, morphology, thermal stability, water absorption, mechanic and surface properties were determined through specific characterization techniques. The optimal polymerization was obtained at (1:2) for BC/PGMA, (1:2:0.2) ratio for BC/GMA/MBA and (1:20) for BC/PPEGMA, with 0.5% of initiator at 60 °C during 6 h. A maximum of 67% and 87% of incorporation percentage was obtained, respectively, for the nanocomposites BC/PGMA/MBA and BC/PPEGMA. BC/PGMA nanocomposites exhibited an increase of roughness and compactation of the three-dimensional structure, an improvement in the thermal and mechanical properties, and a decrease in their swelling ability and crystallinity. On the other hand, BC/PPEGMA showed a decrease of stiffness of three-dimensional structure, improvement in thermal and mechanical properties, an increase in their swelling ability and a decrease the crystallinity. Both BC/polymethacrylate nanocomposites exhibited a basic surface character. The acid treatment showed to be a suitable strategy to modify BC/PGMA nanocomposites through epoxide ring-opening reaction mechanism. Nanocomposites became more compact, smooth and with more water retention ability. A decrease in the thermal and mechanical proprieties was observed.

The new nanocomposites acquired properties useful to biomedical applications or/and removal of heavy metals due to the presence of functional groups.

**Keywords:** bacterial cellulose, nanocomposite, *in situ* radical polymerization, glycidylmethacrylate, poly(ethyleneglycol)methacrylate, chemical treatment.



## RESUMO

Os nanocompósitos de celulose bacteriana/polimetacrilatos têm ganho interesse em inúmeras áreas de estudo e para diversas aplicações. As propriedades atrativas dos monómeros metacrilatos e da celulose bacteriana, BC, possibilitam aos novos nanocompósitos adquirirem características interessantes para diversas aplicações. No presente estudo, os nanocompósitos de BC/poli(glicidilmetacrilato) (BC/PGMA) e BC/poli(etilenoglicol)metacrilato (BC/PPEGMA) foram obtidos através da polimerização radical livre *in situ* do GMA e PEGMA, respetivamente, dentro da rede da BC usando o persulfato de amónia (APS) como iniciador. O *N,N'*-metilenobisacrilamida (MBA) foi usado como agente reticulante nos nanocompósitos de BC/PGMA. A composição química, a estrutura morfológica, a estabilidade química, a absorção de água e as propriedades mecânicas e de superfície foram determinadas. A polimerização ótima foi observada para uma razão de (1:2) para a BC/PGMA, (1:2:0.2) para a BC/PGMA/MBA e a uma razão de (1:20) para o BC/PPEGMA com 0.5 % de iniciador a 60 °C durante 6 h. A percentagem máxima de incorporação de 67% e 87% foi obtida para os nanocompósitos BC/PGMA/MBA e BC/PPEGMA, respetivamente. Os nanocompósitos de BC/PGMA demonstraram uma estrutura rugosa e compacta, um melhoramento nas propriedades mecânicas e térmicas, uma diminuição na sua capacidade de absorção de água e cristalinidade. Por sua vez, os nanocompósitos de BC/PPEGMA apresentaram uma diminuição na rigidez da rede, um melhoramento nas propriedades mecânicas e térmicas, um aumento na sua capacidade de absorção de água e uma diminuição na cristalinidade. Os nanocompósitos de BC/polimetacrilato exibiram um carácter básico à superfície depois da incorporação dos metacrilatos. O tratamento químico ácido demonstrou ser uma estratégia útil para a modificação dos nanocompósitos de BC/PGMA através do mecanismo de abertura do anel epóxi. Os nanocompósitos tornaram-se morfológicamente mais compactos e com a superfície mais lisa. No entanto, as propriedades mecânicas e térmicas decrescem e, a superfície tornou-menos básica. Os novos nanocompósitos apresentam propriedades uteis para aplicações biomédicas ou para a remoção de metais pesados.

**Palavras-chave:** celulose bacteriana, glicidilmetacrilato, poli(etilenoglicol)metacrilato, nanocompósitos, polimerização radical livre *in situ*, tratamento químico.



# TABLE OF CONTENTS

ACKNOWLEDGEMENTS.....	III
LIST OF PUBLICATIONS.....	V
ABSTRACT.....	VII
RESUMO .....	VII
TABLES INDEX.....	XVI
LIST OF ABBREVIATIONS .....	XVIII
 CHAPTER I. Overview of bacterial cellulose .....	 2
1. Cellulose as Biopolymer.....	2
2. Bacterial Cellulose – Historical Outline .....	4
2.1. Biochemistry of Bacterial Cellulose and Biosynthesis Pathways .....	4
2.2. Structure and Properties of Bacterial Cellulose .....	6
2.3. Application of Bacterial Cellulose .....	9
3. Bacterial Cellulose Nanocomposites .....	10
3.1. BC nanocomposites through BC biosynthesis.....	10
3.2. BC nanocomposites through <i>in situ</i> polymerization.....	12
3.3. Acrylate monomers used in BC nanocomposite.....	14
4. Aim of the Study.....	16
 CHAPTER II. New bacterial cellulose/poly(glycidylmethacrylate) nanocomposites films by <i>in situ</i> free radical polymerization .....	 20
1. Introduction.....	21
2. Methodology .....	22
2.1. Material .....	22
2.2. BC nanocomposites preparation .....	22
2.2.1. GMA and GMA/MBA polymerization .....	22
2.2.2. <i>In situ</i> free radical polymerization of GMA and GMA/MBA into BC .....	23
2.3. BC nanocomposites characterization .....	24
2.3.1. Infrared Spectroscopy .....	24

2.3.2.	Energy-dispersive X-ray spectroscopy .....	24
2.3.3.	Scanning electron microscopy .....	24
2.3.4.	X-ray diffraction .....	24
2.3.5.	<sup>13</sup> Carbon Nuclear Magnetic Resonance.....	25
2.3.6.	Swelling ratio.....	25
2.3.7.	Thermogravimetric analyses.....	26
2.3.8.	Dynamic mechanical analyses.....	26
3.	Results and Discussion.....	26
3.1.	<i>In situ</i> free radical polymerization reaction .....	26
3.2.	Optimization of the <i>in situ</i> free radical polymerization .....	28
3.3.	BC nanocomposites characterization .....	30
3.3.1.	Infrared and X-ray Spectroscopy .....	30
3.3.2.	X-ray diffraction .....	32
3.3.3.	<sup>13</sup> Carbon Nuclear Magnetic Resonance.....	33
3.3.4.	Scanning electron microscopy .....	34
3.3.5.	Swelling ratio.....	35
3.3.6.	Thermogravimetric analyses.....	36
3.3.7.	Dynamic Mechanical properties .....	38
4.	Conclusions .....	39

## CHAPTER III. Epoxide ring-opening of bacterial cellulose/poly(glycidylmethacrylate) nanocomposites..... 43

1.	Introduction.....	44
2.	Methodology .....	45
2.1.	BC nanocomposites preparation .....	45
2.2.	Chemical modification of BC nanocomposites .....	45
2.3.	BC nanocomposites characterization .....	46
3.	Results and Discussion.....	47
3.1.	Structural Analysis .....	48
3.2.	Morphological Analyses .....	49
3.3.	Thermal and Mechanical Analyses .....	50
3.4.	Surface properties .....	52

4. Conclusions .....	56
CHAPTER IV. Novel bacterial cellulose/poly(ethyleneglycol) methacrylate nanocomposite films obtained by <i>in situ</i> free radical polymerization .....	
1. Introduction.....	60
2. Methodology .....	61
2.1. Material .....	61
2.2. BC nanocomposites preparation .....	61
2.3. BC nanocomposites characterization .....	62
3. Results and Discussion.....	62
4. Conclusions .....	68
CHAPTER V. Assessment of the surface properties changes of bacterial cellulose/polymethacrylate nanocomposite films by Inverse Gas Chromatography .....	
1. Introduction.....	71
1.1. Inverse gas chromatography .....	71
1.1.1. Surface energy component .....	72
1.1.2. Acid base character .....	73
1.1.3. Isotherm measurements .....	74
2. Experimental methodology .....	75
2.1. Material .....	75
2.2. BC/PGMA and BC/PEGMA nanocomposites.....	75
2.3. IGC measurements.....	76
2.4. Swelling ratio .....	77
2.5. Scanning electron microscopy.....	77
2.6. Energy-dispersive X-ray spectroscopy .....	78
3. Results and Discussion.....	78
3.1. Dispersive component of surface energy .....	78
3.2. Heterogeneity .....	81
3.3. Surface area .....	83
3.4. Acid-base character .....	84
4. Conclusions .....	87

FINAL CONCLUSIONS.....	89
REFERENCES.....	90

## FIGURES INDEX

<b>Figure 1.</b> Molecular structure of cellulose where inter- (blue) and intra- (red) chain hydrogen bonds dashed lines [reproduced from (14)].	3
<b>Figure 2.</b> Morphology characteristics of the different types of cellulose fibers [reproduced from (15)].	3
<b>Figure 3.</b> Schematic of the metabolic pathways of <i>Glucanoacetobacter xylinum</i> and the assembly of cellulose molecules into nanofibrils [reproduced from (6)].	6
<b>Figure 4.</b> A SEM of freeze-dried surface of bacterial cellulose gel [reproduced from (14)].	7
<b>Figure 5.</b> (A) X-ray patterns of BC films and (B) View along the direction 4 (i.e. $[1\bar{1}0]$ for $I_\alpha$ and $[010]$ for $I_\beta$ ) and the displacement of the hydrogen bonding sheets: blue $I_\alpha$ and red $I_\beta$ [reproduced from (3, 13)].	8
<b>Figure 6.</b> Different forms of BC produced by <i>Gluconacetobacter sp.</i> (A) Membrane, (B) Irregular forms, (C) Sphere-like particles [reproduced from (36)].	8
<b>Figure 7.</b> Applications of bacterial cellulose: A – Tubes (blood vessel); B – Branched tube fermented on a branched silicone tube (vascular grafts) [reproduced from (36)]; C –Dressing (wound dressing) [reproduced from (7)]; D – Incorporation of $\text{AgNO}_3$ nanoparticles (antimicrobial activity); E –Paper (filter paper) and F – Colored with aniline blue dye (bioadsorbent) [reproduced from (11)].	9
<b>Figure 8.</b> SEM images of surface morphology of (A) BC and (B) BC/Chitosan film in dry form [reproduced from (41)].	11
<b>Figure 9.</b> (A) Visual appearance of PVA: (a) without BC (b) BC/PVA nanocomposites and (c) BC/PVA nanocomposites after chemical crosslinker and (B) Stress-strain behavior of BC/PVA [reproduced from (39)].	12
<b>Figure 10.</b> (A) Visual appearance of BC/PAEM and all BC/PAEM/MBA nanocomposites. (B) TGA thermograph of BC/PAEM nanocomposites. (C) Swelling of wet BC, BC/PAEM and BC/PAEM/MBA nanocomposites [reproduced from (43)].	13
<b>Figure 11.</b> (A) Visual aspect of BC, BC/PHEMA and BC/PHEMA/PEGDA films and (B) ADSCs proliferation in contact with BC and BC/PHEMA/PEDGA films [reproduced from (40)].	14
<b>Figure 12.</b> Molecular structure of glycidylmethacrylate (GMA).	15

<b>Figure 13.</b> Molecular structure of poly(ethylene glycol) methacrylate (PEGMA).....	16
<b>Figure 14.</b> Schematic reaction of <i>in situ</i> polymerization of GMA/MBA inside BC network. .....	20
<b>Figure 15.</b> Scheme diagram of <i>in situ</i> free radical polymerization reaction of PGMA/MBA inside of BC network. ....	27
<b>Figure 16.</b> Visual images of (a) BC, (b) BC/PGMA and (c) BC/PGMA/MBA nanocomposites.....	28
<b>Figure 17.</b> Effect of reaction time (A), temperature (B), initiator (C), monomer (D) and crosslinker (E) amount in BC <i>in situ</i> free radical polymerization. ....	29
<b>Figure 18.</b> ATR-FTIR of native BC, BC/PGMA and BC/PGMA/MBA nanocomposites. .....	30
<b>Figure 19.</b> XRD patterns of BC, BC/PGMA and BC/PGMA/MBA nanocomposites. ...	32
<b>Figure 20.</b> $^{13}\text{C}$ NMR spectra of native BC, BC/PGMA and BC/PGMA/MBA nanocomposites.....	34
<b>Figure 21.</b> SEM images of BC/PGMA and BC/PGMA/MBA nanocomposites.....	35
<b>Figure 22.</b> Swelling ratio in function of time of BC, BC/PGMA and BC/PGMA/MBA nanocomposites.....	36
<b>Figure 23.</b> TGA and DTGA profile of BC/PGMA and BC/PGMA/MBA nanocomposites and their controls.....	37
<b>Figure 24.</b> Storage modulus $e$ $\tan \delta$ versus temperature of BC and BC/PGMA nanocomposites.....	38
<b>Figure 25.</b> Schematic diagram of the epoxide ring-opening mechanism of BC/PGMA nanocomposites.....	47
<b>Figure 26.</b> $^{13}\text{C}$ NMR spectra of BC/PGMA and BCP/PGMA/MBA nanocomposites before and after chemical treatment.....	48
<b>Figure 27.</b> XRD patterns of BC/PGMA and BC/PGMA/MBA nanocomposites before and after chemical treatment. ....	49
<b>Figure 28.</b> SEM images of BCGMA-CT and BCGMAMBA-CT nanocomposites morphology in different perspectives. The (i), (ii), (iii) and (iv) images correspond to the samples without chemical treatment.....	50

<b>Figure 29.</b> TGA and DTGA of BC/PGMA and BC/PGMA/MBA nanocomposites before and after chemical treatment.....	51
<b>Figure 30.</b> Storage modulus $e \tan \delta$ versus temperature of BCPGMA-CT nanocomposites. ....	52
<b>Figure 31.</b> Heterogeneity profile with n-octane for BC/PGMA/MBA and BCPGMAMBA-CT nanocomposites at 25 °C.....	54
<b>Figure 32.</b> Specific surface energy with polar probes: THF - tetrahydrofuran, DCM - dichloromethane, ETOAc – ethyl acetate, ACN – acetonitrile of BC/PGMA/MBA and BCPGMAMBA-CT nanocomposites at 25 °C. ....	55
<b>Figure 33.</b> Schematic reaction of <i>in situ</i> free polymerization of PEGMA inside BC network. ....	59
<b>Figure 34.</b> Schematic of <i>in situ</i> free radical polymerization reaction of PEGMA inside of BC network [based on (86)]. ....	62
<b>Figure 35.</b> Effect of monomer (PEGMA) amount in BC <i>in situ</i> free radical polymerization. ....	63
<b>Figure 36.</b> ATR–FTIR spectra of BC and BC/PPEGMA nanocomposite. ....	64
<b>Figure 37.</b> SEM images of BC and BC/PPEGMA nanocomposites morphology in different perspectives. ....	65
<b>Figure 38.</b> XRD patterns of BC and BC/PPEGMA nanocomposites. ....	66
<b>Figure 39.</b> Behavior of the swelling ratio in function of time of BC and BC/PPEGMA nanocomposites.....	66
<b>Figure 40.</b> TGA and DTGA profile of BC and BC/PPEGMA nanocomposites.....	67
<b>Figure 41.</b> Storage modulus $e \tan \delta$ versus temperature of BC/PPEGMA nanocomposites. ....	68
<b>Figure 42.</b> Schematic representation of GC and IGC measurements (89). ....	72
<b>Figure 43.</b> SEM images of BC nanocomposites morphology (A) BC; (B) BC/PGMA; (C) BC/PGMA/MBA and (D) BC/PPEGMA. ....	80
<b>Figure 44.</b> Schematic interactions of non-polar and polar probes with surface groups of BC/PGMA/MBA nanocomposites. ....	81
<b>Figure 45.</b> Heterogeneity profile with n-octane for native BC, (A) BC/PGMA and BC/PGMA/MBA and (B) BC/PPEGMA nanocomposites at 25 °C. ....	82

<b>Figure 46.</b> Specific surface energy of BC, BC/PGMA and BC/PGMA/MBA nanocomposites with polar probes: THF - tetrahydrofuran, DCM - dichloromethane, ETOAc – ethyl acetate and ACN – acetonitrile, at 25 °C. ....	85
<b>Figure 47.</b> Specific surface energy of BC and BC/PPEGMA nanocomposites with polar probes: THF - tetrahydrofuran, DCM - dichloromethane, ETOAc – ethyl acetate, ACN – acetonitrile, at 25 °C. ....	85
<b>Figure 48.</b> Heterogeneity profile with dichloromethane for (A) BC, BC/PGMA and BC/PGMA/MBA and (B) BC and BC/PPEGMA nanocomposites, at 25 °C. ....	86

## TABLES INDEX

<b>Table 1.</b> EDX analysis of elemental composition of BC, BC/PGMA and BC/PGMA/MBA nanocomposites (wt %).	32
<b>Table 2.</b> Crystallinity index, $I_c$ , and crystallite size, ACS, of BC/PGMA and BC/PGMA/MBA nanocomposite.	33
<b>Table 3.</b> Thermal degradation, $T_d$ (°C), of BC/PGMA, BC/PGMA/MBA nanocomposites and their controls in study.	38
<b>Table 4.</b> Thermal degradation, $T_d$ (°C), of BC/PGMA and BC/PGMA/MBA nanocomposites before and after chemical treatment.	51
<b>Table 5.</b> Surface properties of BC/PGMA/MBA and BCPGMAMBA-CT nanocomposites at 25°C.	53
<b>Table 6.</b> EDX analysis of elemental composition of BC and BC/PPEGMA nanocomposites (wt %).	64
<b>Table 7.</b> Physical constants of all probes used in IGC experiments.	77
<b>Table 8.</b> Dispersive component of surface energy, $\gamma_s^d$ , swelling ratio, $SW$ , of BC, BC/PGMA and BC/PPEGMA nanocomposites.	79
<b>Table 9.</b> Surface area, $S_{BET}$ , monolayer capacity, $n_m$ and adsorption potential distribution maximum, $A_{max}$ , of BC, BC/PGMA, PC/PGMA/MBA and BC/PPEGMA nanocomposites, at 25 °C with $n$ -octane.	84
<b>Table 10.</b> Acid-base character, $K_A$ and $K_B$ of BC, BC/PGMA BC/PGMA/MBA and BC/PPEGMA nanocomposites, at 25 °C.	87



## LIST OF ABBREVIATIONS

$\Delta G_{ads}$  – Molar energy of adsorption

$\Delta G_{sp}^s$  – Specific component of the surface energy

$\Delta H_{ads}^{sp}$  – Specific enthalpy of adsorption

$\Delta S_{ads}^{sp}$  – Specific entropy of adsorption

$V_N$  – Net retention volume

$AN^*$  - Acceptor numbers

$A_{max}$  – Adsorption potential

$K_A$  – Acid constant

$K_B$  – Basic constant

$S_{BET}$  – Surface area

$W_A$  – Energy of adhesion

$a_m$  – Cross area

$n_m$  – Monolayer capacity

$p^\circ$  - Saturation pressure

$\gamma_L^d$  – Dispersive component of the surface energy of the probe molecule

$\gamma_s$  – Surface energy

$\gamma_s^d$  – Dispersive component of the surface energy

**ADSCs** – Adipose-derived stem cells

**AEM** – 2-Aminoethyl methacrylate

**APS** – Ammonium persulphate

**ATR – FTIR** – Attenuated Total Reflection Fourier Transform Infrared Spectroscopy

**ATRP** – Atom transfer radical polymerization

**BC** – Bacterial cellulose

**BC/PPEGMA** – Bacterial cellulose/poly(ethyleneglycolmethacrylate)

**BC/PGMA** – Bacterial cellulose/poly(glycidylmethacrylate)

**BC/PGMA/MBA** – Bacterial cellulose/poly(glycidylmethacrylate) crosslinker with *N,N'*-methylenebisacrilamide

**BCPGMA-CT** – Bacterial cellulose/poly(glycidylmethacrylate) after chemical treatment

**BCPGMAMBA-CT** – Bacterial cellulose/poly(glycidylmethacrylate) crosslinker with *N,N'*-methylenebisacrilamide after chemical treatment

**BuMA** – Butyl methacrylate

**c-di-GMP** – Cyclic diguanylic acid

**CPMAS <sup>13</sup>C NMR** – Solid-state Cross-Polarization Magic Angle Spinning Carbon-13 Nuclear Magnetic Resonance

**DG** – Degradation profile

**DMA** – Dynamic Mechanical Analysis

**DMAEMA** – *N,N*-dimethylaminoethylmethacrylate

**E'** - Storage modulus

**EDX** – Energy-Dispersive X-ray Spectroscopy

**EOEMA** – 2-Ethoxyethyl methacrylate

**FE-SEM** – Field Emission Scanning Electron Microscopy

**Glc – 1 – P** – Glucose-1-phosphate

**Glc – 6 – P** – Glucose-6-phosphate

**GMA** – Glycidylmethacrylate

**GMMA** – Glycerol monomethacrylate

**HEMA** – 2-Hydroxyethyl methacrylate

**IGC** – Inverse Gas Chromatograph

**MBA** - *N,N'*-Methylenebisacrilamide

**MMA** – Methyl methacrylate

**PAAc** – Poly(acrylic acid)

**PDE-A and PDE-B** – c-di-GMP phosphodiesterases A and B

**PEG** – Poly(ethylene glycol)

**PEGDA** – Poly(ethylene glycol)diacrylate

**PEGMA** – Poly(ethyleneglycol)methacrylate

**PGMA** – Poly(glycidylmethacrylate)

**PVA** – Poly(vinyl alcohol)

**RAFT** – Reversible addition-fragmentation chain transfer polymerization

**SW** – Swelling ratio

**TGA** – Thermogravimetric Analysis

**UDPG** – Uracil diphosphate glucose

**UGPase** – UDPG-pyrophosphorylase

**XRD** – X-ray diffraction

***DN*** – Donor number

***N*** – Avogadro's number

***R*** – Gas constant

***T*** – Temperature

***Td*** – Thermal degradation

***a*** – Area occupied by probe molecule

***c*** – Heat of sorption

***n*** – Amount adsorbed

***p*** – Partial pressure



## CHAPTER I

### *Bacterial cellulose and Nanocomposites world – General Introduction*

---



## CHAPTER I. Overview of bacterial cellulose

### 1. Cellulose as Biopolymer

Originally from Greek and employed for the first time by the Swedish chemist Berzelius in 1833, *polymers* (*poli*, many; *meros*, parts) are defined as large molecules (macromolecules) synthesized from simple molecules, *monomers*, linked by covalent bonds by polymerization processes (1-3).

Cellulose is the most abundant natural polymer because it is the main component of the plant cell walls. It can be found in large amount in wood [above 50% (w/w)] and cotton [above 94% (w/w)] (3). Due to its versatility and properties, cellulose can be applied into different areas such as pulp and paper production, textiles, construction materials, cosmetics, pharmaceutical industries as excipient and as a source for biofuel production (4, 5). Through chemical processes like *e.g.* methylation and acetylation, cellulose derivatives can be produced such as cellulose ethers and cellulose esters for other's applications (3, 5-8). The increase interest and demand for vegetable cellulose derivatives had augmented the consumption of wood as a raw material, being the cellulose production approximately  $1.5 \times 10^{12}$  tons per year. This value represents a major fraction of the total biomass produced which contributes to the deforestation and global environmental issues (4, 9, 10).

Cellulose was described for the first time by Anselm Payen in 1836 as "*a resistant fibrous solid that remains behind after treatment of various plant tissues with acids and ammonia, and after subsequent extraction with water, alcohol, and ether*" (11). It consists in a linear homopolymer composed by *D*-glucose monomer glycosidically linked covalently in a  $\beta(1-4)$  conformation through acetal functions, between the hydroxyl groups of C1 and C4 carbon atoms. It is attributed a molecular formula of  $(C_6H_{10}O_5)_n$  where  $n$  is the degree of polymerization of glucose (Figure 1) (9, 11, 12). Two adjacent structural units constitute the basic repeating unit called disaccharide cellobiose of the linear polymer (9). The linear configuration of cellulose is stabilized by the intra-chain hydrogen bonds between the hydroxyl groups and the oxygens of the adjacent ring molecules. Besides that, the interaction between hydroxyls groups and oxygens of neighboring molecules via inter-chain hydrogen bonds promote the aggregation

of multiple cellulose chains resulting into nanofibrils. Combining both intra- and inter-chain hydrogen bonding, turns the polymer relatively stable and give fibrils high axial stiffness (13). Cellulose is insoluble in water, with high mechanical resistance and with a chemical composition of 43.6–45 % carbon, 6.0–6.5 % hydrogen and the remainder oxygen. The length of fibers depends of the source of cellulose and can range between 100 up to 10,000 nm (4).

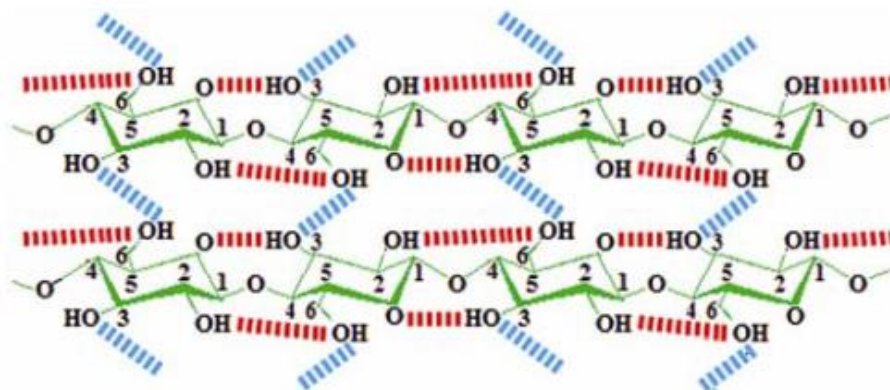


**Figure 1.** Molecular structure of cellulose where inter- (blue) and intra- (red) chain hydrogen bonds dashed lines [reproduced from (14)].

Cellulose with different morphologies can be obtained from conventional plant fibers following adequate procedures as pulping processes (mechanical and chemical), acid hydrolysis, steam explosion, high-intensity ultrasonification, among others (Figure 2) (4).

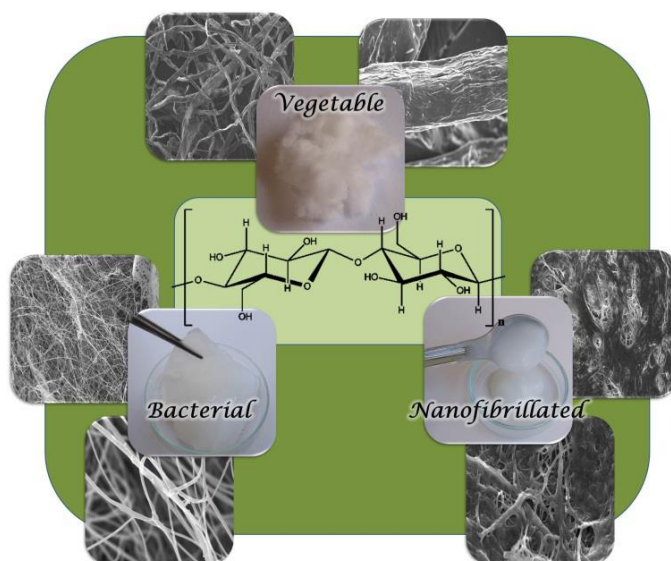


**Figure 2.** Morphology characteristics of the different types of cellulose fibers [reproduced from (15)].

## 2. Bacterial Cellulose – Historical Outline

Adrian J. Brown discovered in 1886 a gelatinous membrane as a product of microbial fermentation of acetic acid from the “vinegar plant” or “mother” (6, 16, 17). Afterwards, their chemical structure resembles that of native cellulose (cell-wall) through X-ray diffraction. It was verified a crystallography typical of cellulose I, with two cellobiose units arranged parallel in units cell and tended to have a specific planer orientation in dried film (14). This gelatinous membrane was denominated as bacterial cellulose, BC, and the “vinegar plant”, as *Acetobacter* (nowadays *Gluconacetobacter*) *xylinum*. As an exopolysaccharide, BC was prompted a number of studies in order to better understand its biosynthesis pathways and properties (18-20). BC can be produced in laboratory by several genera of bacteria such as *Gluconacetobacter*, *Entrobacter*, *Rhizobium*, *Agrobacterium* and *Sarcina* sp during their biosynthesis (12). Innumerable bacteria strains have been reported as BC producers. Known as a gram-negative, aerobic, straight, slightly bent rods or ellipsoidal with dimensions of 0.6 x 4  $\mu\text{m}$ , *Gluconacetobacter* strains are characterized as BC producers (6). For example, *Gluconacetobacter sacchari* was reported as a high efficient producer of BC for the first time by Trovatti *et al* (2011) with production yields of 2.7 g/L after 96h (21).

In recent years, BC has gained interest in numerous areas of study and in a variety of applications due to its unique and specific properties such as high degree of crystallinity (80-90%), high water retention capacity (99% of own weight), high purity (free hemicellulose and lignin), high degree of polymerization (above 8000 wherein sometimes getting even 16,000 or 20,000), ultrafine fibrous network, high tensile strength, water holding ability, porosity, biocompatibility, hydrophilicity, non-toxicity and a relatively simple production and efficient in terms of costs (9, 11, 17, 22, 23). The BC display a typical Young's modulus in the range of 15-35 GPa with a tensile strength ranging between 200-300 MPa (9, 11).

### 2.1. Biochemistry of Bacterial Cellulose and Biosynthesis Pathways

Extensive research and reviews regarding the metabolic pathways of BC, genetic and strains of cellulose-producing of BC have been reported (3, 24-27). *Gluconacetobacter xylinum* is the most commonly model bacteria strain studied due to its ability to produce cellulose

from a wide range of carbon/nitrogen sources, being the rate of cellulose production proportional to that of cell growth (6, 18, 28-30). Several studies indicate that the carbon sources present in the medium influence the yield of BC as well as the bacteria strains and the culture conditions: static and shaking (11, 29-35).

Two metabolic pathways operate in *G. xylinum* for BC production: the pentose phosphate cycle (oxidation of carbohydrates) and the citrate acid cycle (oxidation of organic acid and related compounds). *G. xylinum* is unable to metabolize glucose in the absence of oxygen due to the lack or weakly present phosphofructose kinase, which is required for glycolysis. Glucose is the most common monosaccharides used as a carbon source in order to obtain cellulose. Four fundamental enzymatic steps occur (i) phosphorylation of glucose by glucokinase, (ii) isomerization of glucose-6-phosphate (Glc-6-P) to glucose-1-phosphate (Glc-1-P) by phosphoglucomutase, (iii) synthesis of UDP-glucose (UDPG) by UDPG-pyrophosphorylase (UGPase) and (iv) cellulose synthase reaction (Figure 3) (6, 18, 24).

UDPG is the immediate sugar nucleotide precursor of cellulose synthesis and for  $\beta(1-4)$  glucan polymerization reaction. This enzyme allows an improved activity in BC producers of c.a. 100x orders of magnitude (24). When disaccharides (sucrose or maltose) are used as carbon source, the biosynthesis of BC initiates with the hydrolysis of disaccharides into monosaccharides (fructose and glucose). Then, they are metabolized by the bacteria strain. The molecular mechanisms of glucose polymerization into long and unbranched cellulose chains are still nuclear, since the pathways of UDPG are relatively not well known. Cyclic diguanylic acid (c-di-GMP) acts like an allosteric activator of the membrane-bound cellulose synthase and display an important role in the biosynthesis of BC as a regulatory element (6). The activity of c-di-GMP phosphodiesterases A and B (PDE-A and PDE-B) stopped the activity of cellulose synthase. PDE-A cleaves the c-di-GMP to form pGpG which is degraded, producing two molecules of 5'-GMP. The activity of PDE-A is selectively inhibited by  $\text{Ca}^{2+}$  ions (24).

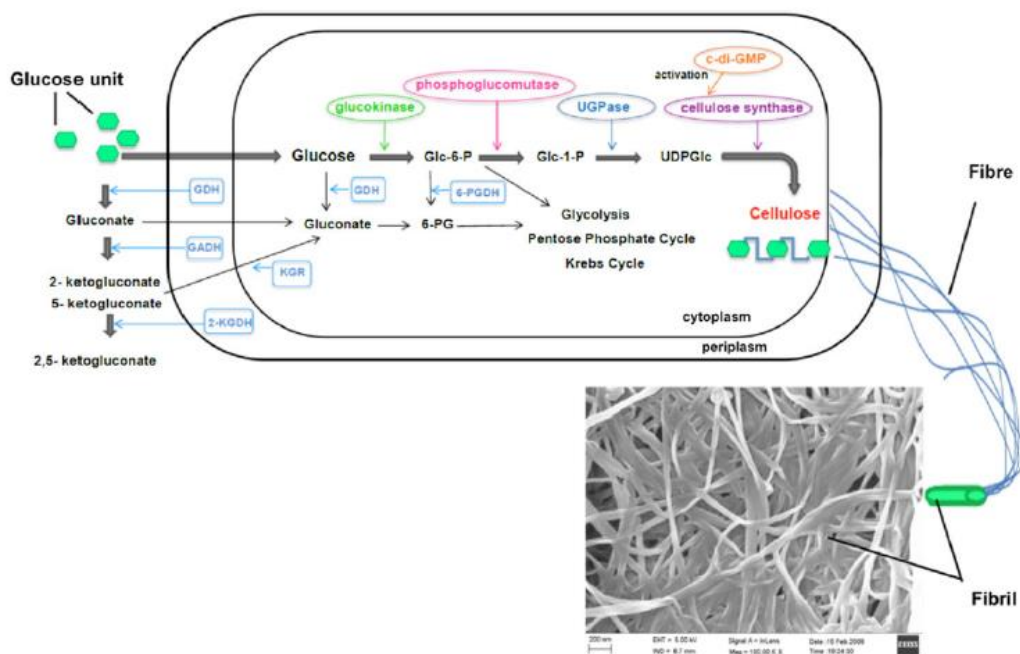


**Figure 3.** Schematic of the metabolic pathways of *Glucanoacetobacter xylinum* and the assembly of cellulose molecules into nanofibrils [reproduced from (6)].

Cellulose is synthesized in microorganisms in two intermediary steps: (i) the formation of  $\beta(1-4)$  glucan chains and (ii) the assembly and crystallization of cellulose chains. The cellulose molecules are initially synthesized inside the bacteria and then spun through cellulose export components to form protofibrils with a diameter c.a. of 2 – 4 nm. A ribbon shaped microfibril of approximately 80 nm is assembled from these protofibrils. Cellulose synthase is the catalyst for biosynthesis of cellulose, which polymerizes the glucose units into the  $\beta(1-4)$  glucan chains (6).

## 2.2. Structure and Properties of Bacterial Cellulose

Structurally, BC possess an identical molecular formula  $(C_6H_{10}O_5)_n$  of the vegetable cellulose as shown in Figure 1 (9, 11, 12). The process of biosynthesis of BC comprises two main stages: linear polymerization of the glucose units catalyzed by the enzyme cellulose synthase, followed by crystallization of the linear chains. The polymerization of  $\beta(1-4)$  glucan starts from 300 to 10,000 glucose unit in order to form a linear polymer. This linear polymer chain assembles with other adjacent chains to form aggregates (subfibrils) with 1.5

nm width, that further combine with another one to form semi-crystalline nanofibrils with 3.5 nm width. The nanofibrils combine between them, originating bundles and then the macroscopic ribbon shapes (Figure 4) (9, 11). The size of nanofibrils and their spatial arrangement strongly influences the BC crystallinity, which depends on two factors: source (organism) and synthesis conditions (9, 11).

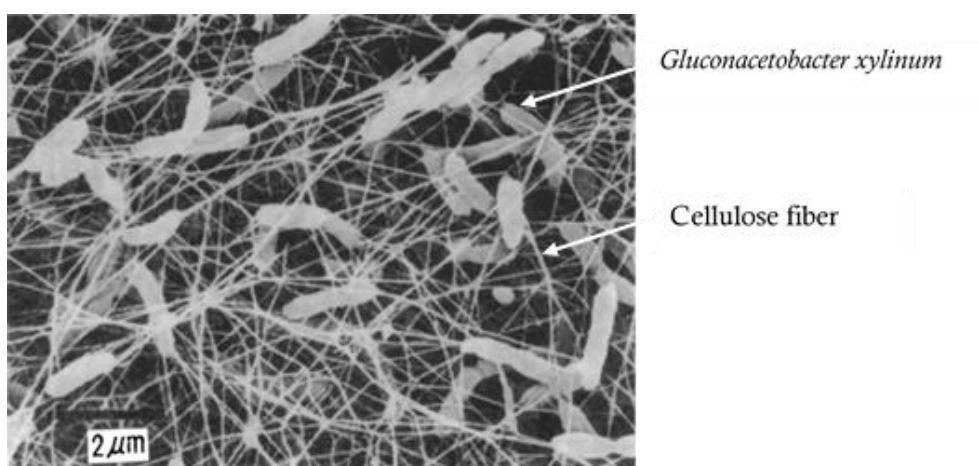


**Figure 4.** A SEM of freeze-dried surface of bacterial cellulose gel [reproduced from (14)].

Cellulose type I is the most common form biosynthesized and detected by X-rays (Figure 5), consisting in two  $\beta(1-4)$  glucan chains oriented parallel to each other in a monocyclic unit cell and arranged uniaxially (11). Native cellulose exhibited two different structural crystals, cellulose  $I_\alpha$  and  $I_\beta$ . The cellulose  $I_\alpha$  is crystallized in larger-size nanofibrils while cellulose  $I_\beta$  is formed in smaller-size nanofibrils being thermodynamically more stable (3). Also, the allomorph forms differ in the unit cell:  $I_\alpha$  show a triclinic unit and  $I_\beta$  a monoclinic unit cell. The ratio  $I_\alpha/I_\beta$  depends from species to species (3). The aggregates form nanofibrils of width approximately 100 nm denominated fibrillary bands and these form the tridimensional network structure. The 3-D micro and nanofibrillar structure of bacterial cellulose influence the majority of its properties (9, 11). Bacterial cellulose, compared with vegetal cellulose, had higher degree of polymerization, a higher degree of crystallinity and higher size of crystallites (9, 11). These structural differences induce considerable differences in terms of physical properties, particularly in terms of the mechanical strength (9, 11).

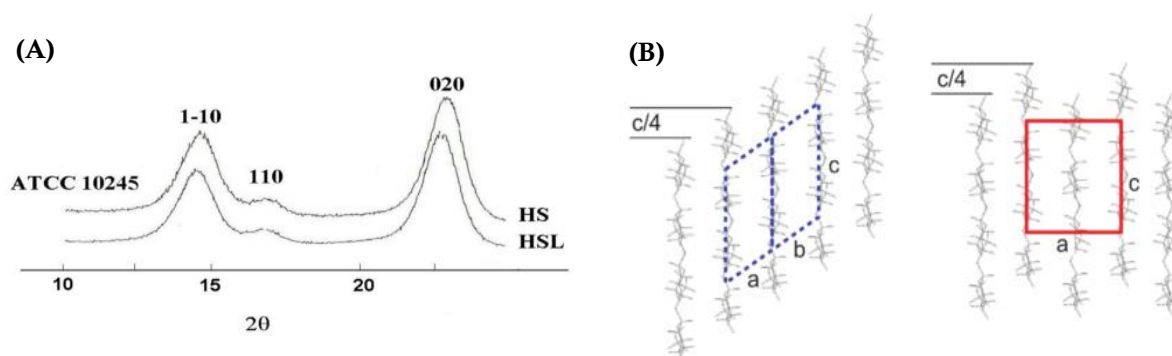


**Figure 5.** (A) X-ray patterns of BC films and (B) View along the direction 4 (i.e.  $[1\bar{1}0]$  for  $I_\alpha$  and  $[010]$  for  $I_\beta$ ) and the displacement of the hydrogen bonding sheets: blue  $I_\alpha$  and red  $I_\beta$  [reproduced from (3, 13)].

BC can be obtained in static and agitated culture media showing three different forms: membrane, irregular shapes and sphere-like particles (Figure 6). BC membranes are produced in static conditions at the air-liquid medium interface and have been commonly used for different applications due to their suitable properties.

In contrast, irregular shapes and spheres of BC are produced under agitated culture. Typically, BC produced in agitated culture media showed lower cellulose  $I_\alpha$  content, lower Young's modulus, higher swelling and have potential to be used in food, healthcare and materials applications (36).

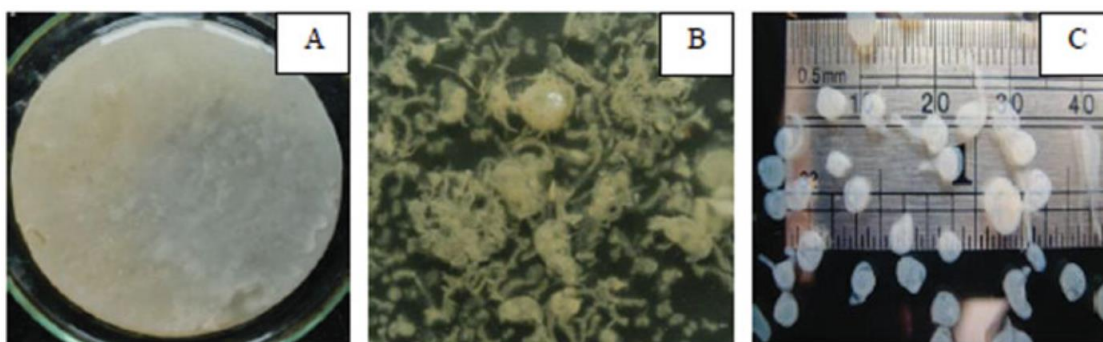


**Figure 6.** Different forms of BC produced by *Gluconacetobacter* sp. (A) Membrane, (B) Irregular forms, (C) Sphere-like particles [reproduced from (36)].

### 2.3. Application of Bacterial Cellulose

BC is one of the finest examples of Nature's art, with a singular morphology and unique properties, and is gaining increasing interest as an excellent biopolymeric material to be employed in a wide range of applications in different areas (Figure 7), namely in the:

- (i) Biomedical and biotechnology fields: artificial skin, artificial blood vessels, artificial cornea, heart valve prosthesis, artificial urethra, artificial bone, artificial cartilage, artificial porcine knee menisci and delivery drug, hormone and protein, reinforcement material for wound dressings, scaffolds for tissue engineering and soft tissue replacement (7, 11);
- (ii) Environmental and agricultural fields: dye decolorization, biadsorbent for heavy metal removal and improvement of quality of soil with application of BC (11);
- (iii) Electronic field: reinforcement transparent flat-panel (11);
- (iv) Food fields: *nata-de-coco* manufacture (11);
- (v) Industrial fields: papermaking (11);
- (vi) Reinforcement as composites (11).

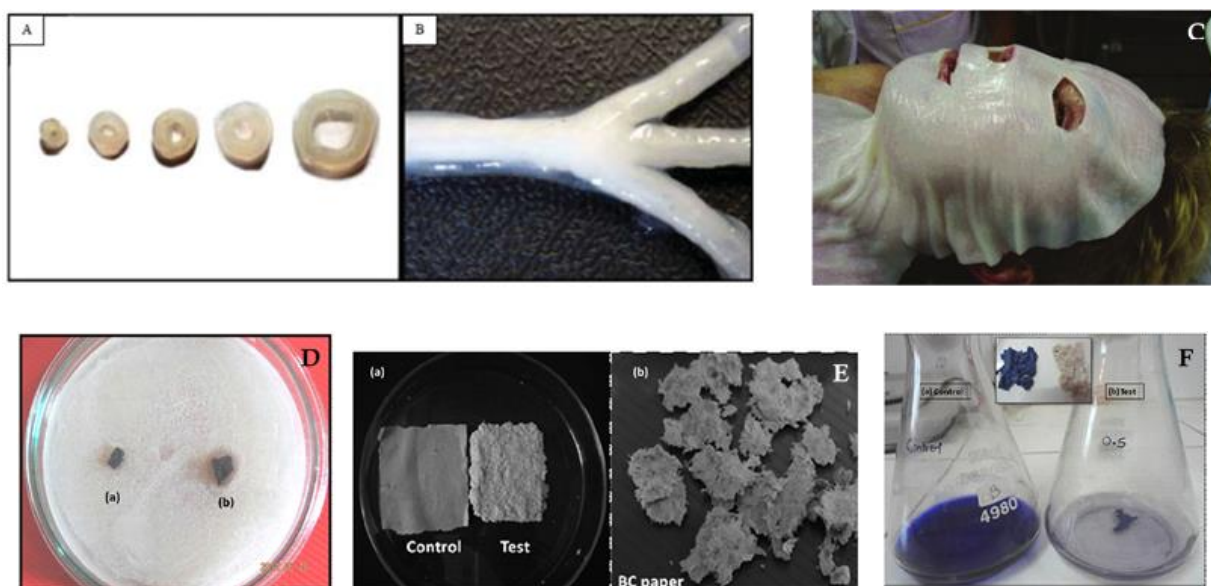


**Figure 7.** Applications of bacterial cellulose: A – Tubes (blood vessel); B – Branched tube fermented on a branched silicone tube (vascular grafts) [reproduced from (36)]; C –Dressing (wound dressing) [reproduced from (7)]; D – Incorporation of AgNO<sub>3</sub> nanoparticles (antimicrobial activity); E –Paper (filter paper) and F – Colored with aniline blue dye (bioadsorbent) [reproduced from (11)].

### 3. Bacterial Cellulose Nanocomposites

Nanocomposites were defined for the first time as “*a multi-phase compound in which one of the phases has a length scale in the nanometer range*” by Roy and co-workers in 1980’s. A more practical definition was introduced by Komarneni in 1992 that defined nanocomposites as “*composites of more than a Gibbsian solid phase where at least one-dimension is in the nanometer range and typically all solid phases are in the 1-20 nanometer range*” (37).

BC nanocomposites have been studied over time due to the excellent properties of these materials. BC can be manipulated in order to improve mechanical performance and biocompatibility, and can be employed in many forms from nano to macro scales for various applications. They can be applied into plant biomimicking, biomedical, electrically conductive materials, catalysis, optical and luminescent materials, proton conductive, separating materials, antimicrobial materials, thermos-responsive, among many another’s (36).

Different approaches for the preparation of BC nanocomposites have been reported in literature (38-41), including: (i) incorporation of desire components in culture medium during BC biosynthesis; (ii) *In situ* polymerization of monomers inside of the BC network and (iii) blending with other polymeric materials. The first’s two approaches are applied in the *in situ* preparation of nanocomposites and are described below.

#### 3.1. BC nanocomposites through BC biosynthesis

One approach for the BC nanocomposites obtainment is the introduction of polymers and/or desirable compounds into the culture medium during BC biosynthesis. This way, the nanocomposite will be produced at the same time as the BC fibrils, through assembly of the desire compounds. In fact, many compounds/polymers have already been incorporated in BC culture media in order to obtain BC nanocomposites. Compounds/polymers such as chitosan (41), carbon fibers, aloe-vera (42), glyoxal (38) or poly (vinyl alcohol) (PVA) (39).

Phisalaphong *et al* (2008) reported a new BC/chitosan film obtained through the supplement of low molecular weight chitosan into the culture medium. The obtained BC/chitosan nanocomposite exhibited a denser homogeneous fibril structure with smaller

pore diameter and higher surface area (Figure 8). Structurally, the introduction of chitosan as a supplement into the culture medium didn't change BC properties such as water vapor transmission rates, average crystallinity index and antimicrobial ability (41).

A new nanostructured film of BC/aloe vera was reported by Saibuatong *et al* (2010) through incorporation of aloe vera into the culture medium during biosynthesis of BC. This assembly resulted in the enhancement of the mechanical properties, water absorption capacity, water vapor transmission rate and crystallinity index. The BC/aloe vera nanocomposite displayed an excellent compatibility and physical properties which make it a good material with a wide range of application in medical areas (42).

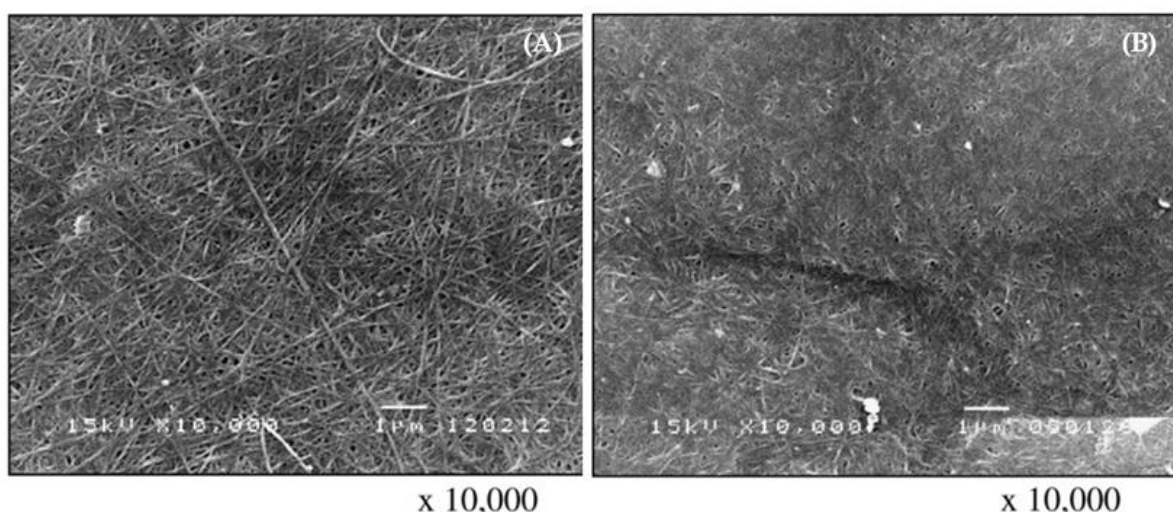


**Figure 8.** SEM images of surface morphology of (A) BC and (B) BC/Chitosan film in dry form [reproduced from (41)].

Castro *et al* (2014) reported the production of BC/PVA nanocomposite films by adding PVA to the culture media followed by chemical crosslinking. The chemical crosslinking, after the biosynthesis, avoid the loss of the PVA matrix during the purification steps improving the functional properties of the nanocomposites, reflected by the good interaction between the PVA matrix and the reinforcement BC phases (Figure 9) (39).

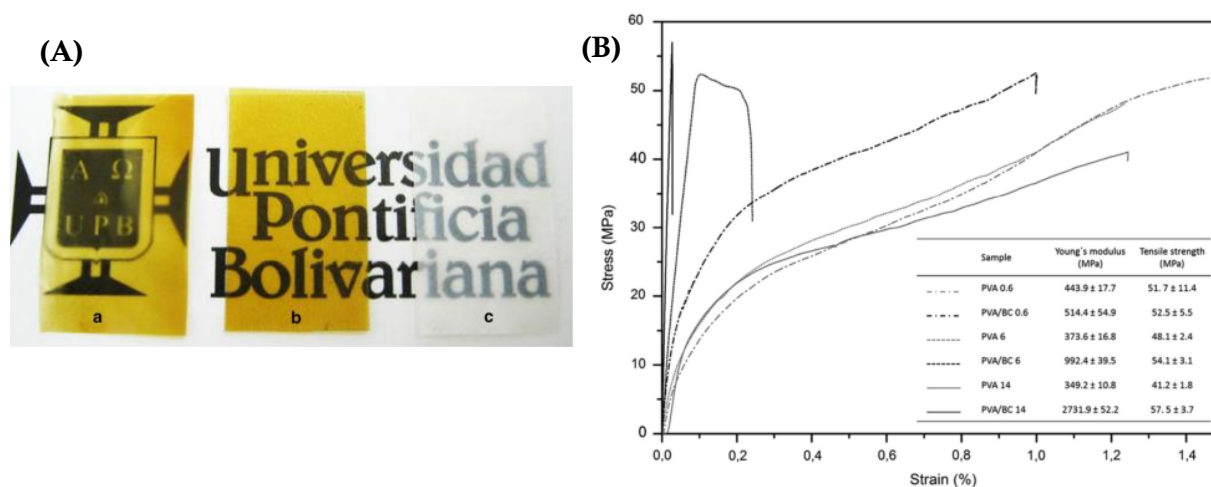


**Figure 9.** (A) Visual appearance of PVA: (a) without BC (b) BC/PVA nanocomposites and (c) BC/PVA nanocomposites after chemical crosslinker and (B) Stress-strain behavior of BC/PVA [reproduced from (39)].

Besides that, these authors reported the glyoxalization of BC films, by introducing glyoxal into the culture medium during the BC biosynthesis. Glyoxalized BC films showed an increase in their hydrophobicity improving the BC properties while keeping its crystallinity (38).

### 3.2. BC nanocomposites through *in situ* polymerization

Another approach to prepare BC nanocomposites is the *in situ* polymerization inside the BC network. This method involves the absorption of a solution with the desire monomer, the initiator and crosslinker (if used in the polymerization) into the BC network, followed by the polymerization reaction. This approach is quite interesting because the final properties of the nanocomposites can be simply tailored by using different monomers or monomers mixtures.

*In situ* polymerization had already been used for the preparation of BC nanocomposites with various methacrylates monomers such as 2-hydroxyethyl methacrylate (HEMA) (22, 40), 2-aminoethyl methacrylate (AEM) (43), glycerol monomethacrylate (GMMA) (22) and 2-ethoxyethyl methacrylate (EOEMA) (22).

Methacrylate monomers are versatile to prepare a series of BC/methacrylate nanocomposites with different properties, due to their chemical structure variability, great availability and easy polymerization (22).

Figueiredo *et al* (2015) reported the preparation of novel BC nanocomposites through *in situ* polymerization of 2- aminoethyl methacrylate (AEM). Variable amounts of AEM and N,N'-methylenebis(acrylamide) (MBA) used as a crosslinker were impregnated into the BC membrane before the polymerization step. The BC/PAEM and BC/PAEM/MBA nanocomposites were very homogeneous suggesting a good distribution of PAEM inside the BC network, and were more translucent than native BC [Figure 10 (A)]. In addition, these nanocomposites showed improved thermal stability and mechanical properties [Figure 10 (B)], a decrease in crystallinity and an increase of swelling ability [Figure 10 (C)] (43).

Furthermore, BC/PAEM nanocomposites (without crosslinker) display antibacterial activity when in contact with a bacterial suspension of a bioluminescent *Escherichia coli* demonstrating to be a good nanomaterial with properties for potential application as antimicrobial wound dressing.

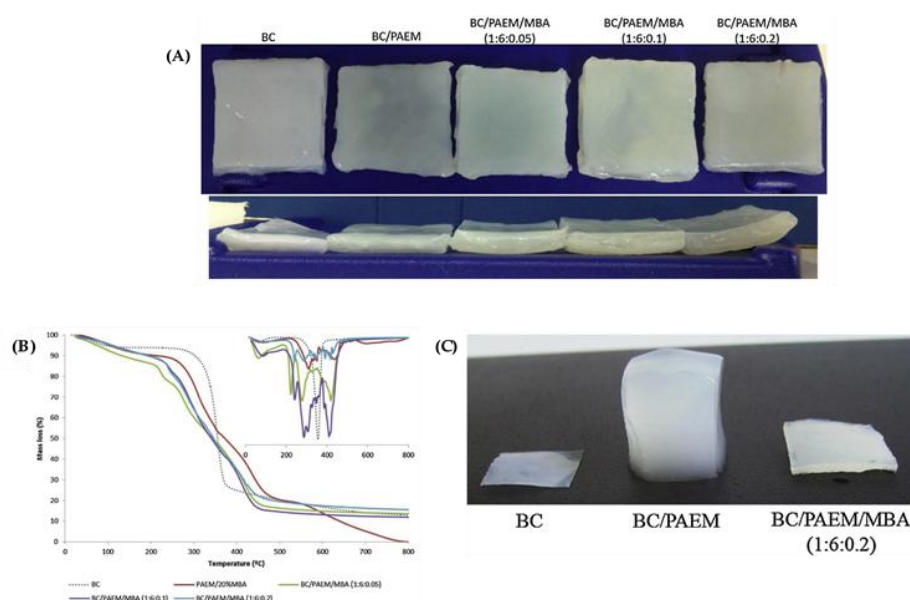


**Figure 10.** (A) Visual appearance of BC/PAEM and all BC/PAEM/MBA nanocomposites. (B) TGA thermograph of BC/PAEM nanocomposites. (C) Swelling of wet BC, BC/PAEM and BC/PAEM/MBA nanocomposites [reproduced from (43)].

In a different study (40), 2-hydroxyethyl methacrylate (HEMA) was used to prepare a series of bacterial cellulose/poly(2-hydroxyethyl methacrylate) nanocomposites films by *in situ* radical polymerization using poly(ethylene glycol) diacrylate (PEGDA) as a crosslinker (40). As in the case of BC/PAEM nanocomposites, the translucency and homogeneity of the BC/PHEMA and BC/PHEMA/PEGDA nanocomposite increased with the amount of monomer and crosslinker polymerized inside the BC network [Figure 11 (A)]. The nanocomposites exhibited improved thermal properties, good swelling ability and a decrease in the storage tensile modulus. Furthermore, the nanocomposites are non-cytotoxic providing favorable cell environment for optimal adhesion and proliferation of adipose-derived stem cells (ADSCs) [Figure 11 (B)]. These makes them promising material for several biomedical applications as for the design of 3D matrices with the purpose of maintaining a cellular niche for stem-mediated tissue regeneration (40).

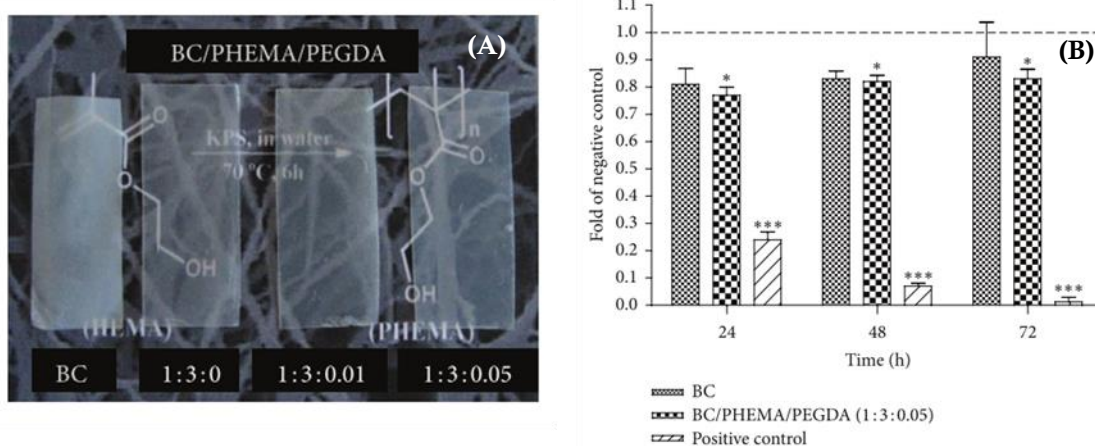


**Figure 11.** (A) Visual aspect of BC, BC/PHEMA and BC/PHEMA/PEGDA films and (B) ADSCs proliferation in contact with BC and BC/PHEMA/PEDGA films [reproduced from (40)].

### 3.3. Acrylate monomers used in BC nanocomposite

Acrylate monomers such as acrylic acid, 2-ethylhexyl acrylate, 2-hydroxyethyl methacrylate (22), methyl methacrylate (MMA), butyl methacrylate (BuMA) (44), *N,N*-dimethylaminoethyl methacrylate (DMAEMA) (45) are typically used for polymerization reaction due their high reactivity.

### Glycidylmethacrylate

Among acrylate monomers, glycidylmethacrylate (GMA) is of particular interest because it presents two polymerizable groups: the epoxide and the methacrylate (Figure 12). The double bond (C=C) of the methacrylate groups enables it to be subjected to a polymerization process through radical polymerization reaction. The functional groups of GMA can react with BC hydroxyl groups (46). Depending on the selective group polymerizable or copolymerizable, the polymer acquires different reactivity. Most commonly, the polymerization reaction mechanism involves the methacrylate groups while the epoxide groups remaining unreacted (47). Moreover, this monomer offers spacer groups, helping in the flexible movement of the polymer chain, favoring e.g. the adsorption of compounds (48, 49). The hydrolysable ester group has been used due to its relatively low toxicity, polarity, hydrophobicity, good reactivity, excellent biocompatibility and lower price comparatively to others methacrylate monomers, make it an attractive monomer for modification (47, 50-53).

These specificities open the possibility for several applications in the polymer chemistry and technology such as for purification of lysozyme from chicken white egg (49, 50, 54), removal of heavy metals and chromate anions from aqueous solutions (48, 55-58), and in coatings, matrix resins and adhesives (47, 59).

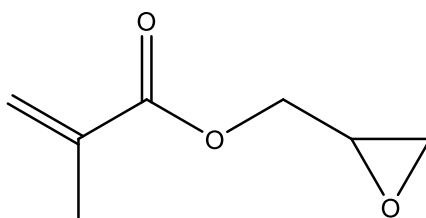


**Figure 12.** Molecular structure of glycidylmethacrylate (GMA).

GMA has already been reported in grafting polymerization from cellulosic backbones using various polymerization systems such as free initiators (54, 55), redox systems like  $\text{H}_2\text{O}_2$ -thiocarbonate,  $\text{H}_2\text{O}_2$ -Cu complex, reversible addition-fragmentation chain transfer polymerization (RAFT) (60), photoinitiation, UV radiation and atom transfer radical polymerization (ATRP) (52, 59).

## Poly(ethylene glycol)methacrylate

Poly(ethylene glycol) (PEG) exhibited unique advantageous properties to be exploited in biomedical and biotechnological devices due their low-toxicity, absence of antigenicity and immunogenicity and inherent ability to prevent protein adsorption (61). Poly(ethylene glycol)methacrylate (PEGMA), a PEG derivative, is another attractive methacrylate monomer due to its amphiphilic nature. This property comes from its water-soluble PEG side chain with a pendant hydroxyl group and its hydrophobic methacrylate group (Figure 13) (62). Due to these properties, PEGMA is one of the most attractive monomers used to prepare biomedical materials such as drug carrier (63), microspheres for transient vascular embolization (62), protein adsorption and immobilization of polysaccharides (64). It is also, used for heavy metals removal (65, 66).

Different approaches of polymerization of PEGMA have been reported in the literature such as photopolymerization (63, 67) and ATRP (61).

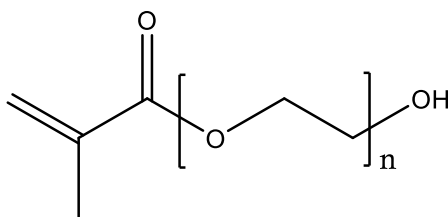


**Figure 13.** Molecular structure of poly(ethylene glycol) methacrylate (PEGMA).

#### 4. Aim of the Study

In view of all issues described above, the aim of the present study is to prepare novel BC nanocomposites for potential biomedical application through *in situ* free radical polymerization of glycidylmethacrylate (GMA) and poly(ethyleneglycol)methacrylate (PEGMA) using *N,N'*-methylenebis(acrylamide) (MBA) as crosslinker.

All BC nanocomposites were characterized in terms of structure, morphology, thermal stability, water absorption, mechanical and surface properties by Attenuated Total Reflection Fourier Transform Infrared Spectroscopy (ATR-FTIR), CPMAS  $^{13}\text{C}$  NMR, X-ray diffraction (XRD), Energy-Dispersive X-ray Spectroscopy (EDX), Field Emission Scanning

Electron Microscopy (FE-SEM), Swelling (SW), Thermogravimetric Analysis (TGA), Dynamic Mechanical Analysis (DMA) and Inverse Gas Chromatography.

The present manuscript is laid out in four different chapters, each one corresponding to scientific papers to be submitted briefly.

## **CHAPTER II**

*New bacterial cellulose / poly(glycidylmethacrylate)  
nanocomposites films by in situ free radical polymerization*

---



## CHAPTER II. New bacterial cellulose/poly(glycidylmethacrylate) nanocomposites films by *in situ* free radical polymerization

### Abstract

Novel bacterial cellulose/poly(glycidylmethacrylate) nanocomposites were prepared by *in situ* free radical polymerization of glycidylmethacrylate using *N,N'*-methylenebisacrilamide as crosslinker. The obtained nanocomposites were characterized in terms of chemical structure, morphology, thermal stability, water absorption and mechanical properties. The optimal conditions achieved for the polymerization were a proportional ratio of 1:2:0.2 (bacterial cellulose/monomer/crosslinker), 0.5% (in respect to monomer) of initiator at 60 °C during 6 h. An incorporation percentage of about 67% was obtained for these experimental conditions. BC nanocomposites exhibited a stiff and compact three-dimensional structure. It was also observed an improvement in thermal and mechanical properties, a decrease in their swelling ability and crystallinity. The new nanocomposites possess epoxy groups in their structure which could react with others molecules, making them suitable for applications in removal of heavy metal or/and proteins.

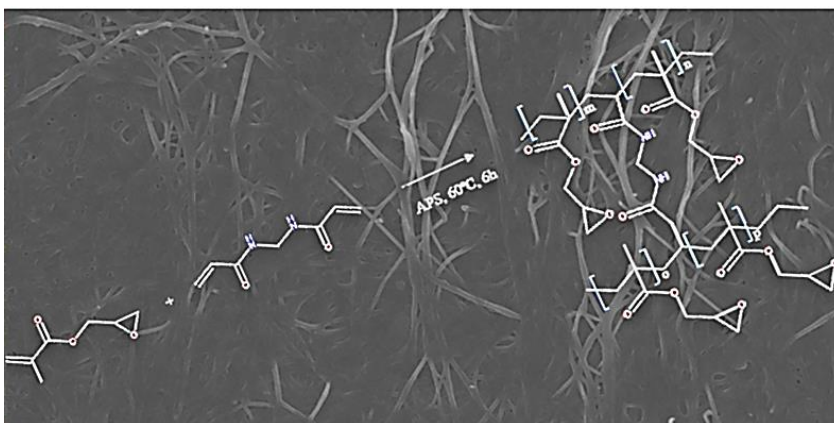


**Figure 14.** Schematic reaction of *in situ* polymerization of GMA/MBA inside BC network.

**Keywords:** bacterial cellulose, glycidylmethacrylate, *in situ* radical polymerization, nanocomposites, morphology, thermal and mechanical properties.

## 1. Introduction

Bacterial cellulose (BC) is a pure form of cellulose produced by several bacteria including *Gluconacetobacter sacchari* which are a gram-negative, rod shaped and strictly aerobic bacteria (16, 17, 21-23). BC confers unique and specific properties such as high degree of crystallinity (80-90%), high water retention capacity (99%), ultrafine fibrous network, high tensile strength, biocompatibility, hydrophobicity and non-toxicity. These properties stand out BC as a good polymer to study having a relatively simple production thus cost efficient (17, 22, 23, 68).

However, BC possess some limitations that restrict its applications as lack of antibacterial properties, optical transparency and stress bearing capability (10). To overcome these limitations, BC nanocomposites have been prepared, consisting in a BC network and reinforcement materials (6, 10, 11, 69). The reinforcement materials improve BC's biological and physiochemical properties (10). BC nanocomposites have been synthesized through *in situ* biosynthesis (38, 42), blended with other polymeric materials (12) and by *in situ* radical polymerization (40, 43).

In the present study, it is exploited the *in situ* radical polymerization of methacrylate monomers into the BC network. Glycidylmethacrylate (GMA) is a methacrylate monomer with two polymerizable groups: the epoxide and the methacrylate groups (double bonds) which offers a wide range of industrial applications in the polymer chemistry and technology namely for purification of lysozyme from chicken white egg (49, 50, 54), removal of heavy metals and chromate anions from aqueous solutions (48, 55-58), in coatings, matrix resins and adhesives (47, 59). Besides that, GMA show a relatively low toxicity, polarity, hydrophobicity and low price which make it an attractive monomer (47, 50-53). GMA has been reported in grafting polymerization on cellulosic backbones using various polymerization systems such as free initiators (54, 55), redox systems like  $\text{H}_2\text{O}_2$ -thiocarbonate,  $\text{H}_2\text{O}_2$ -Cu complex, reversible addition-fragmentation chain transfer polymerization (60), photoinitiation, UV radiation and atom transfer radical polymerization (52, 59).

This work report the development of BC nanocomposite through *in situ* radical polymerization of GMA into BC network using *N,N'*-methylenebisacrilamide (MBA) as crosslinker and ammonium persulphate (APS) as initiator. The optimal conditions of polymerization were determined and the new BC nanocomposites membranes were characterized in term of structural, morphological, water ability, thermal, and viscoelastic properties.

## 2. Methodology

### 2.1. Material

Wet bacterial cellulose (BC) membranes produced by *Gluconacetobacter sacchari* (70) using standard conditions were used. Glycidylmethacrylate (GMA, 97%, with 100 ppm of monomethyl ether hydroquinone as inhibitor), *N,N'*-methylenebisacrilamide (MBA,  $\geq 99.5\%$ ) and ammonium persulphate (APS, 98%) were used as monomer, crosslinker and initiator, respectively. All reagents were purchased from Sigma-Aldrich and used as received. Distilled water was used as solvent in all steps of the procedure.

### 2.2. BC nanocomposites preparation

#### 2.2.1. GMA and GMA/MBA polymerization

A solution of 500 mg of GMA (monomer) and APS (initiator) (0.5% w/w GMA) in distilled water and  $N_2$  atmosphere was prepared. This reaction mixture was placed at 60 °C for 6 hours to prepare the PGMA/MBA polymer. PGMA/MBA polymer was prepared using the same conditions used for PGMA, but with addition of 20% ( $w_{crosslinker}/w_{monomer}$ ) MBA crosslinker to the monomer and initiator solution.

The obtained PGMA/MBA polymer after the reaction time was washed several times with water, while PGMA was washed with methanol, and both were dried at 40 °C overnight, and stored after that in a desiccator until their characterization.

### 2.2.2. *In situ* free radical polymerization of GMA and GMA/MBA into BC

The *in situ* free radical polymerization of GMA inside the BC network was adapted from the procedure described by Figueiredo *et al.* (43). An aqueous reaction mixture containing the monomer ( $w/w_{dry\ BC}$ ) in a ratio of 1:2, 0.5% initiator ( $w/w_{monomer}$ ) and 20% crosslinker ( $w_{crosslinker}/w_{monomer}$ ) (when used in reaction) was prepared. Wet BC membranes were weight and about 60% of their water content was drained. The drained membranes and reaction mixture were purged in N<sub>2</sub> for 30 min. After that the reactional mixture was added to the BC membranes and left for 1 hour at room temperature to occur the incorporation of the monomer (and of the initiator and crosslinker) inside the BC network. Then, the polymerization reaction take place in an oil bath for 6 hours at 60 °C. The obtained nanocomposite membranes were washed with distilled water during 1 hour for 8 times, dried at 40 °C and stored in a desiccator until their characterization.

The percentage of polymer incorporation in the BC network was determined by the sample increasing weight after polymerization and was calculated according to Eq. (1):

$$\% \text{ Incorporation} = \frac{W_{modified\ BC} - W_{BC}}{W_{BC}} \times 100 \quad (\text{Equation 1})$$

where  $W_{BC}$  is the weight of dry bacterial cellulose (g) and  $W_{modified\ BC}$  is the weight of dry bacterial cellulose after *in situ* free radical polymerization (g).

## **2.3. BC nanocomposites characterization**

### **2.3.1. Infrared Spectroscopy**

The infrared spectra were obtained using Attenuated Total Reflection Fourier Transform Infrared Spectroscopy (ATR-FTIR) using a Perkin Elmer FTIR System Spectrum BX spectrophotometer equipped with a single horizontal Golden Gate ATR cell after 32 scans in the  $4000\text{--}500\text{ cm}^{-1}$  range with a resolution of  $4\text{ cm}^{-1}$ .

### **2.3.2. Energy-dispersive X-ray spectroscopy**

The semi-quantitative elemental chemical compositions of the samples were determined by energy-dispersive X-ray spectroscopy (EDX). Semi-quantitative analyses (wt. %) were done for elements (carbon, oxygen and nitrogen) and the  $C/O$  ratio was obtained. EDX experiments were conducted at an accelerated voltage of 5 kV in a Hitachi SU 8090 equipment.

### **2.3.3. Scanning electron microscopy**

Scanning electron micrographs of the surface samples were obtained by Scanning Electron Microscopy (SEM), with a HR-FESEM SU-70 Hitachi equipment operating at 1.5 kV operating in the field emission mode. Samples were deposited on a steel plate and coated with carbon before analysis.

### **2.3.4. X-ray diffraction**

The X-ray diffraction (XRD) measurements were carried out with a Phillips X'pert MPD diffractometer using  $\text{Cu K}\alpha$  radiation. The peaks were deconvoluted using Pearson VII peak functions (Peakfit software) for crystallinity index,  $I_c$ , appearance crystal size (ACS) (38):

$$I_c = 1 - \frac{I_{am}}{I_{002}} \times 100 \% \quad (\text{Equation 2})$$

where  $I_{am}$  is the maximum peak intensity at  $2\theta$  around  $22^\circ$ , representing the crystalline region, and  $I_{002}$  is the minimum peak intensity at  $2\theta$  around  $18^\circ$ , representing the amorphous region. The ACS was calculated using Scherrer's formula:

$$ACS = \frac{(0.9\lambda)}{FWHM \cos \theta} \quad (\text{Equation 3})$$

where FWHM is the width of the peak at half the maximum height.

### 2.3.5. $^{13}\text{C}$ Carbon Nuclear Magnetic Resonance

Solid-state Cross-Polarization Magic Angle Spinning  $^{13}\text{C}$  Carbon Nuclear Magnetic Resonance (CPMAS  $^{13}\text{C}$  NMR) spectra were recorded on a Bruker Avance III 400 spectrometer operating at a B0 field of 9.4 T using 9 kHz MAS with proton  $90^\circ$  pulse of 3 microseconds and a time between scans of 3 seconds.  $^{13}\text{C}$  CPMAS NMR spectra were acquired using a contact time of 2000 (2000) microseconds.  $^{13}\text{C}$  chemical shifts were referenced with respect to glycine (C=O at 176.03 ppm).

### 2.3.6. Swelling ratio

The swelling ratio (SW) of the membranes was determined by immersing the samples in distilled water at room temperature with a minimum of three replicas. The weight increase was periodically measured during 48 hours. For each measurement, the samples were taken out of the water, their wet surfaces immediately wiped dry in filter paper, weighted, and then re-immersed. The SW was calculated using the equation:

$$SW(\%) = \frac{(W_s - W_d)}{W_d} \times 100\% \quad (\text{Equation 4})$$

where,  $W_s$  is the samples weight after swelling and  $W_d$  is the weight of dry sample before swelling.

### 2.3.7. Thermogravimetric analyses

Thermogravimetric analysis (TGA) were carried out with a Shimadzu TGA 50 analyzer equipped with a platinum cell. Samples were heated at a constant rate of 10 °C/min, from room temperature to 800 °C, under a nitrogen flow of 20 mL/min.

### 2.3.8. Dynamic mechanical analyses

Dynamic mechanical analyses were performed using tension as deformation mode (single strain) on a Tritec 2000 DMA (Triton Technologies). For the temperature sweeps, a ramp rate of 2 °C/min was used and samples were heated from –100 to 200 °C, at a frequency of 1 and 10 Hz, with a displacement of 0.005 mm.

## 3. Results and Discussion

### 3.1. *In situ* free radical polymerization reaction

Novel BC nanocomposites were obtained through *in situ* free radical polymerization of GMA into the BC network using MBA as crosslinker and APS as initiator. A schematic illustration of *in situ* polymerization reaction of GMA inside the BC network is illustrated in Figure 15. The *in situ* radical polymerization of GMA occurs through a homolytic cleavage via C=C, initiated by free radical provoked by the dissociation of APS (71).

The crosslinking of PGMA with MBA allows a better incorporation of polymer inside the BC network and consequently the retention of more polymer avoiding its removal through washing (40, 72). This incorporation can change the morphology and properties of

the native bacterial cellulose as perceptible on the visual images of the obtained BC/PGMA and BC/PGMA/MBA nanocomposites (Figure 16).

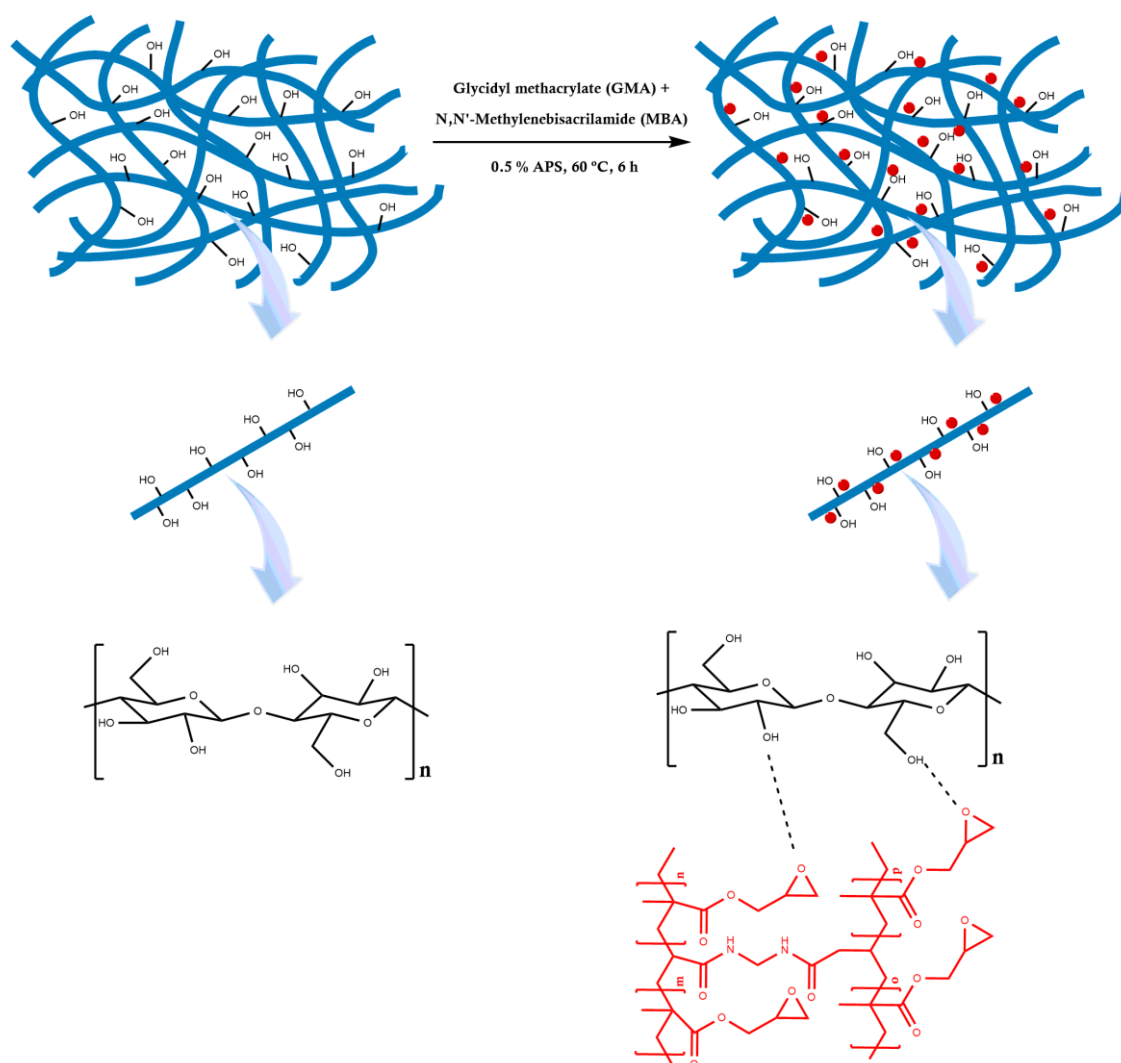


**Figure 15.** Scheme diagram of *in situ* free radical polymerization reaction of PGMA/MBA inside of BC network.

Both synthesized BC/PGMA nanocomposites display an opaque white appearance while native BC exhibits a milky white appearance after air drying. BC/PGMA exhibited as malleable material while the BC/PGMA/MBA materials showed an increased stiffness,

being difficult to remove from the Erlenmeyer after polymerization, which predict new thermal, morphologic and surface properties.

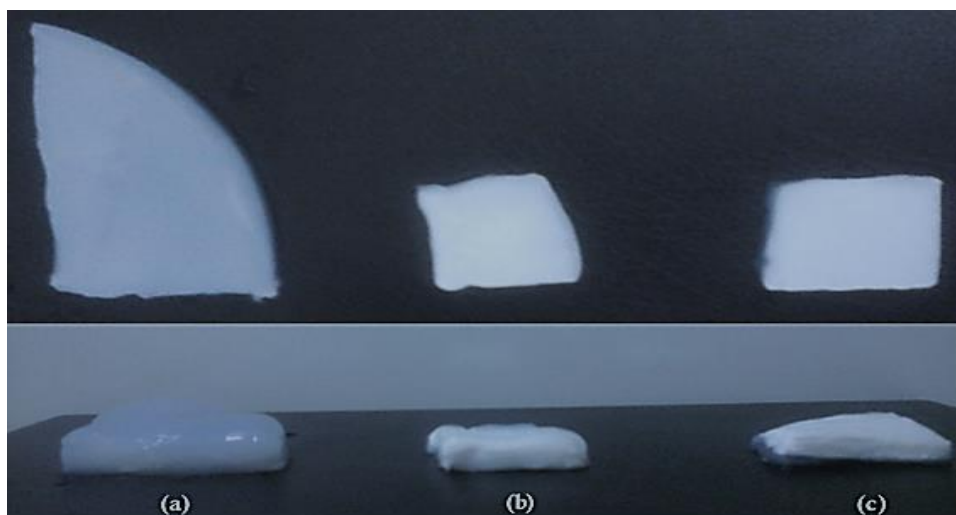


**Figure 16.** Visual images of (a) BC, (b) BC/PGMA and (c) BC/PGMA/MBA nanocomposites.

### 3.2. Optimization of the *in situ* free radical polymerization

The effects of the reaction time and temperature, and monomer, initiator and crosslinker amount on the incorporation yield of the methacrylate polymer were studied in order to establish the optimal conditions for the *in situ* free radical polymerization of GMA and GMA/MBA inside of the BC network. The goal of this study was to obtain the maximum incorporation of polymer and crosslinker inside BC tridimensional network.

The PGMA and PGMA/MBA incorporation percentage was calculated through Equation 1. Figure 17 shows the results achieved for the different conditions tested. The *in situ* free radical polymerizations were carried out for different reaction times, namely 60, 180 and 360 min. As shown in Figure 17 (A), the highest polymer incorporation was attained for 6 hours of reaction for BC/PGMA and BC/PGMA/MBA nanocomposites with 60.8% and 67.3% of polymer incorporation in BC network, respectively. The effect of temperature on polymerization was evaluated at 50, 60 and 70 °C and it was concluded that 60 °C is the optimum temperature in the range considered [Figure 17 (B)]. The diffusion of monomer, initiator and crosslinking from the solution to the BC membrane influences the extension of

the polymerization reaction (56). Thus, it's probable that the number of free radicals increase with the temperature increase (56). Figures 17 (C), (D) and (E) show the effects of the amount of initiator, BC/PGMA and BC/PGMA/MBA ratio, respectively. The best concentration of initiator, BC/PGMA and BC/PGMA/MBA molar ratio (considering the amount of polymer and crosslinker incorporated) tested were 0.5%, (1:2) and (1:2:0.2), respectively. The initiator concentration is referred by other authors as a crucial factor for a successful of polymerization due to the formation of free radicals in solution (73). A lower incorporation percentage at lower concentration of initiator may be related with the deficit of the free radicals and at higher concentration due to the self-combination of the free radicals, causing a failure of chain initiator or enhanced rate of termination which balances the rate of propagation (56).

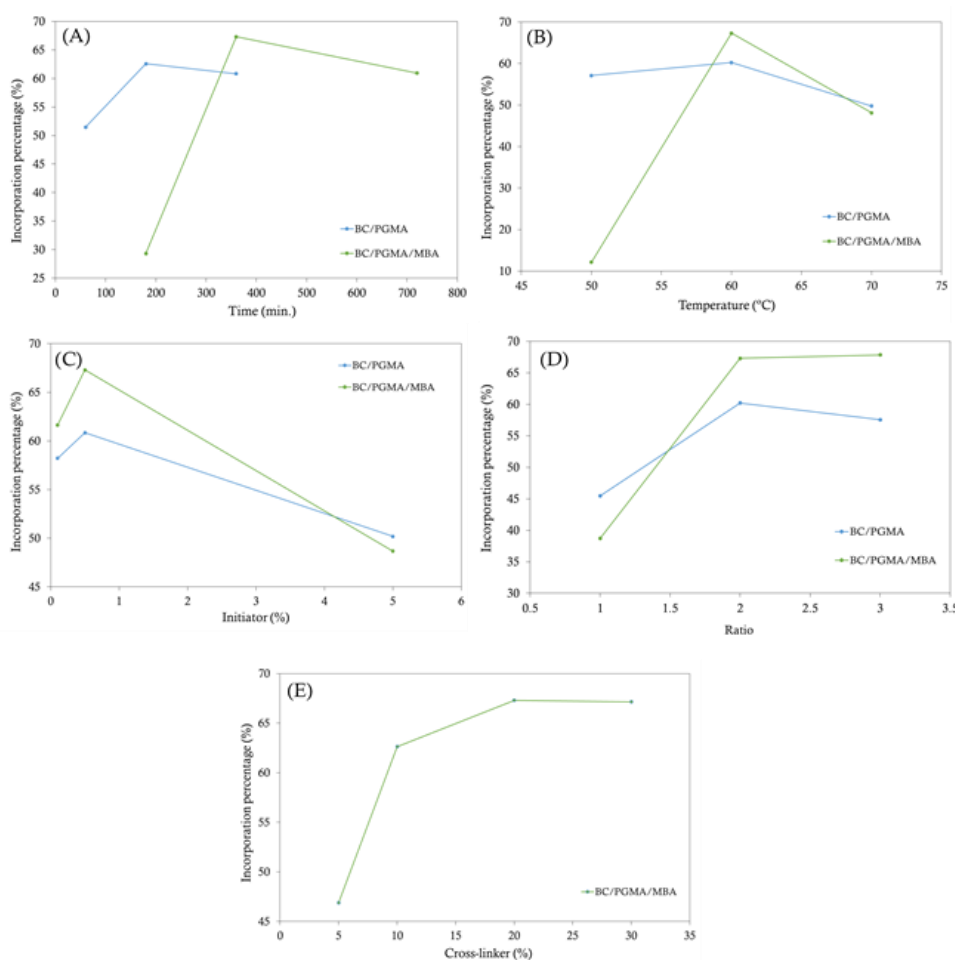


**Figure 17.** Effect of reaction time (A), temperature (B), initiator (C), monomer (D) and crosslinker (E) amount in BC *in situ* free radical polymerization.

### 3.3. BC nanocomposites characterization

Of all ratios of BC/PGMA and BC/PGMA/MBA nanocomposites obtained, the ratio of (1:2) and (1:2:0.2) were chosen to be characterized as they were where the maximum ratio polymerization was achieved.

#### 3.3.1. Infrared and X-ray Spectroscopy

ATR-FTIR analysis was performed in order to confirm the occurrence of the polymerization inside of the BC tridimensional network. Figure 18 shows the ATR-FTIR spectra of BC, BC/PGMA and BC/PGMA/MBA nanocomposites.

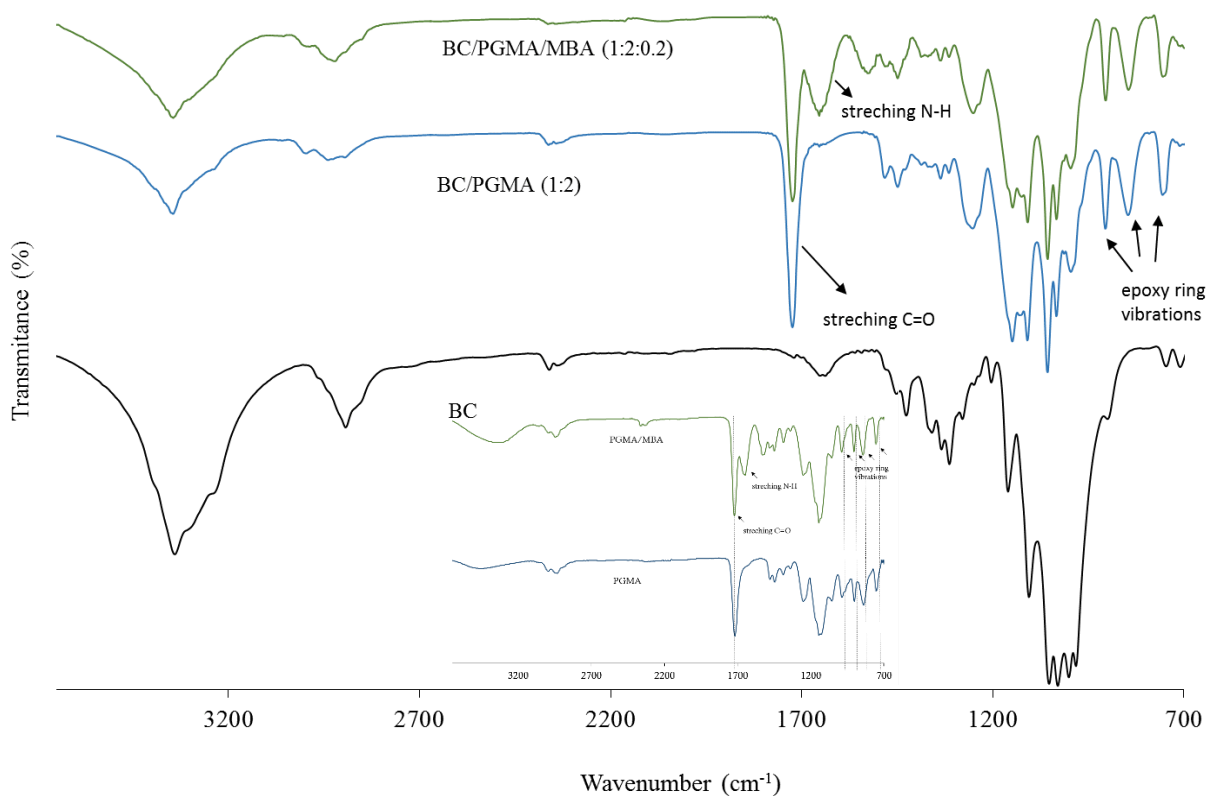


**Figure 18.** ATR-FTIR of native BC, BC/PGMA and BC/PGMA/MBA nanocomposites.

The BC characteristic peaks are visible in all BC nanocomposites spectra at 3338, 2896, 1448, 1148, 1108 and 1060-1028  $\text{cm}^{-1}$  corresponding to the free stretching vibration of the (O–H) group, stretching vibration (C–H), in plan bending (O–H), stretching (C–O–C), deformation (C–H), stretching (C–C) ring of cellulose and stretching (C–O), respectively (43). The two peaks at 3296  $\text{cm}^{-1}$  and 710  $\text{cm}^{-1}$  correspond to the monoclinic  $I_{\alpha}$  allomorph and the peaks at 3240  $\text{cm}^{-1}$  and 750  $\text{cm}^{-1}$  were attributed to the triclinic  $I_{\beta}$  form of BC (38). The appearance of peaks at 1724, 844 and 754  $\text{cm}^{-1}$ , attributed to the vibrations of ester carbonyl group (C=O) and epoxy group of the PGMA chains, respectively, confirms the incorporation of PGMA in the BC network.

The absence of peak at 1660  $\text{cm}^{-1}$  [stretching of methacrylate group (C=C)] indicates that the *in situ* free radical polymerization occurred with success. The presence of the epoxy groups of PGMA confirms the *in situ* polymerization of PGMA into BC only via C=C. The addition of crosslinker, MBA, is visible by the peaks at 1650, 1450 and 1390  $\text{cm}^{-1}$  that correspond to (N–H) and (C–N) acrylamide units. Thus, the characteristic peaks of polymer and crosslinker observed in the BC nanocomposites spectra evidences their incorporation into BC network.

The elemental composition of the BC/PGMA and BC/PGMA/MBA nanocomposites was determined by EDX analysis (Table 1). The major elements in all samples were carbon (C) and oxygen (O). Based on the molecular formula, GMA and BC have a C/O ratio of 1.79 and 0.75, respectively, and MBA has a C/O ratio of 3.02. It's expected that the C amount in BC/PGMA nanocomposite increase due to the PGMA incorporation. According to the obtained results, an increase for C/O ratio was observed in the BC/PGMA nanocomposite. By the other hand, was observed an increase of N amount in BC/PGMA/MBA nanocomposites with a C/N ratio of 6.45. These data evidence the success incorporation of PGMA and MBA into the BC network and are in agreement with ATR-FTIR.

**Table 1.** EDX analysis of elemental composition of BC, BC/PGMA and BC/PGMA/MBA nanocomposites (wt %).

Samples	C	N	O	C/O Ratio
BC	75.37	1.58*	23.05	3.30
BC/PGMA (1:2)	80.70	1.40*	17.90	4.50
BC/PGMA/MBA (1:2:0.2)	72.37	11.22	16.41	4.41

\*impurities due to culture medium.

### 3.3.2. X-ray diffraction

Figure 19 presents the XRD profiles of BC, BC/PGMA and BC/PGMA/MBA nanocomposites. Three peaks characteristic of BC were assigned in the diffraction angle of  $15.4^\circ$ ,  $17.1^\circ$  and  $22.9^\circ$  corresponding to (1 $\bar{1}$ 0), (110) and (200) crystallographic planes for BC/PGMA and BC/PGMA/MBA. The decrease in the intensity indicates a decrease in the crystallinity of BC with the introduction of PGMA and MBA. The peak were deconvoluted in order to determine the crystalline dimensions and crystallinity index,  $I_c$ , showed in Table 2. As expected, the incorporation of the polymers into the BC network change the BC chain organization and leads to a decrease in the crystallinity index and a decrease in the crystallite size.

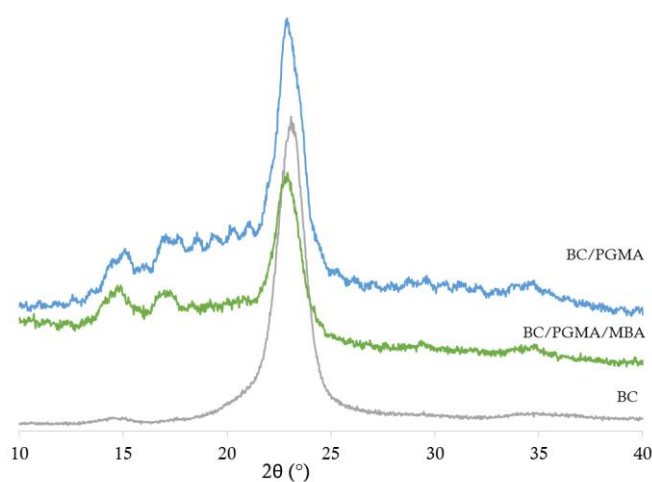


**Figure 19.** XRD patterns of BC, BC/PGMA and BC/PGMA/MBA nanocomposites.

**Table 2.** Crystallinity index,  $I_c$ , and crystallite size, ACS, of BC/PGMA and BC/PGMA/MBA nanocomposite.

Sample	ACS (nm)			$I_c$ (%)
	(110)	(110)	(200)	
BC/PGMA	0.692	2.29	1.98	68.96
BC/PGMA/MBA	0.899	0.907	0.927	56.51

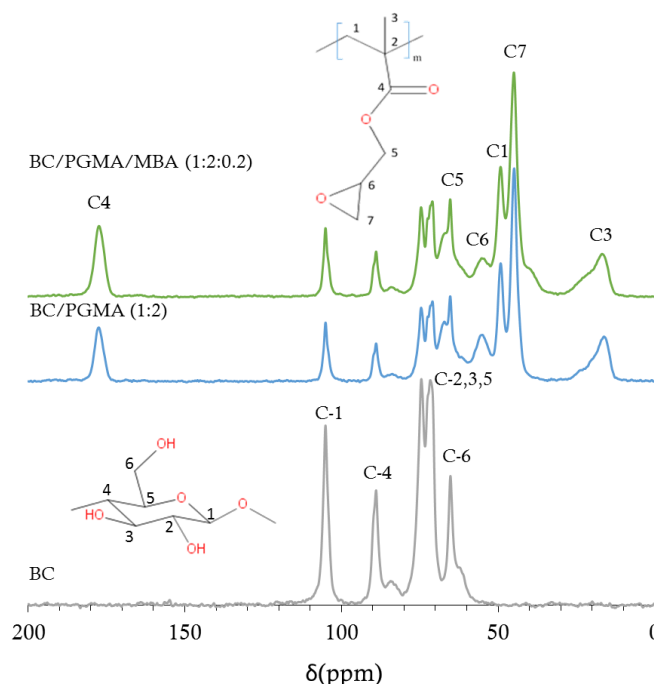
### 3.3.3. $^{13}\text{C}$ Carbon Nuclear Magnetic Resonance

Figure 20 shows the solid-state  $^{13}\text{C}$  NMR spectra of native BC, BC/PGMA and BC/PGMA/MBA nanocomposites films.  $^{13}\text{C}$  NMR spectra of BC display the characteristic resonances of cellulose at  $\delta$  65.2 (C-6), 71.4–74.3 (C-2,3,5), 90.0 (C-4) and 104.8 ppm (C-1).

The resonance at 15.74 ppm correspond to the  $\alpha$ -methyl group and at 48.99 ppm to the backbone methylene carbons atoms. The presence of these signals confirms the success of polymerization inside BC. The methylenoxy group, methyne and methylene carbons of the epoxy group exhibited signal at 65.49, 54.45 and 44.73 ppm, respectively. The resonance signal at 176.99 ppm is attributed to the carbonyl ester carbons of PGMA. Similar results are reported in the literature for PGMA (74-76).

The  $^{13}\text{C}$  NMR spectra of BC/PGMA nanocomposites evidence that the resonance signals correspond of the sum of the starting components (BC and GMA). In BC/PGMA/MBA, the absence of crosslinker resonance signal at 163.88 ppm (amide carbonyl carbons) may be due to the lower content used in mixture reaction.

Furthermore, the absence of  $^{13}\text{C}$  reasonable signals typical of the monomer (GMA) at 127.75 ppm attributed to (C=C), confirming the success of the *in situ* polymerization of GMA into the BC network previously indicated by ATR-FTIR spectra.



**Figure 20.**  $^{13}\text{C}$  NMR spectra of native BC, BC/PGMA and BC/PGMA/MBA nanocomposites.

### 3.3.4. Scanning electron microscopy

SEM analysis was carried out to study the effect of the incorporation of PGMA in the morphology of BC. Figure 21 shows the SEM images of the surface and cross-section views of BC nanocomposites. The surface morphology of BC/PGMA and BC/PGMA/MBA is different when compared with that of native BC which confirms the change in the structural BC network. The incorporation of the PGMA makes the BC network more compact and smoother, although it's still visible the entangled microfibrils characteristic of BC. BC/PGMA/MBA surface exhibited a soft appearance with small spaces between particles in a wide range of sizes (from sub- $\mu\text{m}$  to several  $\mu\text{m}$  wide) and a microporous structure.

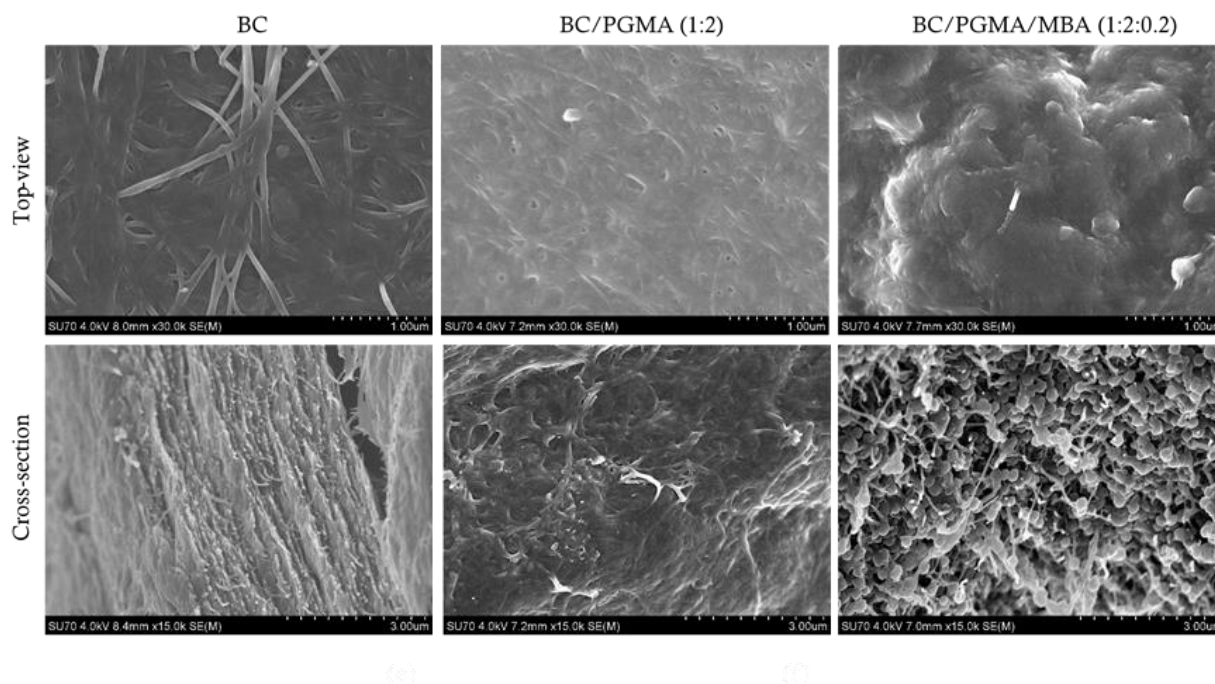


Figure 21. SEM images of BC/PGMA and BC/PGMA/MBA nanocomposites.

### 3.3.5. Swelling ratio

In order to evaluate the rehydration ability of the BC nanocomposites, swelling studies were performed immersing the films in water during 48 h at room temperature. Figure 22 shows the swelling ratios of native BC and nanocomposites. The BC/PGMA and BC/PGMA/MBA nanocomposites display a lower rehydration ability (32.8% and 31.3%, respectively) when compared with native BC (137.7%) after 48 h of immersion. In these study, the addition of a crosslinker promotes crosslinked points in PGMA chains and, consequently, an increase in the number of crosslinking polymer network which results in a decrease of swelling ratio due to the epoxy groups amounts of PGMA into the BC (77). The hydrophobic behavior and interactions of BC/PGMA nanocomposites may promote a more rigid network (78) which are supported and in agreement with SEM analyses and macroscopic observation.

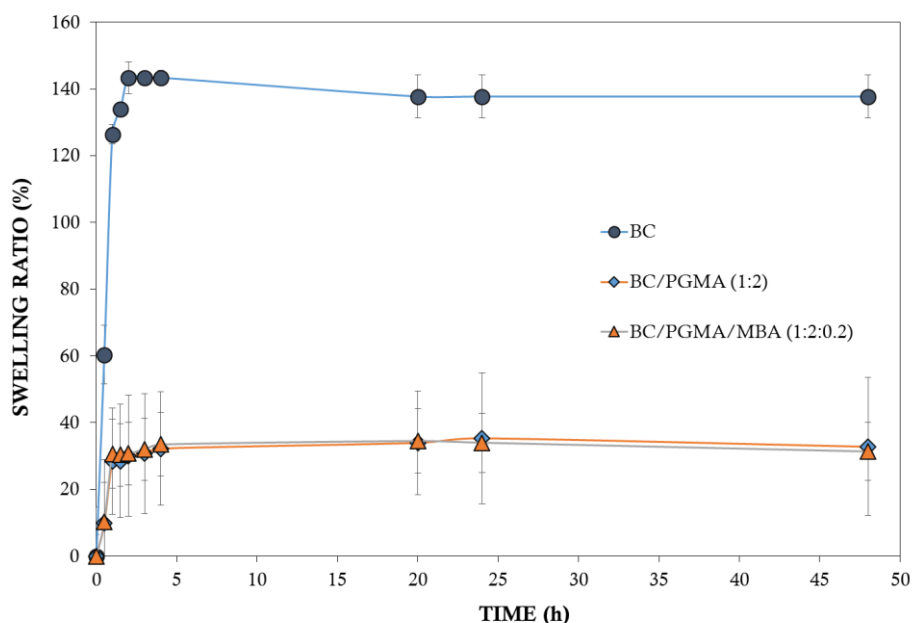
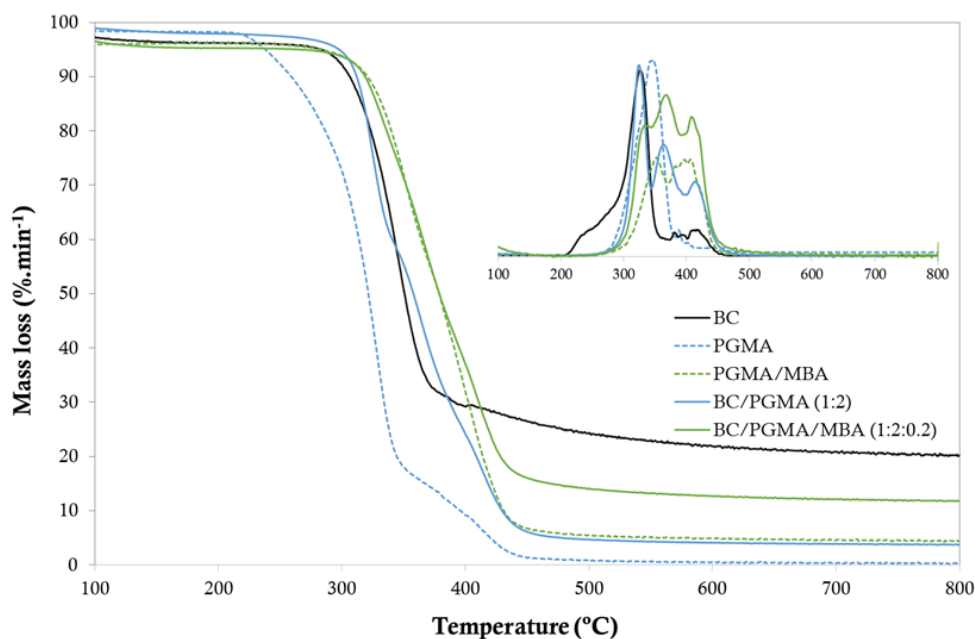


Figure 22. Swelling ratio in function of time of BC, BC/PGMA and BC/PGMA/MBA nanocomposites.

### 3.3.6. Thermogravimetric analyses

Thermogravimetric analyses were carried out with the aim to evaluate the thermal stability and degradation profile of BC/PGMA and BC/PGMA/MBA nanocomposite films. This knowledge is important in numerous applications where materials might be submitted to high temperatures and applied to any material that exhibits a weight change upon heating (79). Beyond the nanocomposites, the native BC and PGMA with and without crosslinker controls were also analyzed for comparison. Figure 23 shows the TGA and DTGA obtained for each samples (controls and nanocomposites) and Table 3 presents their maximum degradation temperatures ( $T_d$ ).

Native BC membranes exhibit one main degradation step at about 347 °C which is typical of cellulose (40, 79). The minor mass loss at around 100 °C is attributed to water evaporation.



**Figure 23.** TGA and DTGA profile of BC/PGMA and BC/PGMA/MBA nanocomposites and their controls.

PGMA display a degradation profile with three main degradation steps at around 326, 388, 414 °C and start their decomposition at 210 °C. The first steps of degradation of PGMA probably may be due to the: (i) depolymerization reaction and (ii) decomposition of esters (72). The minor mass loss at around 414 °C can be attributed to decomposition of units involving side group scission of PGMA (71). The addition of crosslinker turn the polymer more thermally stable and provokes a displacement of the degradation profile evidencing a start decomposition at around 278 °C and possessing a degradation profile at around 352, 398 and 408 °C (Figure 23).

The TGA shows that incorporation of PGMA into the BC network influence the thermal stability and degradation profile. The incorporation of PGMA and PGMA/MBA into the BC increase their stability starting their decomposition, at around 275 °C.

The increase of the  $Td_i$  in nanocomposites suggest a strong interaction and compatibility between the PGMA and cellulose nanofibrils probably due to the establishment of hydrogens bonds between BC nanofibrils and PGMA chains (40).

**Table 3.** Thermal degradation,  $T_d$  (°C), of BC/PGMA, BC/PGMA/MBA nanocomposites and their controls in study.

Samples	$Td_i$	$Tdmax_1$	$Tdmax_2$	$Tdmax_3$
BC	266	347	---	---
PGMA (1:0)	210	326	388	414
PGMA/MBA (1:0.2)	278	352	398	408
BC/PGMA (1:2)	273	321	363	413
BC/PGMA/MBA (1:2:0.2)	277	336	367	407

### 3.3.7. Dynamic Mechanical properties

The viscoelastic properties of BC/PGMA and BC/PGMA/MBA nanocomposites were evaluated through dynamic mechanical analysis. Figure 24 shows the variation of the storage modulus and  $\tan \delta$  of BC/PGMA and BC/PGMA/MBA nanocomposites.

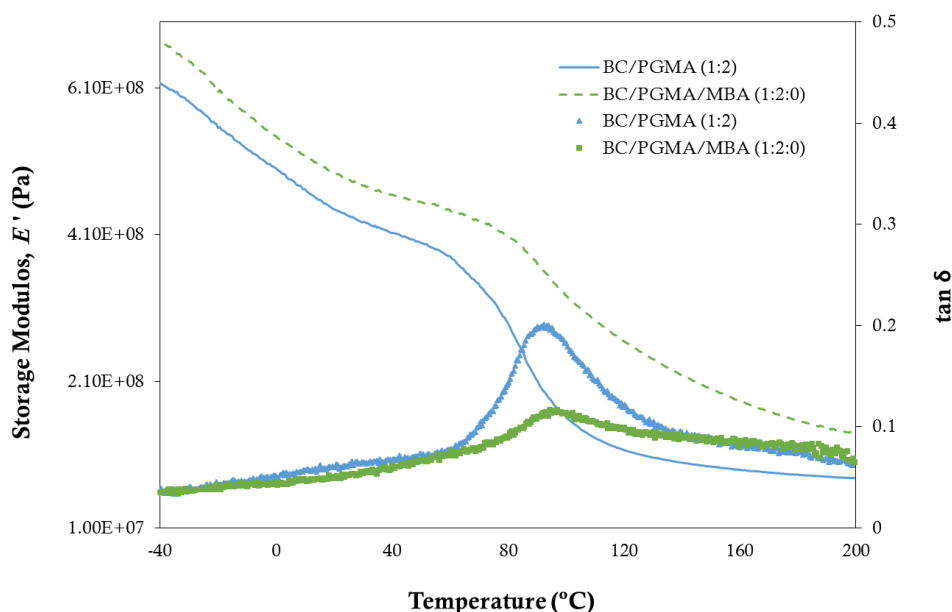


**Figure 24.** Storage modulus e  $\tan \delta$  versus temperature of BC and BC/PGMA nanocomposites.

The storage modulus trace of the nanocomposites,  $E'$ , shows only one transition. The results obtained showed that the incorporation of PGMA provokes a decrease of storage

modulus when compared with native BC (40). This is due to the fact that PGMA is an amorphous polymer, which decreases the crystallinity of the nanocomposites. The addition of cross-linker leads to an increase of 11% in  $E'$  and of 7 % in  $\tan \delta$  indicating that the cross-linker make the nanocomposites with a tighter and higher stiffness BC network. The  $T_g$  obtained from the  $\tan \delta$  peak also increase with the crosslinker addition from 90.2 to 96.5 °C.

## 4. Conclusions

Bacterial cellulose/poly(glycidylmethacrylate) nanocomposites (BC/PGMA) were obtained through *in situ* polymerization of glycidylmethacrylate using *N,N'*-methylenebisacrilamide, MBA, as crosslinker and ammonium persulphate as initiator. The maximum monomer incorporation into the bacterial cellulose occurs at (1:2) for BC/PGMA and at (1:2:0.2) ratio for BC/PGMA/MBA, with 0.5 % of initiator, at 60 °C during 6 h. The incorporation of the PGMA makes the BC network more compact and smooth and allows an improvement in their thermal and mechanical properties. It's also observed that the addition of a crosslinker allows a better retention of the polymer into BC network which makes the new nanocomposite to exhibit a roughness and more compact three-dimensional structure. Moreover, an improvement in thermal and mechanical properties was observed. Both BC nanocomposites display a decrease in their water retention ability and in the crystallinity degree. The new BC nanocomposites exhibited properties that can be applied for absorbent materials for the removal of heavy metals and/or proteins due to the fact they possess epoxy groups in their structure which could react with other molecules.



## CHAPTER III

*Epoxide ring-opening of bacterial  
cellulose / poly(glycidylmethacrylate) nanocomposites*



## CHAPTER III. Epoxide ring-opening of bacterial cellulose/poly(glycidylmethacrylate) nanocomposites

### Abstract

New nanocomposites were prepared by epoxide ring-opening reaction mechanism of bacterial cellulose/poly(glycidylmethacrylate) without (BC/PGMA) and with crosslinker, *N,N'*-methylenebisacrilamide (BC/PGMA/MBA). To make it, the BC/PGMA and BC/PGMA/MBA nanocomposites were subject to chemical treatment to promote epoxide ring-opening reactions. A replacement of the epoxy groups for hydroxyls groups occurred in an aqueous solutions at pH 3.5. After chemical treatment, the methacrylate nanocomposites, BCPGMA-CT and BCPGMAMBA-CT, present a more compact and smoother structure. It was also observed a decrease in thermal properties, mechanical properties, and crystallinity, but an increase in their water retention ability. The surface became with less basic character and occurred an increase in surface area. The reported methodology give rise to new and interesting methacrylate nanocomposites.

**Keywords:** bacterial cellulose, glycidylmethacrylate, nanocomposites, chemical treatment, epoxy-ring opening.

## 1. Introduction

Recently, bacterial cellulose (BC) has gained considerable attention as a source for the development of new materials including nanocomposites due to its excellent properties such as high purity, high degree of crystallinity (80-90%), high water retention capacity (99%), ultrafine fibrous network and high tensile strength (17, 22). Combining the excellent properties of BC with those of methacrylate monomers, such as high reactivity and availability, bacterial cellulose/methacrylate nanocomposites have been prepared and evaluated for different biomedical applications such as wound dressing (43).

Glycidylmethacrylate (GMA), among other methacrylate monomers, have received particular attention because of the presence of two polymerizable groups: the epoxide and the methacrylate groups. As polymer, it offers a wide range of industrial applications in polymer chemistry and technology such as for purification of lysozyme from chicken white egg (49, 50, 54), removal of heavy metals and chromate anions from aqueous solutions (48, 55-58), in coatings, matrix resins and adhesives (47, 59). Furthermore, GMA show a relatively low toxicity, polarity, hydrophobicity and low price comparatively to other methacrylate monomers which make them an attractive monomer for the polymer synthesis (47, 50-53).

PGMA has been reported as grafted to different materials such as cellulose (49, 50) via C=C, functionalizing the epoxy group, through epoxy ring-opening, with other molecules as adsorbent material.

BC/PGMA nanocomposites, synthesized through *in situ* free radical polymerization using *N,N'*-methylenebisacrilamide, MBA, exhibited a great retention of the polymer inside the BC network. Without crosslinker, these nanocomposites display a smoother and compact network and with crosslinker, a rough, compact, dense and crosslinked network. Both BC nanocomposites display an improvement in their thermal and mechanical properties and, a decrease in the swelling ratio and crystallinity.

In the present study, a simple methodology was developed using the chemical treatment that occurs in an aqueous solution at pH 3.5, to epoxide ring-opening of PGMA

inside BC network of BC/PGMA and BC/PGMA/MBA nanocomposites as a way to obtain a microporous and crosslinked nanocomposite.

The obtained materials were characterized in terms of their structural and chemical composition, crystallinity, morphology, thermal stability, water absorption, mechanical properties and surface properties.

## 2. Methodology

### 2.1. BC nanocomposites preparation

Wet bacterial cellulose (BC) membranes produced by *Gluconacetobacter sacchari* (70) using standard conditions were used. The BC/PGMA/MBA nanocomposites were obtained through the methodology described in “Section 2.2. of Chapter II: *New Bacterial cellulose/poly(glycidylmethacrylate) nanocomposites films by in situ radical polymerization*” of present monography.

### 2.2. Chemical modification of BC nanocomposites

The chemical modification of BC/PGMA and BC/PGMA/MBA nanocomposites was based in procedure described by Reis *et al* (2009) (80). Wet BC/PGMA and BC/PGMA/MBA nanocomposites membranes were drained in order to remove the excess of water and immersed in 2 mmol % HCl aqueous solution. Then, the reaction mixture was placed at 140 °C during 4 hours and under constant stirring (100 rpm). After this period, the membranes were washed in distilled water until neutral pH, dried at 40 °C and kept in a desiccator until characterization.

Along this paper, the terminology of samples are described below: BC/PGMA–bacterial cellulose membrane with poly(glycidylmethacrylate); BC/PGMA/MBA – bacterial cellulose membrane poly(glycidylmethacrylate) crosslinking *N,N'*-methylenebisacrilamide; BCPGMA-CT – chemical treatment of bacterial cellulose membrane with

glycidylmethacrylate and BCPGMAMBA-CT – chemical treatment of bacterial cellulose membrane with glycidylmethacrylate crosslinking *N,N'*-methylenebisacrilamide.

### 2.3. BC nanocomposites characterization

The obtained BC/PGMA nanocomposite were characterized in terms of chemical composition, morphology, thermal stability, water absorption, mechanic and surface properties by ATR-FTIR, EDX, CPMAS <sup>13</sup>C NMR, FE-SEM, XRD, TGA, SW, DMA and IGC, respectively. The methodology applied for each methods is described in “Section 2.3. of Chapter II: *New Bacterial cellulose/poly(glycidylmethacrylate) nanocomposites films by in situ radical polymerization*” of present manuscript, expect the IGC analysis which is described below.

#### Inverse Gas Chromatography measurements

The BC nanocomposites were packed in the standard glass silanized (dymethyldichlorosilane; Repelcote BDH, UK) columns with 0.2 cm ID and 30 cm in length by vertical tapping about 2 hours. The columns with the samples were conditioned 8 h at 40 °C. After conditioning, pulse injections were carried out with a 0.25 mL gas loop. Four *n*-alkanes (heptane, octane, nonane and decane) were used for measurements of the dispersive component of the surface energy at 20, 25 and 30 °C. Four polar probes (tetrahydrofuran, dichloromethane, acetonitrile and ethyl acetate) were used to determine the specific component of surface energy and acid-base character ( $K_A$  and  $K_B$ ) at 25 °C. The isotherm experiments were undertaken with *n*-octane, tetrahydrofuran and dichloromethane at 25 °C for all samples tested. All experiments were carried out at 0% relative humidity with a helium flow rate of 10 ml/min and at least in duplicate, producing an error less than 4%.

IGC measurements were carried out on a commercial inverse gas chromatograph (*iGC*, Surface Measurements Systems, London, UK) equipped with flame ionization (FID) and thermal conductivity (TCD) detectors. The *iGC* system is fully automatic with SMS *iGC* Controller v1.8 control software. Data were analysed using *iGC* Standard v1.3 and

Advanced Analysis Software v1.25. The calculation methodology is described exhaustively in Chapter V of the present manuscript.

### 3. Results and Discussion

BC/PGMA and BC/PGMA/MBA nanocomposites were subject to a chemical treatment in order to promote the reaction of epoxy groups of the PGMA with hydroxyl group of cellulose chain through epoxide ring-opening. The effect of attachment of PGMA in structure, morphology, swelling, thermal, mechanical and surface properties was evaluated through ATR-FTIR,  $^{13}\text{C}$  NMR, XRD, EDX, FE-SEM, SW, TGA, DMA and IGC techniques.

A probably scheme illustrating the epoxide ring-opening mechanism of BC/PGMA/MBA nanocomposites is shown in Figure 25.

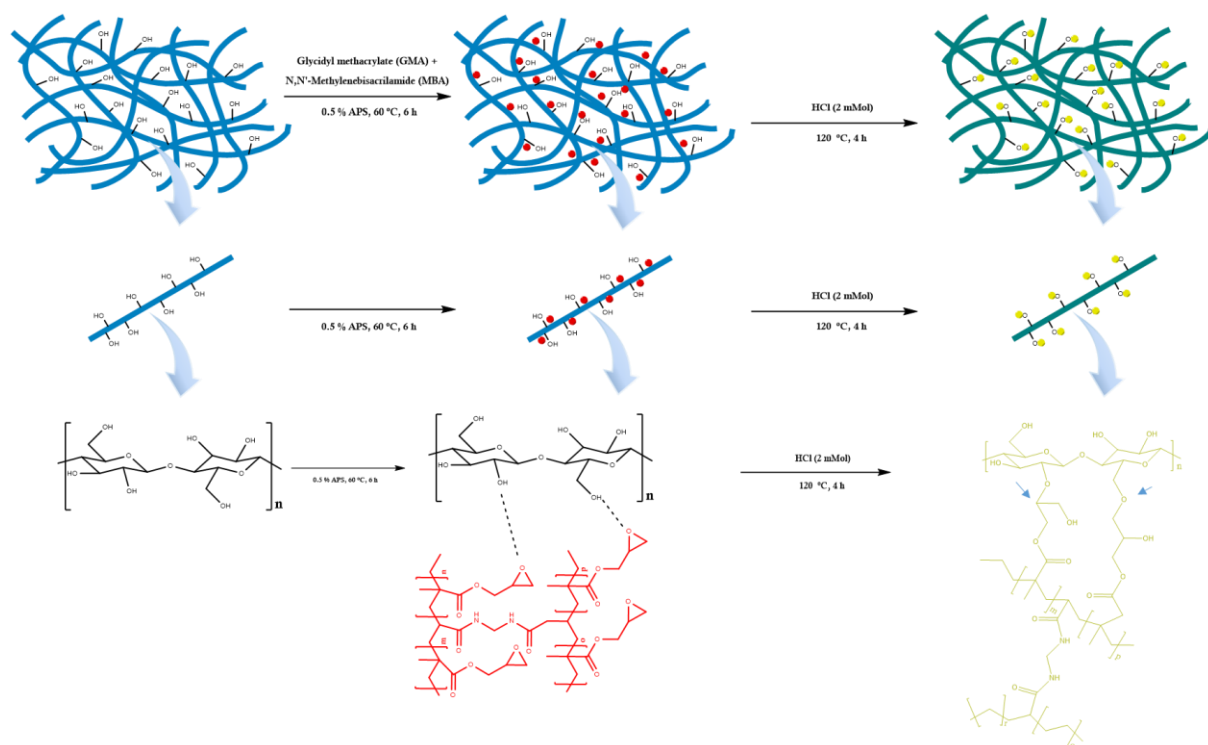


**Figure 25.** Schematic diagram of the epoxide ring-opening mechanism of BC/PGMA nanocomposites.

### 3.1. Structural Analysis

After incorporation of PGMA with and without crosslinker into the bacterial cellulose network, the chemical modifications occurred in aqueous solutions at pH 3.5 through epoxide ring-opening mechanism. Reis *et al* (2009) reported a similar mechanism to explain the chemical modifications of other macromolecules, poly(vinyl alcohol) (PVA) and poly(acrylic acid) (PAAc) with PGMA.

$^{13}\text{C}$  NMR spectra of BCPGMA-CT and BCPGMAMBA-CT nanocomposite films was carried out and shown in Figure 26. The nanocomposites display characteristics resonance signals of BC/PGMA nanocomposites with exception at 65.12 and 70.59 ppm which is assigned to the carbon of ring-opening with an additional signal at 63.42 ppm for BCPGMA-CT. These results suggest that the epoxide ring-opening forms, preferentially, a hydroxyl group as reaction products. It's also observed an increase in the intensity signal at 60.1 ppm which is attributed to the  $(-\text{O}-\text{CH}_2-)$  atoms. The presence of these signals confirms the epoxide ring-opening reaction by the binding of PGMA chain to hydroxyls groups of cellulose backbone.

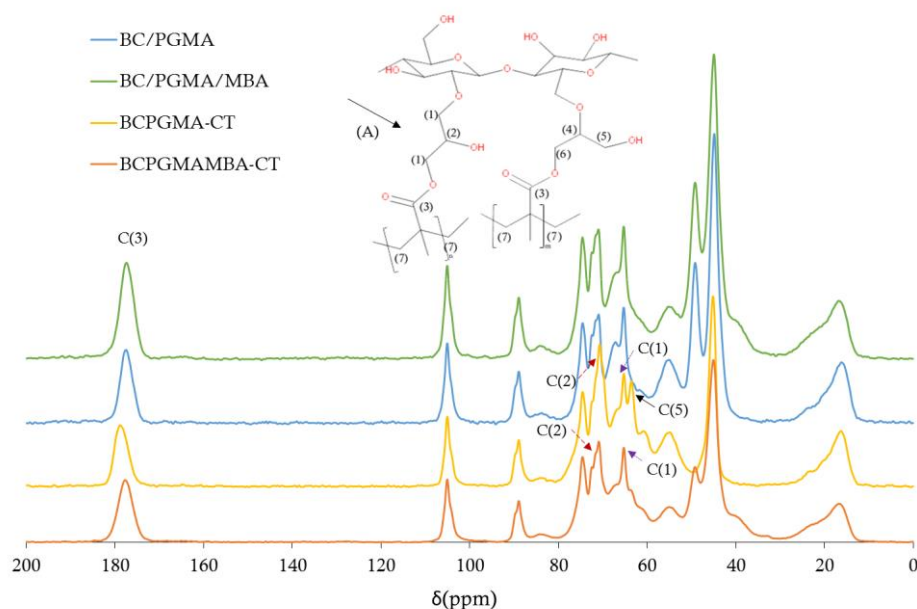


**Figure 26.**  $^{13}\text{C}$  NMR spectra of BC/PGMA and BCP/PGMA/MBA nanocomposites before and after chemical treatment

XRD analysis of the nanocomposites was carried out with the aim to know how the chemical modifications affect the degree of crystallinity of nanocomposites. The crystallinity index ( $I_c$ ) obtained for BCGMA-CT and BCPGMAMBA-CT was 38% and 43%, respectively. The XRD patterns (Figure 27) and  $I_c$  obtained for BCGMA-CT and BCPGMAMBA-CT nanocomposites show that a significant decrease in the crystallinity occurs after the chemical treatment, displaying a decrease in the intensity of peaks at  $2\theta$  (1 $\bar{1}$ 0), (110) and (200) when compared with BC/PGMA and BC/PGMA/MBA nanocomposites ( $I_c$  = 69% and 56%, respectively). This happens probably due to the attachment of PGMA chain to cellulose backbone, which decrease the structural arrangement of BC fibrils.

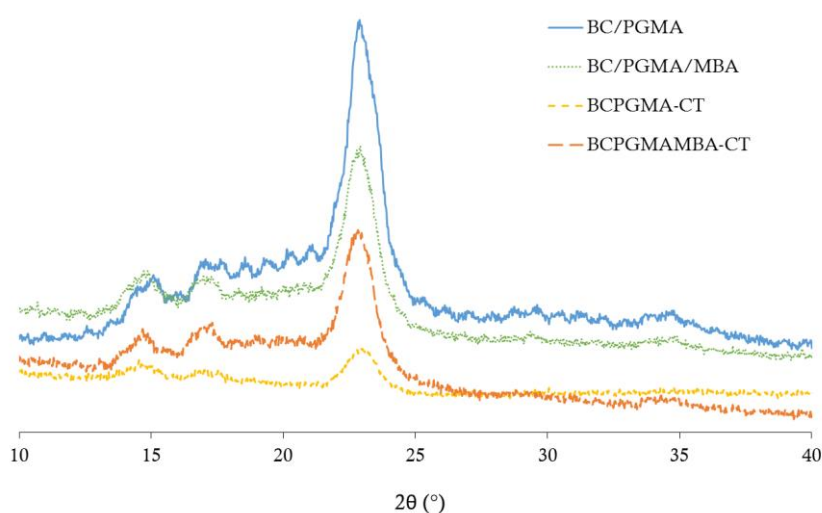


**Figure 27.** XRD patterns of BC/PGMA and BC/PGMA/MBA nanocomposites before and after chemical treatment.

### 3.2. Morphological Analyses

SEM images reveal that the surface morphology changed with the chemical treatment. The BC hydroxyls group reaction with epoxy ring of PGMA seems to make the BC network surface more homogeneous probably due to the linkage between PGMA and cellulose chain [Figure 28 (b) and (d)]. At surface, the microfibril of BC was more exposed to the surface in

both samples but more compact with chemical modification as shown in Figure 28 (a) and (c). Thus, the chemical treatment of the BC /PGMA nanocomposites change their morphology at surface and inside, turning it more compact and smooth which, consequently, affect the properties of the BC nanocomposites.

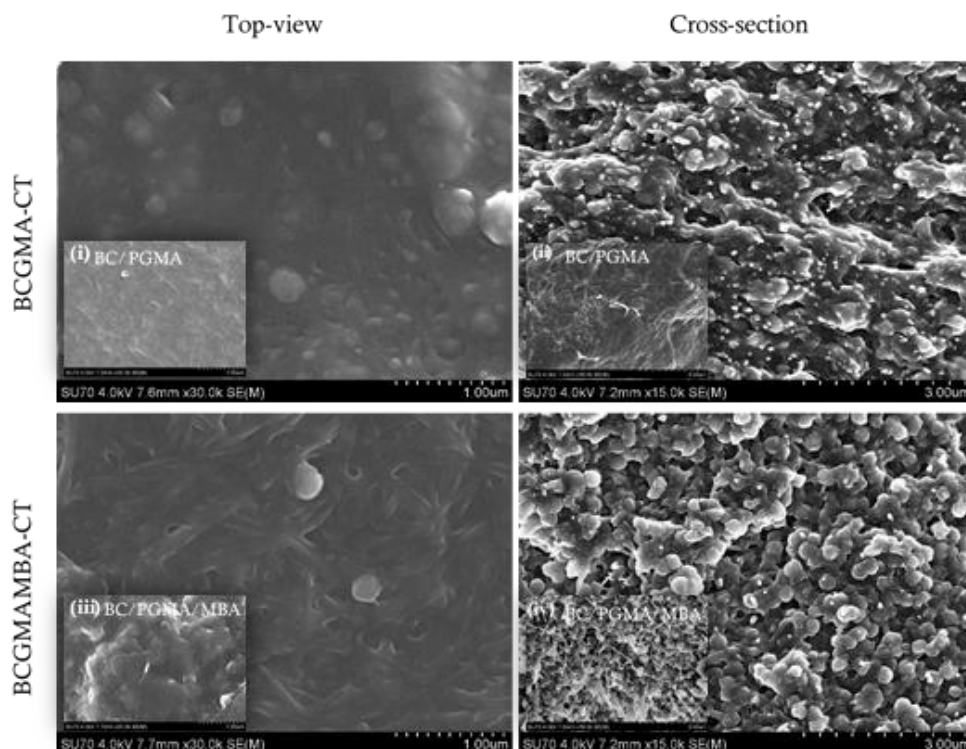


**Figure 28.** SEM images of BCGMA-CT and BCGMAMBA-CT nanocomposites morphology in different perspectives. The (i), (ii), (iii) and (iv) images correspond to the samples without chemical treatment.

### 3.3. Thermal and Mechanical Analyses

Figure 29 exhibit the TGA and DTGA achieved for nanocomposites and Table 4 show the maximum temperature of thermal degradation,  $T_d$ , obtained for each sample. The minor mass loss at around 100 °C is attributed to water evaporation of samples. BCPGMA-CT nanocomposites display a degradation profile with three main degradation steps similar to BC/PGMA nanocomposites. It's observed the maximum degradation temperature of PGMA which suggests that doesn't occur the degradation of PGMA polymer provoked by temperature or/and acid aqueous solution.

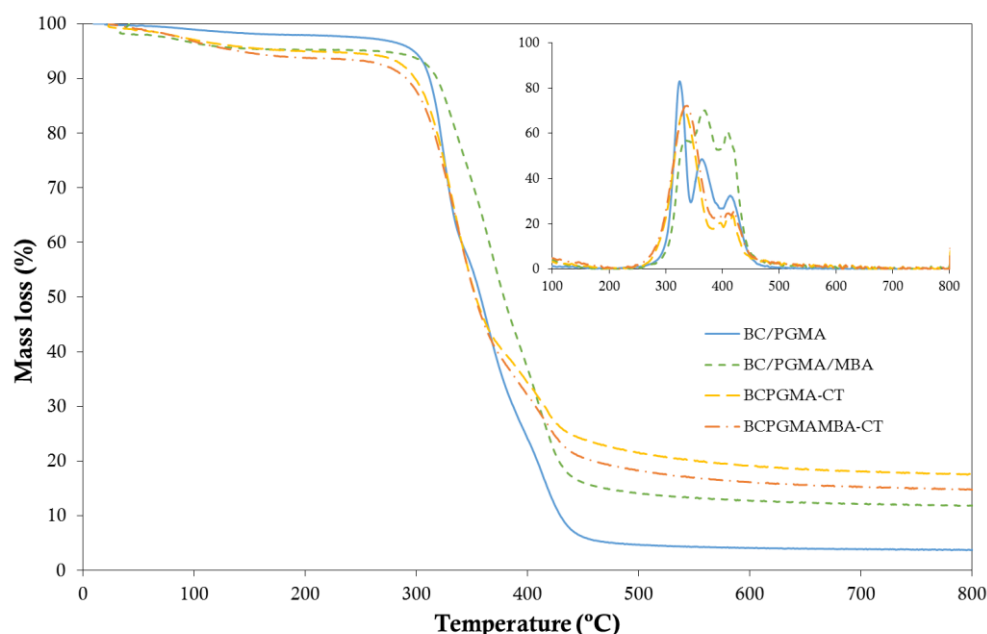


**Figure 29.** TGA and DTGA of BC/PGMA and BC/PGMA/MBA nanocomposites before and after chemical treatment

**Table 4.** Thermal degradation,  $T_d$  (°C), of BC/PGMA and BCP/PGMA/MBA nanocomposites before and after chemical treatment.

Samples	$Td_i$	$Tdmax_1$	$Tdmax_2$	$Tdmax_3$
BC/PGMA	273	321	363	413
BC/PGMA/MBA	277	336	367	407
BCPGMA-CT	250	337	394	421
BCPGMAMBA-CT	265	332	398	417

Observing the TGA results, it's evident that the epoxy ring of the BC/PGMA nanocomposite affects the thermal stability of the fibers, and is related with the chemical modification of BC network.

Dynamic mechanical analysis allows to evaluate the influence of chemical treatment on the BC network viscoelastic properties. Figure 30 shows the variation of the storage tensile modulus and  $\tan \delta$  of BCPGMA-CT and BCPGMAMBA-CT nanocomposites. It's observed that the storage modulus,  $E'$ , started early the transition coinciding in the glass transition

zone in both nanocomposites. The chemical treatment increase the storage modulus compared with BC/PGMA and BC/PGMA/MBA nanocomposites as well as the  $T_g$  obtained from the  $\tan \delta$  peak (90.2 to 146.4 °C and 96.5 to 99.2 °C, respectively) (as described in *Section 3.3.6. of Chapter II*). These results suggest that the reaction of epoxy group of PGMA chain to cellulose backbone via (–OH), increase the amorphous content (supported by XRD pattern). Moreover, these results also indicates that the nanocomposites became less rigid than initial BC/PGMA nanocomposites.

BCPGMA-CT and BCPGMAMBA-CT exhibited distinct mechanical performance which make these simple chemical treatment a good strategy to obtain nanocomposites for new applications.

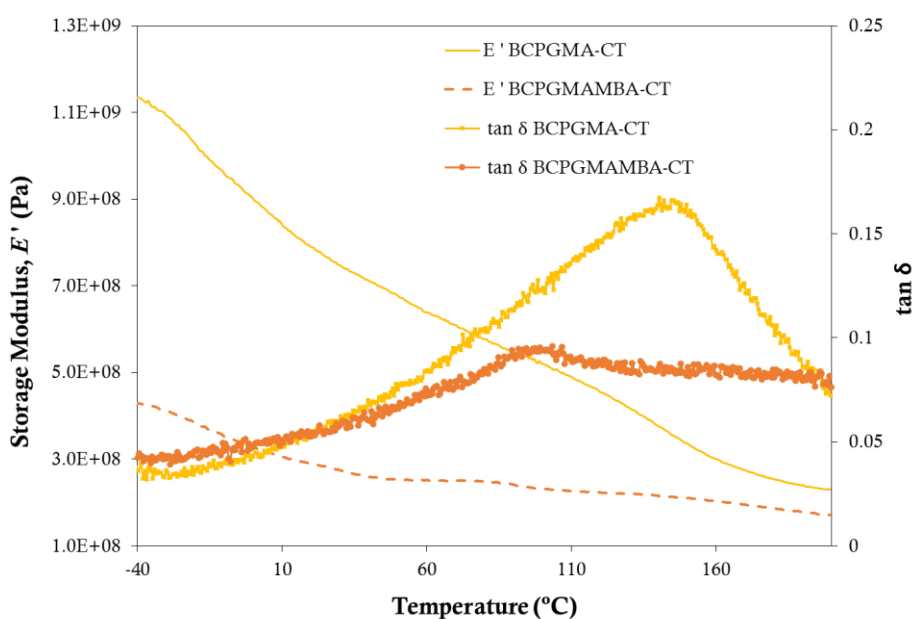


**Figura 30.** Storage modulus e  $\tan \delta$  versus temperature of BCPGMA-CT nanocomposites.

### 3.4. Surface properties

In order to study the effect of the chemical treatment in the nanocomposites surface, IGC analysis was performed. This knowledge allows the prediction of its compatibility with other materials. Parameters such as dispersive component of the surface energy,  $\gamma_s^d$ , specific

component of the surface energy,  $\Delta G_s^{sp}$ , surface area,  $S_{BET}$ , monolayer capacity,  $n_m$ , adsorption potential,  $A_{max}$ , acid character,  $K_A$  and basic character,  $K_B$ , were determined.

BCGMAMBA-CT exhibited a lower  $\gamma_s^d$  (37% less) when compared with BC/PGMA/MBA (Table 5), suggesting that the surface became less hydrophobic due to a decrease of the number or/and energy of the active sites.

**Table 5.** Surface properties of BC/PGMA/MBA and BCPGMAMBA-CT nanocomposites at 25°C.

	BC/GMA/MBA	BCGMAMBA-CT
$\gamma_s^d$ (mJ/m <sup>2</sup> )	82.93	51.91
$K_A$	0.13	0.10
$K_B$	0.56	0.23
$K_B/K_A$	4.31	2.36
$S_{BET}$ (m <sup>2</sup> /g)	0.83	3.61
$n_m$ (mmol/g)	2.18	9.52

Dispersive component of surface energy,  $\gamma_s^d$ , acid,  $K_A$ , and basic,  $K_B$ , character, surface area,  $S_{BET}$ , monolayer capacity,  $n_m$ .

The energetic profile of the surface heterogeneity is determined by the BET model (81) through the injection of different concentrations of *n*-octane probe and provides an energetic “map” of the nanomaterial surface. Figure 31 shows the heterogeneity profile for BC/PGMA/MBA and BCPGMAMBA-CT nanocomposites at 25 °C. After chemical modifications, the nanocomposite shows a higher number of actives sites but less energetics with a peak maximum at 9.71 kJ/Mol, suggesting that the chemical treatment decrease  $\gamma_s^d$  by the presence of less energetic actives sites at the surface of the nanocomposite.

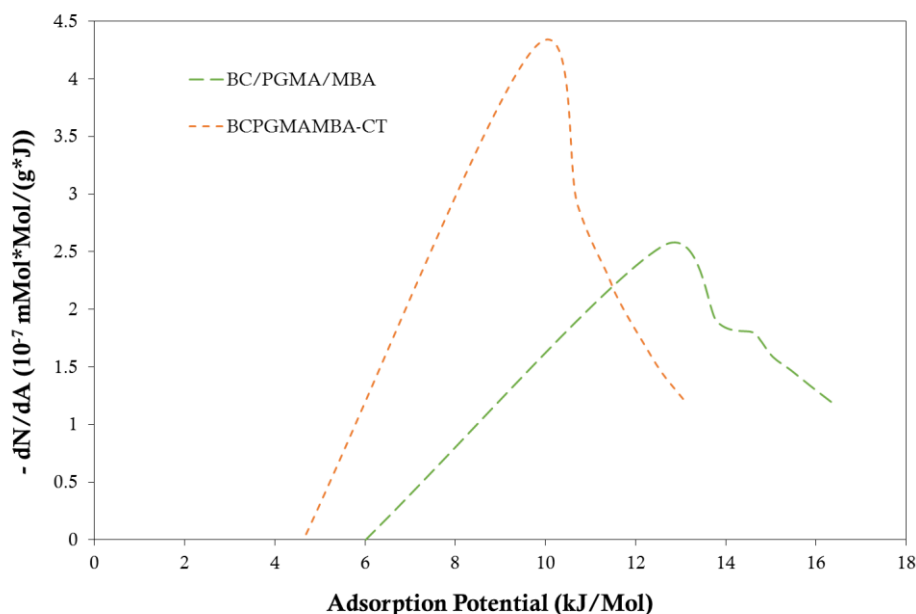


**Figure 31.** Heterogeneity profile with *n*-octane for BC/PGMA/MBA and BCPGMAMBA-CT nanocomposites at 25 °C.

The chemical treatment to the BCPGMAMBA-CT nanocomposite increase significantly the  $S_{BET}$  and the monolayer capacity as shown in Table 5. This increase may be due to the particular size decrease or the increase of surface porosity/rugosity (82). As seen in SEM images, the surface became more roughness after the chemical treatment.

The specific component of surface energy,  $\Delta G_s^{sp}$ , was determined through injection of polar probes and is present in Figure 32. The modification in the  $\Delta G_s^{sp}$ , indicates that the chemical treatment change the polar groups in the nanocomposite. The nanocomposites exhibited the maximum interaction with acetonitrile, which is an amphoteric probe, since it reacts with both acid and basic groups in the nanocomposite surfaces. The chemical treatment decrease the  $\Delta G_s^{sp}$  values for all probes which suggest that occurs a decrease in polar active sites at the surface of the nanocomposite. This decrease was more significant for the dichloromethane (acid probe: 43%) than for tetrahydrofuran (basic probe: 29%). These results indicate that the BCPGMAMBA-CT nanocomposites exhibit more acid sites in the surface due to the epoxide ring-opening which give rise to hydroxyls groups - the acid groups.

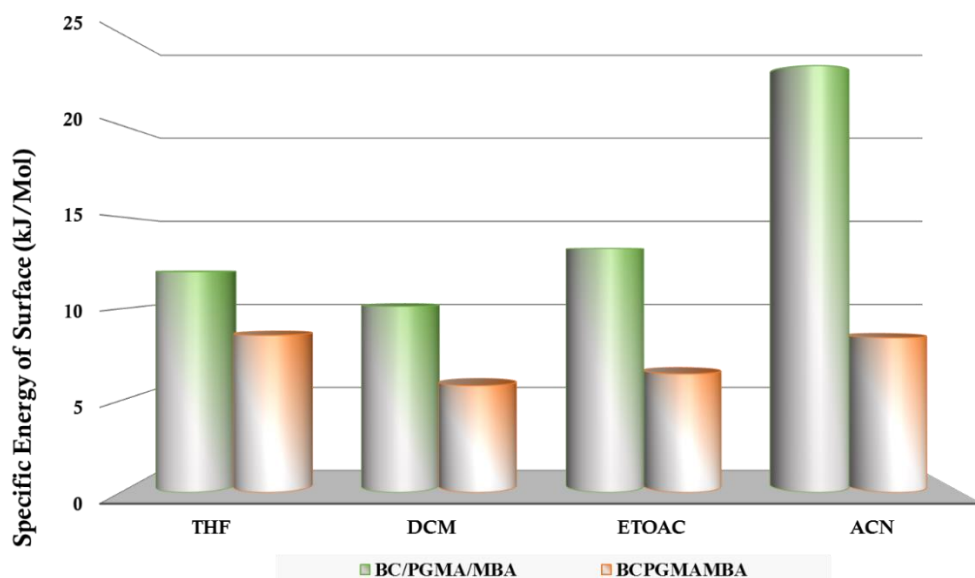


**Figure 32.** Specific surface energy with polar probes: THF - tetrahydrofuran, DCM - dichloromethane, ETOAc – ethyl acetate, ACN – acetonitrile of BC/PGMA/MBA and BCPGMAMBA-CT nanocomposites at 25 °C.

The  $\Delta G_s^{sp}$  is converted into acid-base number using the Guttmann's concept (83), and the results (Table 5) show that the chemical treatment decrease the base constant,  $K_B$ , with a  $K_B/K_A$  ratio 55% lower than BC/PGMA/MBA. Thus, the increase in the character exhibited in BC nanocomposites derives from the epoxide ring-opening, which decrease the basic groups (epoxide).

The know rehydration ability of the bacterial cellulose is attributed to the presence of hydroxyls groups. The BCGMAMBA-CT nanocomposite exhibits a swelling ratio of 227%, a considerable increase of c.a. 7 times plus when compared with BC/PGMA/MBA nanocomposite (31%). These results are in agreement with  $\gamma_s^d$  trend data discussed previously and reinforces the epoxide ring-opening process during the chemical treatment.

## 4. Conclusions

Natural polymers are able to react with many modifiers agents such as glycidylmethacrylate, a bifunctional compound, in order to obtain new composites. Epoxide ring-opening reaction was a suitable strategy to modify the bacterial cellulose/poly(glycidylmethacrylate) nanocomposites. In order to do that, the BC/PGMA and BC/PGMA/MBA nanocomposites were subjected to chemical treatment. The morphology of BCPGMA-CT and BCPGMAMBA-CT nanocomposites is more compact and smooth. A decrease in thermal and mechanical properties was observed while an increase of the amorphous content and water retention ability in the new bacterial cellulose nanocomposites was verified. The surface of BCPGMA-CT and BCPGMAMBA-CT nanocomposites present a less basic character and an increase of the surface area was observed. The reported methodology gives rise to new and interesting methacrylate nanocomposites.

## CHAPTER IV

*Novel bacterial cellulose / poly(ethyleneglycol)methacrylate  
nanocomposite films obtained by in situ free radical  
polymerization*



## CHAPTER IV. Novel bacterial cellulose/poly(ethyleneglycol) methacrylate nanocomposite films obtained by *in situ* free radical polymerization

### Abstract

New bacterial cellulose/methacrylate nanocomposite were prepared by the *in situ* free radical polymerization of poly(ethyleneglycol)methacrylate, (PEGMA), inside the BC network using ammonium persulphate, (APS), as radical initiator. Chemical composition, morphology, thermal stability, water absorption and mechanic properties were determined. The optimal conditions achieved for polymerization were a ratio of (1:20) for bacterial cellulose/monomer with 0.5% of initiator during 6 h at 60 °C. The maximum incorporation percentage achieved was 87%. With the incorporation of the polymer, films became less stiff and displayed a translucent-yellow color. The incorporation of the PPEGMA hydrophilic chains originates an improvement of the thermal and mechanical properties and also their swelling ability. A decrease in the crystallinity occurred due to the increase of the structural entropy. The new nanocomposite acquires properties able to be applied in biomedical materials.

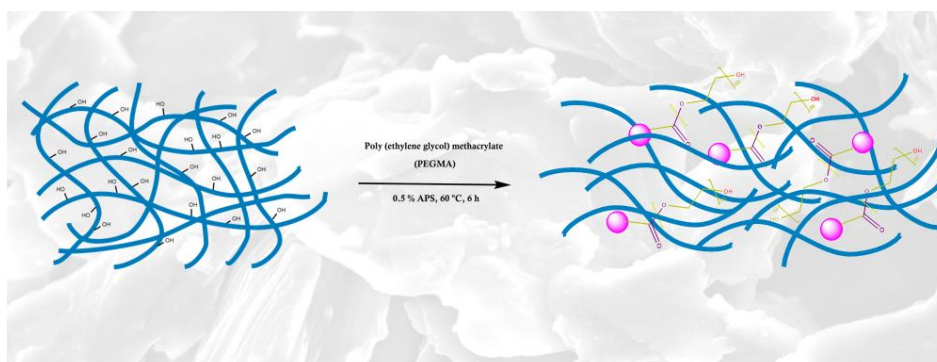


**Figure 33.** Schematic reaction of *in situ* free polymerization of PEGMA inside BC network.

**Keywords:** bacterial cellulose, PEGMA, *in situ* radical polymerization, nanocomposites

## 1. Introduction

Recently, several studies have been reported using bacterial cellulose as a starting component to obtain bacterial cellulose based nanocomposites. Bacterial cellulose produced by *Gluconacetobacter* sp acquires excellent properties such as high purity, degree of crystallinity (80-90%), high water retention capacity (99%), ultrafine fibrous network and high tensile strength (17, 22). Besides that, they are biocompatible, hydrophilic and non-toxic (11).

Bacterial cellulose/methacrylate nanocomposites have been prepared with different methacrylate monomers which provide a wide range of materials with adjustable properties due to their variability in chemical structure, possibility of adapting the physicochemical properties, great availability and easy to polymerization. (22) Wound dressing (43), design of 3D matrices (40), removal of heavy metal and chromate anions from aqueous solutions (48, 55-58), coatings, matrix resins and adhesives (47, 59) were some applications of bacterial cellulose based methacrylate's nanocomposites.

Poly (ethylene glycol) (PEG) display unique properties which are advantageous to biomedical and biotechnological applications due its low-toxicity, absence of antigenicity and immunogenicity and inherent ability to prevent protein adsorption (61). Poly(ethyleneglycol)methacrylate (PEGMA), one PEG derivatives, is an attractive methacrylate monomer due to its amphiphilic nature which comes from its water-soluble PEG side chain with a pendant hydroxyl group and its hydrophobic methacrylate group (62). PEGMA was used for biomedical materials such as drug carrier, microspheres for transient vascular embolization (62), protein adsorption and immobilization of polysaccharides (64) and heavy metal removal (65, 66).

PPEGMA can be produced by different polymerization approaches such as suspension polymerization (65, 84), UV-initiated free radical polymerization (85) and atom transfer radical polymerization (ATRP) (61).

The present study reports the development of BC nanocomposite through *in situ* radical polymerization of PEGMA into BC network using APS as initiator. The optimal polymerization conditions were determined and the obtained BC/PPEGMA nanocomposite characterized in terms of chemical composition, morphology, thermal stability, water absorption and mechanic properties.

## 2. Methodology

### 2.1. Material

Wet bacterial cellulose (BC) membranes using in standard conditions was used (70). Poly(ethyleneglycol)methacrylate (PEGMA, 97%, with 100 ppm of monomethyl ether hydroquinone as inhibitor, average of  $M_n = 500$ ) and ammonium persulphate (APS, 98%) were used as monomer and initiator, respectively. All reagents were purchased from Sigma-Aldrich and used as received. Distilled water was used as a solvent in all procedure steps.

### 2.2. BC nanocomposites preparation

The *in situ* polymerization of PEGMA inside the BC network was adapted from the procedure described by Figueiredo *et al* (43). Wet BC membranes were weight and 60% of its water content was drained. A reaction mixture containing the monomer ( $w/w_{dry\ BC}$ ) in a ratio of 1:20, 0.5% initiator ( $w/w_{monomer}$ ) was prepared in an aqueous solution and purged in  $N_2$  for 30 min. as well as the drained membrane. After that, the reactional mixture was added to the BC membrane and left for 1 hour at room temperature to occur the monomer incorporation (and of the initiator and crosslinker) inside the BC network. Then, the polymerization reaction was left reacting for 6 hours at 60°C. The obtained nanocomposite membranes were washed with distilled water during 1 hour for 8 times, dried at 40 °C and stored in a desiccator until their characterization.

The optimum percentage of polymer incorporation in the BC was determined by the sample increasing weight after polymerization and was calculated according to Eq. (1)

$$\% \text{ Incorporation} = \frac{w_{modified\ BC} - W}{W} \quad (\text{Equation 5})$$

where  $W$  is the weight of dry bacterial cellulose (g) and  $W_{modified\ BC}$  is the weight of the dry bacterial cellulose after *in situ* radical polymerization (g).

## 2.3. BC nanocomposites characterization

The obtained BC/PPEGMA nanocomposite was characterized in terms of chemical composition, morphology, thermal stability, water absorption and mechanic properties by ATR-FTIR, XRD, EDX, FE-SEM, TGA, SW and DMA, respectively. The methodology applied for each methods is described in “Section 2.3. of Chapter II: *New Bacterial cellulose/poly(glycidylmethacrylate) nanocomposites films by in situ radical polymerization*” of present monography.

## 3. Results and Discussion

BC/PPEGMA nanocomposites were prepared by the *in situ* free polymerization of PEGMA incorporation into the BC network using APS as initiator. The schematic representation of the polymerization is shown in Figure 34.

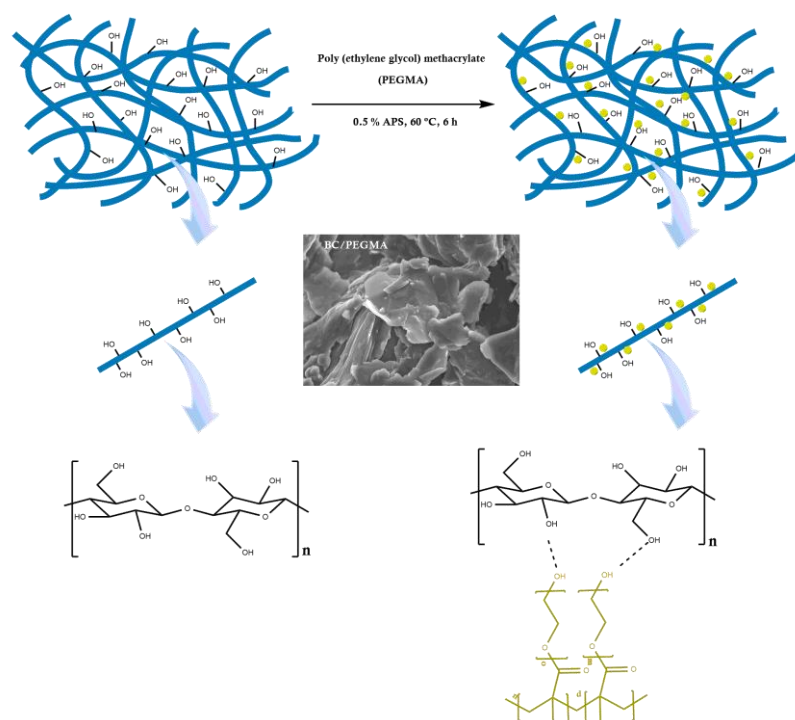


**Figure 34.** Schematic of *in situ* free radical polymerization reaction of PEGMA inside of BC network [based on (86)].

The *in situ* radical polymerization of PEGMA occurs through a homolytic cleavage via C=C, initiated by free radical provoked by the dissociation of APS (71).

Different reaction conditions were studied. The optimal conditions (considering the amount of polymer incorporated) determined for this polymerization were a ratio of (1:20) for bacterial cellulose/monomer with 0.5% of initiator at 60 °C during 6 h resulting in a polymer incorporation percentage of about 87% into the BC network (Figure 35).

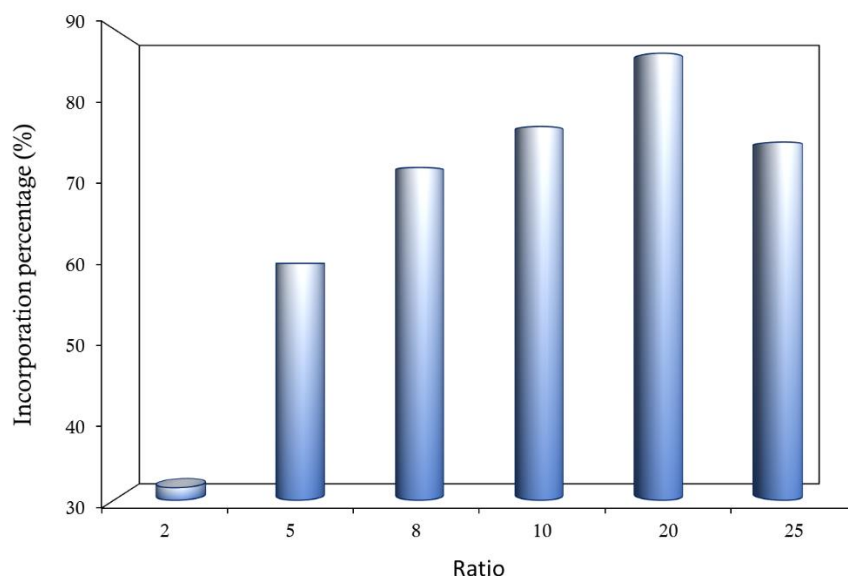


**Figure 35.** Effect of monomer (PEGMA) amount in BC *in situ* free radical polymerization.

The obtained BC/PPEGMA nanocomposites display a translucent-yellow color while native cellulose exhibits a milky white appearance. It's also observed a decrease of stiffness of the BC network, suggesting that the incorporation of polymer occurs into the cellulose network.

This new nanocomposite was characterized in terms of structure, morphology, rehydration ability, thermal and mechanical properties. ATR-FTIR analysis was performed to confirm the incorporation of polymer inside of BC tridimensional network. Figure 36 shows the ATR-FTIR spectra of BC and BC/PPEGMA (1:20).

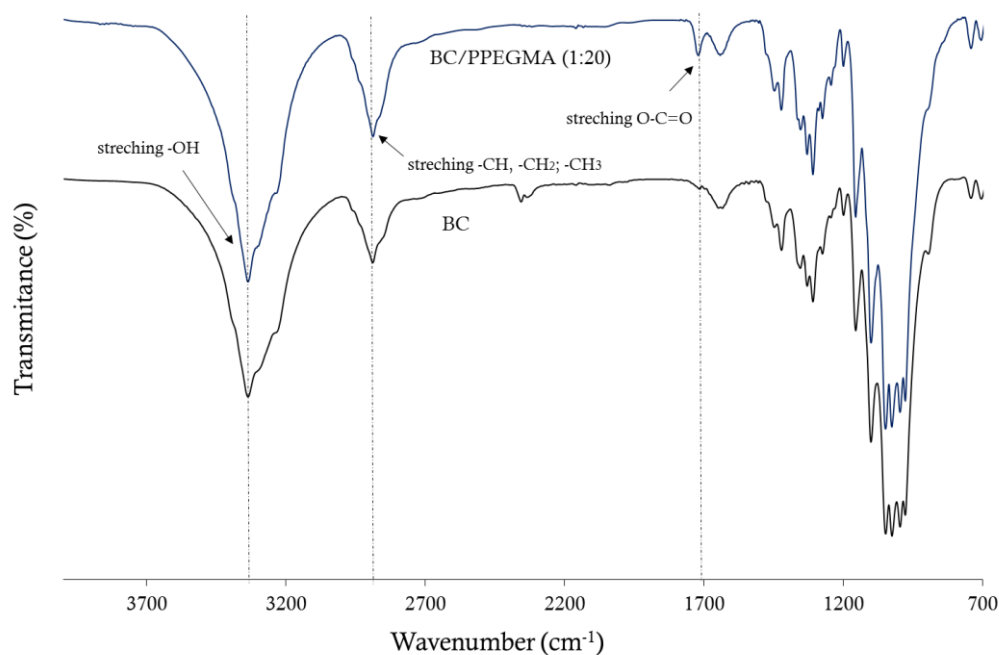


**Figure 36.** ATR-FTIR spectra of BC and BC/PPEGMA nanocomposite.

The ATR-FTIR spectra of the BC/PPEGMA nanocomposites exhibited, in addition to the characteristic peaks of native BC (described in *Section 3.3.1. of Chapter II*) a absorption band at  $1720\text{ cm}^{-1}$ , attributed to the carboxyl groups of methacrylate ester units ( $\text{O}-\text{C}=\text{O}$ ). Additionally, the intensification of the absorption at  $2894\text{ cm}^{-1}$ , assigned to the vibrations of the  $\text{CH}$ ,  $\text{CH}_2$  and  $\text{CH}_3$  and at  $3340\text{ cm}^{-1}$ , attributed to the PEG terminal hydroxyl groups (65, 85), confirm the success of incorporation of PPEGMA into the BC network. Moreover, the absence of the characteristic  $\text{C}=\text{C}$  stretching vibrations at  $1660\text{ cm}^{-1}$  indicates that the polymerization of PEGMA occurs into the three-dimensional network.

A decrease of 12% in the  $\text{C}/\text{O}$  ratio in BC/PPEGMA nanocomposites, determined by EDX (Table 6) evidence the increase of hydroxyl groups ( $-\text{OH}$ ) and ester groups ( $\text{O}-\text{C}=\text{O}$ ) into the network of BC, arising from the presence of PPEGMA in BC network.

**Table 6.** EDX analysis of elemental composition of BC and BC/PPEGMA nanocomposites (wt %).

Samples	C	O	C/O Ratio
BC	75.37	23.05	3.30
BC/PPEGMA (1:20)	73.14	25.23	2.90

As expected, the incorporation of hydrophilic groups from PPEGMA into the three-dimensional BC network leads to changes in the morphology of the membranes as revealed by SEM analysis (Figure 37). Comparatively with native BC, BC/PPEGMA nanocomposites display a denser, compact and homogeneous surface morphology with scattered between cellulose microfibrils. Inside of the network, thin laminated-type flakes leaves were spread throughout the network. BC/PPEGMA nanocomposite network exhibit particles with a wide range of sizes (from sub- $\mu\text{m}$  to several  $\mu\text{m}$  wide). The SEM images evidences that the incorporation of PPEGMA only occurs inside of the network.

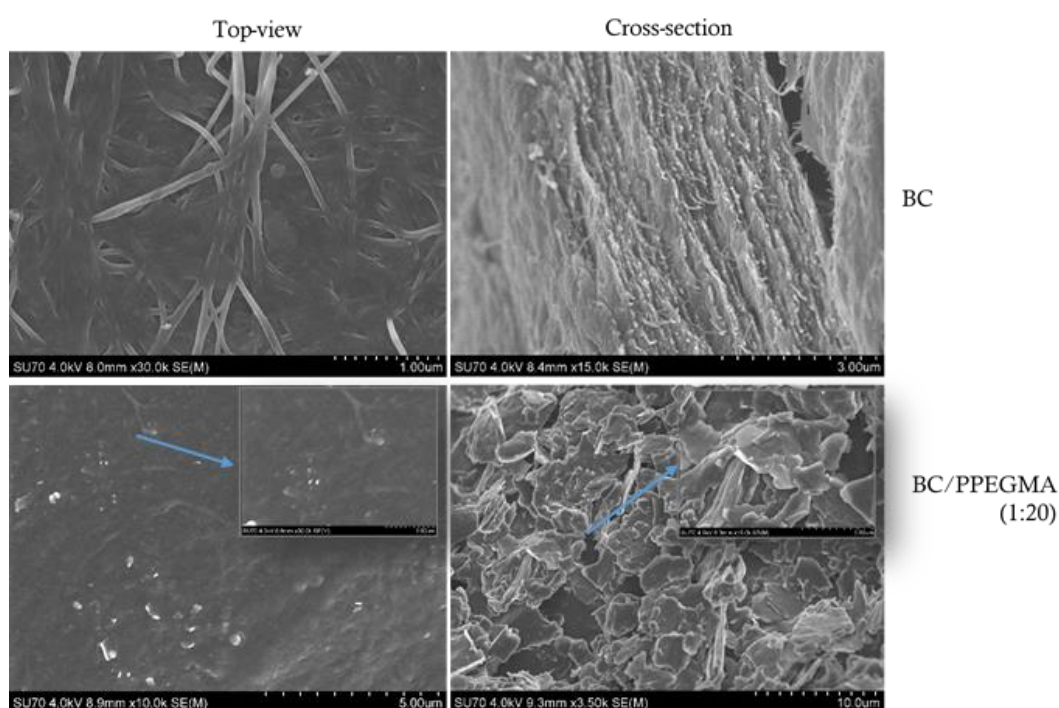


**Figure 37.** SEM images of BC and BC/PPEGMA nanocomposites morphology in different perspectives.

The incorporation of PPEGMA can decrease the crystallinity of BC network due to the BC fibrils disorganization. In the XRD profile of BC/PPEGMA, only one characteristic diffraction peak of BC at  $2\theta$  of  $22.9^\circ$ , corresponding to the (200) crystallographic planes was observed (Figure 38). The crystallinity index obtained for BC/PPEGMA was 39.40% with smaller crystallite dimensions (0.877 nm). This high decrease in the crystallinity index is in line with the 87% of PEGMA incorporation.

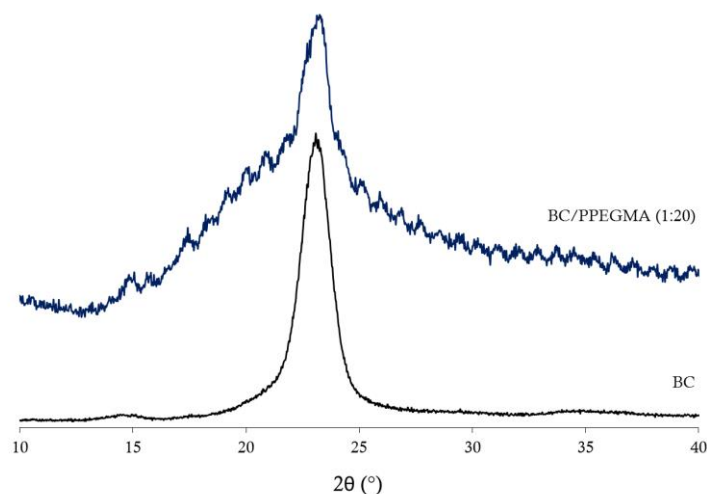


**Figure 38.** XRD patterns of BC and BC/PPEGMA nanocomposites.

In order to evaluate the absorption of water and rehydration ability of the new BC nanocomposites, the swelling studies were performed by immersion of the membranes in water during 48 h at room temperature. Figure 39 shows the swelling ratios of native bacterial cellulose and of the new BC/PPEGMA nanocomposites. Both samples absorbed water in different ratios, reaching an equilibrium at 24 h. The introduction of PPEGMA chain with hydroxyls groups ( $-\text{OH}$ ) and ester groups ( $\text{O}-\text{C}=\text{O}$ ) promotes an increase in the hydrophilicity character of the samples, exhibiting an increment of 213% in the water absorption when compared with native BC.

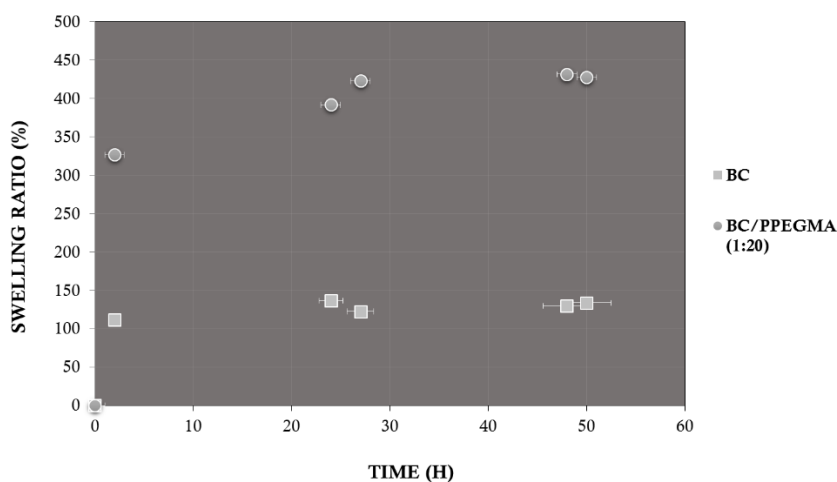


**Figure 39.** Behavior of the swelling ratio in function of time of BC and BC/PPEGMA nanocomposites.

The thermal stability and degradation profile of BC/PPEGMA nanocomposites was evaluated by thermogravimetric analysis as shown in Figure 40. Native bacterial cellulose membranes were also analyzed for comparison purposes. As described in *Section 3.3.5. of Chapter II*, native BC exhibit one main degradation step with maximum degradation temperature at about 347 °C (42, 80). The addition of PPEGMA decrease the stability when compared to BC, starting their decomposition at around 266 °C and exhibited a degradation profile with two main step degradation at around 342 and 402 °C.

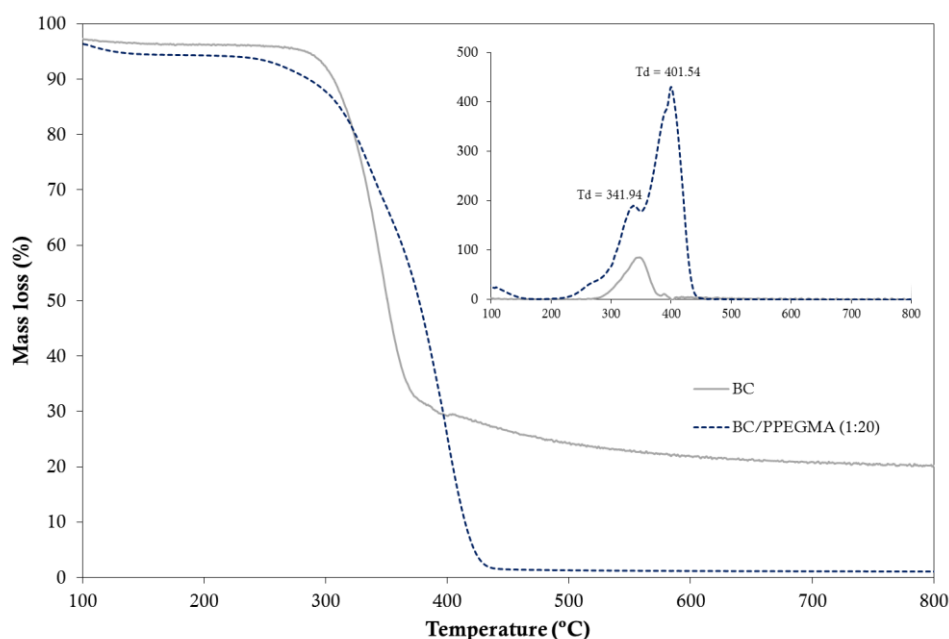


**Figure 40.** TGA and DTGA profile of BC and BC/PPEGMA nanocomposites.

The influence of PPEGMA incorporation on the viscoelastic properties of the novel BC/PPEGMA nanocomposites was evaluated by DMA. Figure 41 shows the variation of the storage tensile modulus and  $\tan \delta$  of BC/PPEGMA nanocomposites films. The storage modulus,  $E'$ , shows only one transition that start for a temperature lower than -43% (before the beginning of the analysis). These results show that the incorporation of PPEGMA originates a remarkable decrease in the  $E'$  compared with native BC (40) due to fact that PEGMA incorporation lead to a decrease of the film crystallinity as obseved by XRD analysis. These results indicated that the incorporation of PPEGMA into the BC network results in a decrease of the rigidity of the membrane.

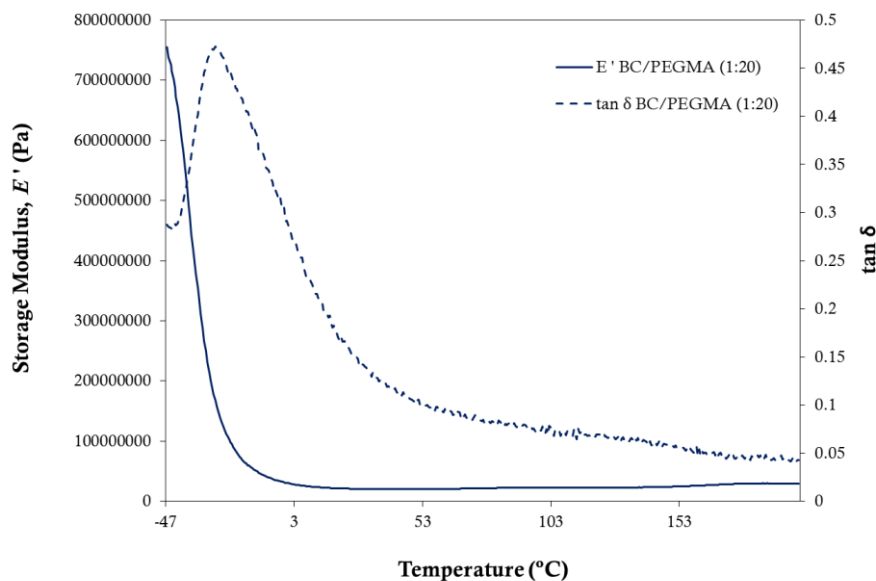


Figure 41. Storage modulus e tan  $\delta$  versus temperature of BC/PPEGMA nanocomposites.

## 4. Conclusions

New bacterial cellulose/poly(ethyleneglycol)methacrylate nanocomposite, BC/PPEGMA was obtained by *in situ* radical polymerization of PEGMA inside the BC network. BC/PPEGMA nanocomposite display a translucent yellow appearance and have new thermal, morphologic and surface characteristics. The incorporation of the hydrophilic PEGMA inside the BC network lead to a decrease of the stiffness of three-dimensional structure, improve the thermal and mechanical properties, increase their swelling ability as well as of amorphous content.

## **CHAPTER V**

*Assessment of the surface properties changes of bacterial  
cellulose/polymethacrylate nanocomposite films by Inverse Gas  
Chromatography*

## CHAPTER V. Assessment of the surface properties changes of bacterial cellulose/polymethacrylate nanocomposite films by Inverse Gas Chromatography

### Abstract

Bacterial cellulose/polymethacrylate nanocomposites have been receiving attention in the last years due to the availability and attractive properties of methacrylate monomers. In this work, bacterial cellulose/poly(glycidylmethacrylate) and bacterial cellulose/poly(ethylene glycol)methacrylate nanocomposites were prepared by *in situ* free radical polymerization. Inverse Gas Chromatography was used to study surface properties namely surface energy, surface area, heterogeneity and acid-base character. The results show the successful incorporation of methacrylate polymers into the bacterial cellulose. The incorporation of glycidylmethacrylate decrease the hydrophilicity and increase the porosity and roughness of the bacteria cellulose network. In the case of poly(ethyleneglycol)methacrylate incorporation, an increase of hydrophilicity and a decrease of the porosity and roughness, was observed. Both methacrylate polymers incorporation made the bacterial cellulose film surface more basic and consequently more reactive with the acid compounds, thus allowing new applications.

**Keywords:** Nanocomposites, bacterial cellulose, poly(glycidylmethacrylate), poly(ethyleneglycol)methacrylate, surface properties, IGC.

## 1. Introduction

Nanocomposites are defined as '*composites of more than a Gibbsian solid phase where at least one-dimension is in the nanometer range and typically all solid phases are in the 1-20 nanometer range*' by Komarneni in 1992 . Recently, several studies have been reported using bacterial cellulose as a starting component and/or the base to obtain bacterial cellulose nanocomposites. Bacterial cellulose possesses excellent properties such as high purity, degree of crystallinity (80-90%), high water retention capacity (99%), ultrafine fibrous network and high tensile strength (17, 22). Furthermore, it exhibits excellent biocompatibility and non-toxicity, being a great material to be employed in a wide range applications in different areas (6, 11, 69).

Bacterial cellulose/poly(methacrylate) nanocomposites have been receiving attention by researchers due to their availability and attractive properties. These properties can be employed in nanocomposites for biomedical applications such as wound dressing (43) and design of 3D matrices (40). Glycidylmethacrylate (GMA) and poly(ethyleneglycol)methacrylate (PEGMA) are two attractive methacrylate due to their properties. GMA possess two functional groups, the epoxide and the methacrylate groups (double bonds), which offers a wide range of industrial applications in polymer chemistry and technology (49, 50, 54). PEGMA, one poly(ethyleneglycol) derivate, confers an amphiphilic nature, which comes from its water-soluble PEG side chain with a pendant hydroxyl group and its hydrophobic methacrylate group (62).

In this paper, the modification of the surface properties of bacterial cellulose with the methacrylate compounds (glycidylmethacrylate and poly(ethyleneglycol)methacrylate) through *in situ* radical polymerization was evaluated. Thermodynamic and morphologic parameters such as dispersive and specific surface energy, acid–base surface character, surface area and heterogeneity were determined using Inverse Gas Chromatography (IGC).

### 1.1. Inverse gas chromatography

Physical chemical properties of the surface nanocomposites can be determinated by IGC. This technique is simple, fast and sensitive, giving great accuracy of the results. Unlike

GC, in IGC the nonvolatile material to be investigated is immobilized in a chromatographic column (stationary phase) and through passage of molecules probe with known properties, it is obtained the characteristic of the solid, at infinite dilution (Figure 42). Thermodynamic parameters such as surface energy, acid-basic character, enthalpy, entropy, adsorption isotherm, adsorption potential, heterogeneity and kinetic parameters such as diffusion, permeability and solubility can be determined through this technique (87, 88).

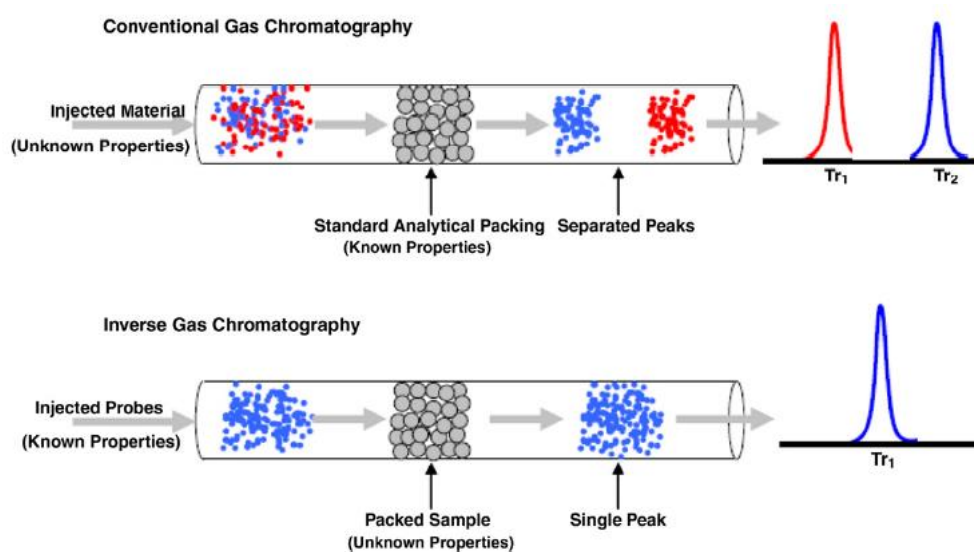


Figure 42. Schematic representation of GC and IGC measurements (89).

### 1.1.1. Surface energy component

The surface energy of a solid,  $\gamma_s$ , characterizes the active energy in the surface of the solid and can be given as the sum of the dispersive component,  $\gamma_s^d$ , which describes all the van der Waals forces interactions and specific component,  $\gamma_s^{sp}$ , which expresses acid-base character (87):

$$\gamma_s = \gamma_s^d + \gamma_s^{sp} \quad (\text{Equation 6})$$

The retention time obtained from the interaction between the probe molecules and the surface of the solid allows us to obtain the volume of probe molecules used, that is directly related to the energy of adsorption (90),  $\Delta G_{ads}$ :

$$\Delta G_{ads} = RT \ln V_N + K \quad (\text{Equation 7})$$

where  $R$  is the gas constant,  $K$  is a constant depending on the chosen reference state,  $T$  is the column temperature and  $V_N$  is the net retention volume. According Fowkes *et al*,  $\Delta G_{ads}$  is related to the energy of adhesion,  $W_A$ , by the equation:

$$RT \ln V_N = 2N_A(\gamma_s^d)^{1/2} a(\gamma_L^d)^{1/2} + K \quad (\text{Equation 8})$$

where  $\gamma_L^d$  is the dispersive component of the surface energy of the probe molecule,  $a$  is the area occupied by probe molecule and  $N$  is the Avogadro's number.  $\gamma_s^d$  can be calculated from the slope of the obtained line made a plot of  $\Delta G_{ads}$  versus  $a(\gamma_L^d)^{1/2}$  of the series of  $n$ -alkanes.

### 1.1.2. Acid base character

Knowledge of the surface materials acid or basic character is important to understand their interaction with polar molecules. The polar molecules and solid interactions involve: dispersive,  $\Delta G_{ads}^d$ , and specific,  $\Delta G_{ads}^{sp}$ , interactions (92). The specific energy of adsorption  $\Delta G_{ads}$  is determined by the equation:

$$\Delta G_{ads} = \Delta G_{ads}^d + \Delta G_{ads}^{sp} \quad (\text{Equation 9})$$

$\Delta G_{ads}^{sp}$  can be determined by the following relation (92):

$$\Delta G_{ads}^{sp} = RT \ln V_N - RT \ln V_{N(ref)} \quad (\text{Equation 10})$$

where  $V_N$  is the net retention volume for the polar probe and  $V_{N(\text{ref})}$  is the net retention volume established by the  $n$ -alkane reference line for the same polar probe. From  $\Delta G_{ads}$  it's possible to determine the surface enthalpy of adsorption,  $\Delta H_{ads}$  and surface entropy of adsorption,  $\Delta S_{ads}$  through the following relation (92):

$$\frac{\Delta G_{ads}}{T} = \frac{\Delta H_{ads}}{T} - \Delta S_{ads} \quad (\text{Equation 11})$$

$\Delta H_{ads}^{sp}$  and  $\Delta S_{ads}^{sp}$  can be established using the  $\Delta G_{ads}^{sp}$  in the previous equation.  $\Delta G_{ads}^{sp}$  can be used to quantify the Lewis acidity and basicity of the non-volatile material with the following equation (92):

$$\frac{\Delta H_{ads}^{sp}}{AN^*} = \frac{DN}{AN^*} \times K_A + K_B \quad (\text{Equation 12})$$

where  $AN^*$  and  $DN$  are Gutmann's (83) modified acceptor and donor numbers, respectively;  $K_A$  is a Lewis acidity constant and  $K_B$  is a Lewis basicity constant.

### 1.1.3. Isotherm measurements

Using a wide variety of probe molecules at different temperatures, it's obtained the adsorption isotherm by the BET equation (93):

$$\frac{p}{n(p^\circ - p)} = \frac{1}{n_m c} + \frac{c-1}{n_m c} \times \frac{p}{p^\circ} \quad (\text{Equation 13})$$

where  $n_m$  is the monolayer capacity;  $n$  the amount adsorbed;  $p$  the partial pressure;  $p^\circ$  the saturation pressure and  $c$  is related with the heat of sorption. Knowing the monolayer capacity and the cross area,  $a_m$ , of a probe molecule, the surface area,  $S_{BET}$ , can be calculated by the following equation (93):

$$S_{BET} = a_m n_m N_A \quad (\text{Equation 14})$$

where  $N_A$  is the Avogadro constant.

Through the adsorption isotherm, the heterogeneity of the surface can be deduced from the adsorption potential,  $A$  by the following equation:

$$A = RT_S \ln \left( \frac{p^c}{p} \right) \quad (\text{Equation 15})$$

## 2. Experimental methodology

### 2.1. Material

Wet bacterial cellulose (BC) membranes in standard conditions were used (70). Glycidyl methacrylate (GMA, 97%, with 100 ppm of monomethyl ether hydroquinone as inhibitor), poly (ethylene glycol) methacrylate (PEGMA, average  $M_n$  500, containing 900 ppm monomethyl ether hydroquinone as inhibitor), N,N'-methylenebisacrilamide (MBA,  $\geq 99.5\%$ ) and ammonium persulphate (APS, 98%) were purchase in Sigma-Aldrich and were used as received. The chemical reagents used for IGC measurements such as non-polar and polar molecules were GC grade ( $>99\%$  purity) supplied by Sigma-Aldrich. The methane gas (reference probe) and helium (carrier gas), of high purity ( $>99.99\%$ ), were supplied by Air Liquide Company.

### 2.2. BC/PGMA and BC/PEGMA nanocomposites

The bacterial cellulose nanocomposites were obtained through the methodology described in “*Section 2.2. Chapter II: Bacterial cellulose/poly (glycidyl-methacrylate) nanocomposites films by in situ radical polymerization*” and *Chapter IV: In situ radical polymerization of bacterial cellulose/poly(ethyleneglycol)methacrylate nanocomposites films*”

Briefly, wet membranes were drained to remove the excess of water. In a separate Erlenmeyer, the membrane and the reaction mixture were purged in nitrogen for 30 min. being added, posteriorly through a syringe. After 1 hour at room temperature, the reaction

took place in an oil bath for 6 hours at 60°C. The BC nanocomposites prepared were washed during 1 hour several times, dried at 40°C and kept in a desiccator until their characterization.

The reaction mixture to the BC/PGMA was prepared in an aqueous solution with (1:2) ratio of monomer, BC:GMA, (w/w), initiator, APS, 0.5% ( $w_{\text{initiator}}/w_{\text{monomer}}$ ) and cross-linking, MBA, 20% ( $w_{\text{crosslinker}}/w_{\text{monomer}}$ ) (when used).

For BC/PEGMA nanocomposites, the reaction mixture was prepared in an aqueous solution with (1:20) ratio BC:PEGMA (w/w) and initiator, 0.5% ( $w_{\text{initiator}}/w_{\text{monomer}}$ ).

### 2.3. IGC measurements

IGC measurements were carried out on a commercial inverse gas chromatograph (*i*GC, Surface Measurements Systems, London, UK) equipped with flame ionization (FID) and thermal conductivity (TCD) detectors. The *i*GC system is fully automatic with SMS *i*GC Controller v1.8 control software. Data were analysed using *i*GC Standard v1.3 and Advanced Analysis Software v1.25.

The sample were packed in the standard glass silanized (dymethyldichlorosilane; Repelcote BDH, UK) columns with 0.2 cm ID and 30 cm in length by vertical tapping about 2 h. The columns with the samples were conditioned 8 h at 40 °C and 2 h at the measurements conditions, to stabilize the columns. After conditioning, pulse injections were carried out with a 0.25 ml gas loop. Four *n*-alkanes (heptane, octane, nonane and decane) were used for measurements of the dispersive component of surface energy at 20, 25 and 30 °C. Four polar probes (tetrahydrofuran, dichloromethane, acetonitrile and ethyl acetate) were used to determine the specific component of surface energy and acid-base character ( $K_A$  and  $K_B$ ) at 25 °C. The physical constants for the probes used in IGC are presented in Table 7. The isotherm experiments were undertaken with *n*-octane, tetrahydrofuran and dichloromethane at 25 °C. All experiments were carried out at 0% relative humidity with a helium flow rate of 10 ml/min at least in duplicate, producing a reproducibility error of less than 4%.

**Table 7.** Physical constants of all probes used in IGC experiments.

Probe	$a(10^{-19} \text{ m}^2)$	$\gamma_L^d(\text{mJ/m}^2)$	$DN(\text{kcal/mol})$	$AN^*(\text{kcal/mol})$	$DN/AN^*$
<i>n</i> -Heptane	5.73	18.4	-	-	-
<i>n</i> -Octane	6.30	21.3	-	-	-
<i>n</i> -Nonane	6.90	22.7	-	-	-
<i>n</i> -Decane	7.50	23.4	-	-	-
Dichloromethane	2.45	24.5	0.0	20.4	-
Acetonitrile	2.14	27.5	14.1	4.7	3.00
Ethyl Acetate	3.30	19.6	17.1	1.5	11.4
Tetrahydrofuran	2.90	22.5	20.0	0.5	40.0

a: Cross-sectional area;  $\gamma_L^d$ : surface tension;  $AN^*$ : electron acceptor number  $[0.288(AN - AN_d)]$ ; DN: electron donor number. (83, 94)

## 2.4. Swelling ratio

The swelling ratio ( $SW$ ) of the membranes was determined by immersing the samples in distilled water at room temperature with a minimum of three replicates. The weight was periodically measured during 48 hours. For each measurement the samples were taken out of the water, their wet surfaces immediately wiped dry in filter paper, weigh, and then re-immersed. The  $SW$  was calculated using the equation below:

$$SW(\%) = \frac{(W_s - W_d)}{W_d} \times 100\% \quad (\text{Equation 16})$$

where,  $W_s$  is the weight of bacterial cellulose after swelling and  $W_d$  is the weight of dry bacterial cellulose before swelling.

## 2.5. Scanning electron microscopy

Scanning electron microscopy (SEM) micrographs of the BC nanocomposite surfaces were obtained on a HR-FESEM SU-70 Hitachi equipment operating at 1.5 kV in the field emission mode. Samples were deposited on a steel plate and coated with carbon before analysis.

## 2.6. Energy-dispersive X-ray spectroscopy

The semi-quantitative elemental chemical compositions of the samples were determined by energy-dispersive X-ray spectroscopy (EDX). Semi-quantitative analyses (wt. %) were done for carbon, oxygen and nitrogen and the  $C/O$  ratio was obtained. EDX experiments were conducted at an accelerated voltage of 5 kV in a Hitachi SU 8090 equipment.

## 3. Results and Discussion

IGC measurement allows to know the changes that occur in the materials surface properties due to different modification processes. This data enables the knowledge of their compatibility and behaviour with other molecules and modifications agents.

In order to study the influence of the poly(glycidylmethacrylate) (PGMA) and poly(ethyleneglycol)methacrylate (PPEGMA), on the surface properties of the bacterial cellulose (BC) produced by *Gluconacetobacter sacchari*, native BC and BC nanocomposites were subjected to inverse gas chromatography (IGC) analysis. The dispersive component of the surface energy,  $\gamma_s^d$ , specific component of the surface energy,  $\Delta G_s^{sp}$ , surface area,  $S_{BET}$ , monolayer capacity,  $n_m$ , adsorption potential,  $A_{max.}$ , acid character,  $K_A$  and basic character,  $K_B$  were determined.

### 3.1. Dispersive component of surface energy

$\gamma_s^d$  was determined by the injection of non-polar molecules ( $n$ -alkanes probes) and obtained plotting  $RT \ln V_n$  against  $a(\gamma_L^d)^{1/2}$  at different temperatures (Eq. 8). Table 8 shows the results obtained for  $\gamma_s^d$  in native BC and BC methacrylate nanocomposites. The correlation coefficient was good, ranging between 0.987 and 0.998.

**Table 8.** Dispersive component of surface energy,  $\gamma_s^d$ , swelling ratio,  $SW$ , of BC, BC/PGMA and BC/PPEGMA nanocomposites.

Samples	$\gamma_s^d$ (mJ/m <sup>2</sup> )			$SW$ (%)
	20 °C	25 °C	30 °C	
BC	58.53	51.8	47.41	137.84
BC/PGMA	59.10	55.21	51.96	32.80
BC/PGMA/MBA	88.25	82.93	78.31	31.36
BC/PPEGMA	35.54	35.42	36.24	431.64

The BC under study, produced by *Gluconacetobacter sacchari*, displays an higher  $\gamma_s^d$  than those reported by Castro *et al* (39.64 mJ/m<sup>2</sup>) produced by *Gluconacetobacter medellensis* (38). This can be attributed to the biosynthesis process of bacterial cellulose. The bacteria strain and synthesis conditions can influence the cellulose chains arrangement and consequently the crystallinity of BC. Cellulose type I is the common form produced by the bacteria exhibiting two allomorph forms: monoclinic  $I_\alpha$  allomorph and triclinic  $I_\beta$  form, distinguishing themselves by their spatial arrangement of nanofibrils (9, 11, 13, 14). In this particular case, the results suggest that the relative  $I_\beta$  form is higher than  $I_\alpha$  allomorph (as shown in Section 2.1. of Chapter II. *New Bacterial cellulose/poly(glycidylmethacrylate) nanocomposites films through in situ radical polymerization*) which is more stable (38).

The incorporation of PGMA, an epoxide methacrylate monomer, leads to an increase of 7% in the  $\gamma_s^d$  value. This result suggest that the *in situ* radical polymerization that occurs inside of BC didn't significantly affect the dispersive component of the surface. This inside incorporation can be observed through the SEM images [Figure 43 (B)]. Furthermore, the obtained swelling values for BC/PGMA/MBA reinforce the idea that the bacterial cellulose increase their hydrophobicity probably due to the intra- and inter-chain hydrogen bonding with PGMA which make this active sites less accessible to water absorption. Figure 44 shows a schematic illustration of apolar and polar probe interactions with BC/PGMA/MBA nanocomposites at surface.

With the addition of crosslinker, MBA, it was observed an increase of 51% in the  $\gamma_s^d$  value. Yang and Zhai (2012) reported that the water contact angle increased in cellulose fibers grafted with GMA, due to the replacement of the polar hydroxyl groups by glycidyl groups,

ester and epoxy groups, that exhibit a less polar character. In the present study, the *in situ* free radical polymerization of GMA crosslinked with MBA inside BC network probably leads to two effects: (i) the increase in the number of glycidyl groups exposed in the surface which present a less polar character, making it more hydrophobic or/and (ii) the change of the spatial arrangement of microfibrils leaving them more exposed to surface (as shown in Figure 43 (C)).

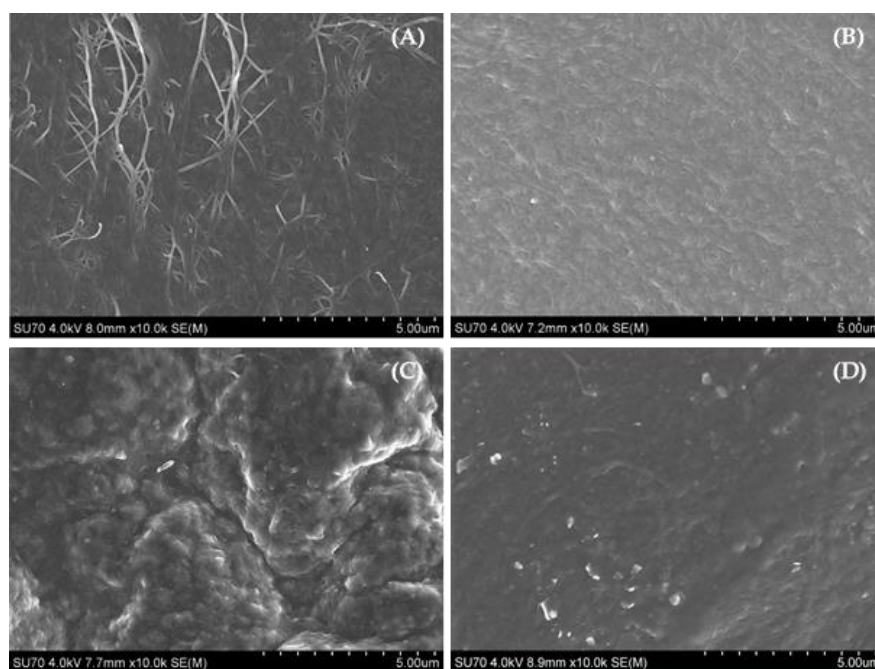


**Figure 43.** SEM images of BC nanocomposites morphology (A) BC; (B) BC/PGMA; (C) BC/PGMA/MBA and (D) BC/PPEGMA.

However, the incorporation of the PPEGMA, change differently the surface properties of BC. PPEGMA has an amphiphilic nature which arises from the pendant hydroxyl group and its hydrophobic methacrylate group. BC/PPEGMA nanocomposite exhibited a decrease in the  $\gamma_s^d$  value to 36.42 mJ/m<sup>2</sup> at 25 °C (40% less). This result suggests that the incorporation of PPEGMA decreases the number of non-polar active sites probably due to the increase of ester bonds and hydroxyls groups from PPEGMA exposed at nanocomposite surface. As shown in SEM images [Figure 43 (D)], the BC/PPEGMA exhibited a dense surface arising of incorporation which probably favours the probes interaction with the polar active sites. The decrease in the C/O ratio (2.90) in the

BC/PPEGMA nanocomposites compared to  $C/O$  ratio (3.30) in the native BC evidence this supposition. Besides that, the water retention ability shows an increase of 213 % compared with native BC which means that the BC, acquire a hydrophilic character after incorporation of PPEGMA, in agreement with the  $\gamma_s^d$  decrease.

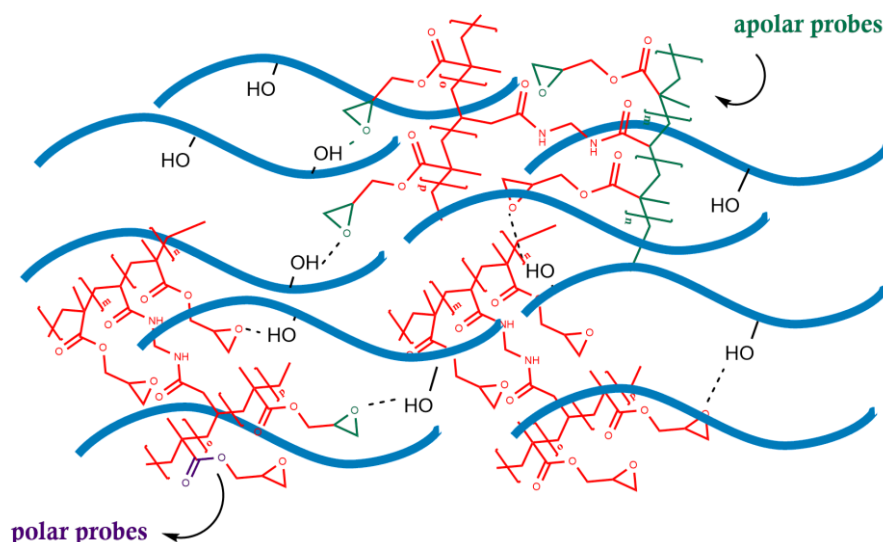


**Figure 44.** Schematic interactions of non-polar and polar probes with surface groups of BC/PGMA/MBA nanocomposites.

### 3.2. Heterogeneity

The dispersive energetic profile of the surface heterogeneity is determined by BET model (81) injecting different concentrations of a *n*-octane probe. The heterogeneity profile for BC and BC nanocomposites at 25 °C are shown in Figure 45. BC/PGMA/MBA nanocomposites exhibited an increase of the active sites energy, opposite to the BC/PPEGMA nanocomposites where occurs a decrease of active sites energy when compared with native BC. This behaviour is aligned with the results obtained to the dispersive component of surface energy and described previously.

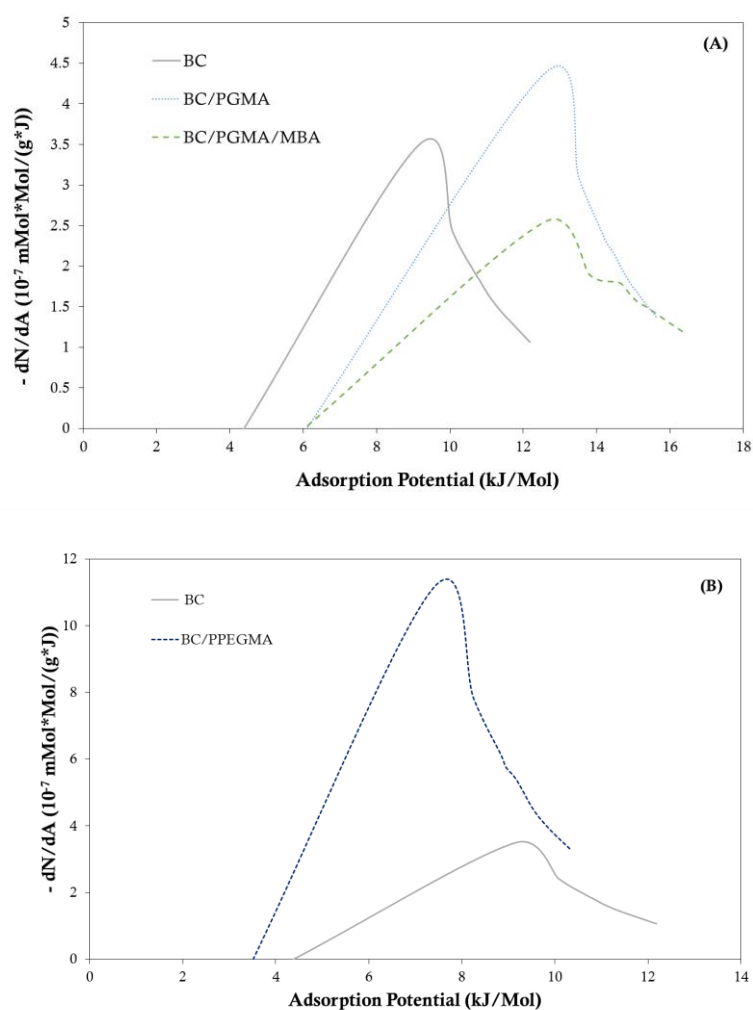


**Figure 45.** Heterogeneity profile with *n*-octane for native BC, (A) BC/PGMA and BC/PGMA/MBA and (B) BC/PPEGMA nanocomposites at 25 °C.

The BC/PGMA show one peak maximum ( $A_{max}$ ) at 12.59 kJ/mol with a high number of active sites. In the presence of the crosslinker, BC/PGMA/MBA, present two peak maximum, ( $A_{max}$ ) at 12.58 and 14.76 kJ/mol, significantly more energetics compared with native BC [Figure 45 (A)]. The addition of crosslinker plays an important function in retaining more monomer into the BC network, having a great effect in  $\gamma_s^d$ , making the surface with more energetic dispersive active sites which increase significantly the  $\gamma_s^d$ . This non-polar character probably comes from the alkanes chains introduced by more polymerization of GMA being more affordable to the nanocomposite surface (as supported by SEM images – Figure 43).

In the BC/PPEGMA nanocomposites one peak maximum ( $A_{max}$ ) at 7.38 kJ/Mol is found with an increase number of less energetic actives sites [Figure 45 (B)], which make the nanocomposite have smaller  $\gamma_s^d$ . This result suggests that the introduction of PPEGMA into the BC network leads to more accessible the non-polar PEG groups.

### 3.3. Surface area

The isotherm measurements with *n*-octane at different concentrations BET model (81) were performed. Symmetrical peaks were obtained and a linear adsorption isotherm described by Henry's Law was observed. These indicates that the interactions between materials and the probe molecule occurs predominantly via the high-energy sites (93). Besides that a type I isotherm was observed, which is characteristic for microporous materials with relatively small external surfaces (96).

The surface area ( $S_{BET}$ ) of bacterial cellulose range between 0.83 m<sup>2</sup>/g and 12.59 m<sup>2</sup>/g and the monolayer capacity ( $n_m$ ) range between 2.18 μmol/g and 33.17 μmol/g (Table 9). These results show that the polymerization with the two methacrylates had different effects in the particle morphology. BC/PGMA and BC/PPEGMA nanocomposites increased the  $S_{BET}$  in 57 % and 219 %, respectively, when compared with native BC, which means: (i) a significant decrease in the particles size or/and (ii) increase in its porosity or roughness (89). SEM images (Figure 43) show that the porosity increase when both polymers were added to BC network.

The addition of crosslinker had an opposite behaviour, decreasing significantly the  $S_{BET}$  in 79 %, which means that occurs an increase of particle size or/and a decrease in porosity/roughness. This can be due to the more compact and dense surface formed after incorporation of PGMA/MBA as supported by SEM images (Figure 43).

**Table 9.** Surface area,  $S_{BET}$ , monolayer capacity,  $n_m$  and adsorption potential distribution maximum,  $A_{max}$ , of BC, BC/PGMA, PC/PGMA/MBA and BC/PPEGMA nanocomposites, at 25 °C with *n*-octane.

Samples	$S_{BET}$ (m <sup>2</sup> /g)	$n_m$ (μMol/g)	R <sup>2</sup>
BC	3.94	10.38	0.9994
BC/PGMA	6.20	16.35	0.9989
BC/PGMA/MBA	0.83	2.18	0.9957
BC/PPEGMA	12.59	33.17	0.9499

### 3.4. Acid-base character

BC, GMA and PEGMA have in its structure polar groups able to interact and exchange the specific interactions with polar probes. Injecting tetrahydrofuran, dichloromethane, ethyl acetate and acetonitrile, the specific component of surface energy,  $\Delta G_s^{sp}$ , was determined and is showed in Figures 46 and 47, respectively.

The high interaction between acetonitrile (amphoteric probes) and the nanocomposites evidence the presence of both acid and basic groups in the nanocomposites surface.

To the BC/PGMA nanocomposites the  $\Delta G_s^{sp}$  increase for all probes which suggest that occurs an increase in polar active sites at the surface. This increase is more significant for the acid probe (dichloromethane) compared to the basic probe (tetrahydrofuran), indicating of an increase in the basic active sites in the surface. The energetic profile of dichloromethane showed that it occurs due to an increase of the active sites number with high energy [Figure 48 (A)]. These results suggest that the incorporation of monomer and the addition of crosslinker affects the acid-base surface character making more basic groups at the surface.

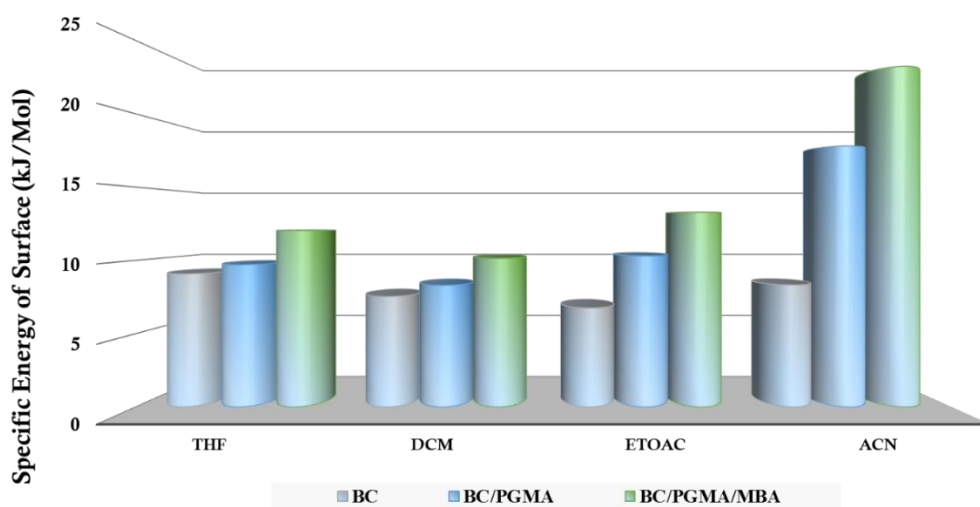


**Figure 46.** Specific surface energy of BC, BC/PGMA and BC/PGMA/MBA nanocomposites with polar probes: THF - tetrahydrofuran, DCM - dichloromethane, ETOAc – ethyl acetate and ACN – acetonitrile, at 25 °C.

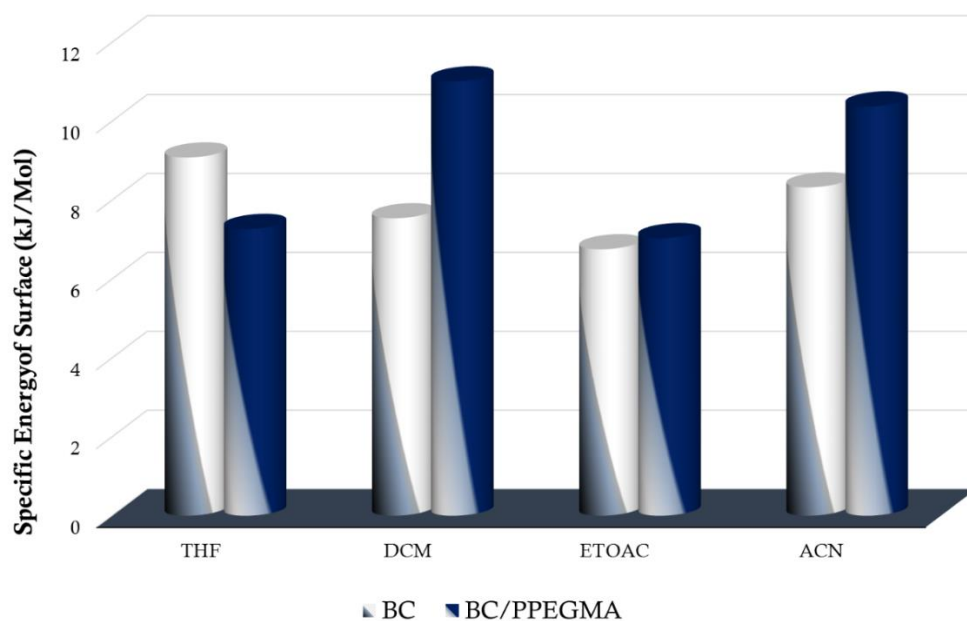


**Figure 47.** Specific surface energy of BC and BC/PPEGMA nanocomposites with polar probes: THF - tetrahydrofuran, DCM - dichloromethane, ETOAc – ethyl acetate, ACN – acetonitrile, at 25 °C.

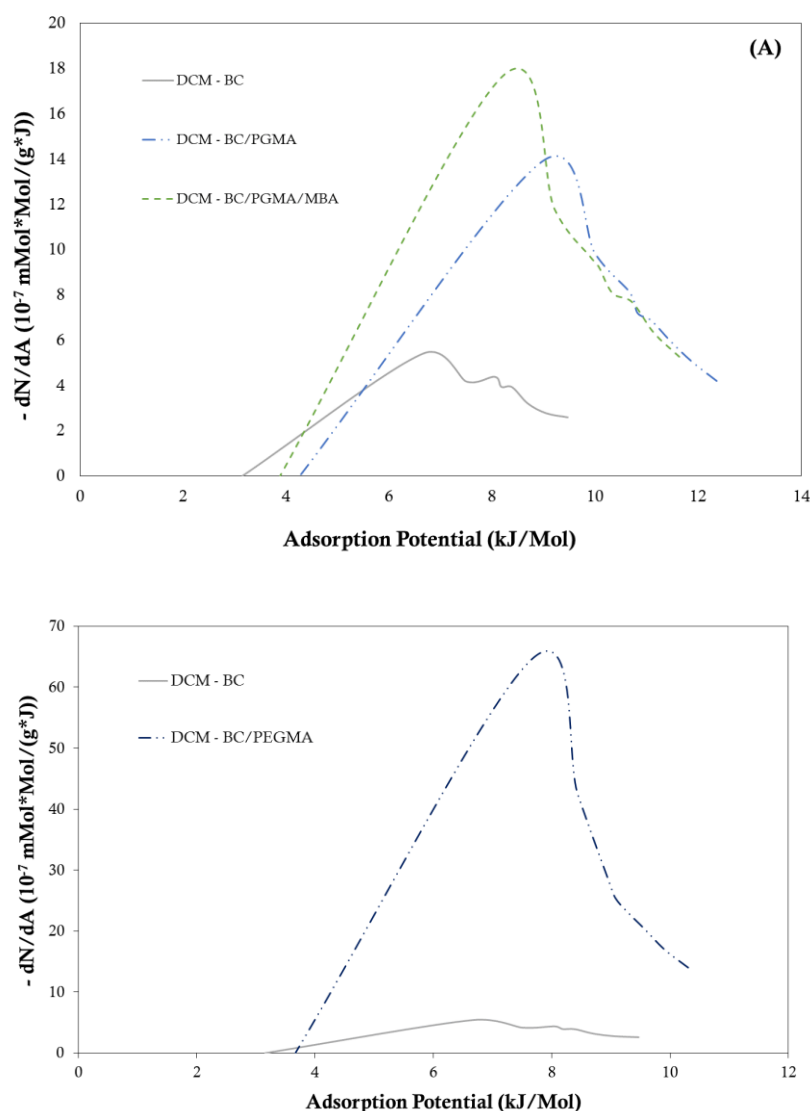


**Figure 48.** Heterogeneity profile with dichloromethane for (A) BC, BC/PGMA and BC/PGMA/MBA and (B) BC and BC/PPEGMA nanocomposites, at 25 °C.

To the BC/PPEGMA nanocomposites, a higher increase in the  $\Delta G_s^{sp}$  for dichloromethane (Figure 47) was observed. The dichloromethane energetic profile [Figure 48 (B)] show an increase in the number of active sites. This observation suggests more basic groups at nanocomposites surface accessible for interactions.

The calculated  $\Delta G_s^{sp}$  is converted into acid-base number using the Guttmann's concept (83). Table 10 present the obtained values for acid-base constants,  $K_A$  and  $K_B$ , for bacterial cellulose nanocomposites. The surface basicity exhibited in native BC is higher than the one found by Castro *et al* (2015), which reported a  $K_B/K_A$  ratio of 1.80. This result suggests

a different arrangement of the cellulose groups at the surface with less hydroxyls groups available to interactions. The incorporation of basic groups such as (C–O–C) in BC/PGMA and BC/PPEGMA nanocomposites leads to an increase of the base constant,  $K_B$ , showing a  $K_B/K_A$  ratio about four times higher.

Taking into account the energetic profile, the increase in the basic character exhibited in BC nanocomposites derives from the increased number of more energetic basic active sites due to the incorporation of methacrylates compounds into BC network.

**Table 10.** Acid-base character,  $K_A$  and  $K_B$  of BC, BC/PGMA BC/PGMA/MBA and BC/PPEGMA nanocomposites, at 25 °C.

Samples	$K_A$	$K_B$	$K_B/K_A$	$R^2$
BC	0.10	0.23	2.27	0.9873
BC/PGMA	0.10	0.42	4.20	0.9868
BC/PGMA/MBA	0.13	0.56	4.31	0.9862
BC/PPEGMA	0.08	0.34	4.25	0.9668

## 4. Conclusions

The incorporation of methacrylate monomers into the BC network through *in situ* radical polymerization is a suitable method to change the BC properties for the production of new nanocomposites aiming new applications. Inverse Gas Chromatography shows that the incorporation of glycidylmethacrylate and poly(ethyleneglycol)methacrylate modify the bacterial cellulose which leads:

- (i) in BC/poly(glycidylmethacrylate), to an increase in the dispersive component of surface energy (decrease in hydrophilicity) and an decrease the surface area when the crosslinked was added;
- (ii) in BC/(poly(ethylene glycol)methacrylate), to a significant decrease in the in the dispersive component of surface energy (increase of hydrophilicity) and a decrease in surface area;

- (iii) in both BC/methacrylate nanocomposites, to a great increase of the basic surface character.

## FINAL CONCLUSIONS

BC as support for nanocomposite films has been exploited for numerous applications and their combination with methacrylate monomers allow to obtain new nanomaterials with different properties to apply in various fields, namely biomedical applications or/and remove heavy metals.

*In situ* free radical polymerization of glycidylmethacrylate, GMA, and poly (ethylene glycol) methacrylate, PEGMA, occurred into the BC network using ammonium persulphate, APS, as initiator and N,N'-methylenebisacrilamide, MBA, as crosslinker in BC/PGMA. The optimal conditions determined for polymerization was (1:2) ratio for BC/PGMA, (1:2:0.2) for BC/PGMA/MBA and (1:20) for BC/PPEGMA with 0.5 % of initiator during 6 h at 60 °C. A maximum incorporation percentage of 60, 67 and 87 %, were obtained respectively. Compared with native BC, the BC/PGMA nanocomposites exhibited a roughness and a compact three-dimensional structure, an improvement in thermal and mechanical properties, a decrease in their swelling ability and a lower crystallinity. Unlike, the BC/PPEGMA had shown a decrease of stiffness of three-dimensional structure and an increase in their swelling ability. However, an improvement in thermal and mechanical properties and an increase in the amorphous content it's observed. Both BC nanocomposites present basic surface character.

Chemical treatment proved to be a good and simple strategy to modified BC/PGMA nanocomposites through epoxide ring-opening reaction mechanism. The replacement of hydroxyls groups of cellulose chains occurs for the linkage of GMA chains by epoxy group. Nanocomposites became more compact, smooth and with more water retention ability. A decrease in the thermal and mechanical proprieties was observed.

As future perspectives, the reactivity of epoxy group as absorbent material, it's an interesting as well as the biocompatibility of all BC polymethacrylate nanocomposites for biomedical applications for application as adsorbent material for removal of heavy metal or/and proteins.

## REFERENCES

1. The chemistry of polymers. Second edition ed: RSC Paperbacks; 1997. 22 p.
2. Chawla P, Bajaj I, Survase S, Singhal R. Fermentative production of microbial cellulose. *Food Technol Biotechnol*. 2009;47:107-24.
3. Keshk S. Bacterial cellulose production and its industrial applications. *J Bioprocess Biotechniq*. 2014;4:1-10.
4. Khalil H, Bhat A, Yusra A. Green composites from sustainable cellulose nanofibrils: A review. *Carbohydr Polym*. 2012;87:963-79.
5. Shokri J, Adibkia K. Application of cellulose and cellulose derivatives in pharmaceutical industries. *Intech*. 2013:47-66.
6. Lee K, Buldum G, Mantalaris A, Bismarck A. More than meets the eye in bacterial cellulose: biosynthesis, bioprocessing, and applications in advanced fiber composites. *Macromol Biosci*. 2014;14:10-32.
7. Fu L, Zhang J, Yang G. Present status and applications of bacterial cellulose-based materials for skin tissue repair. *Carbohydr Polym*. 2013;92:1432-42.
8. Xu X, Liu F, Jiang L, Zhu J, Haagenson D, Wiesenborn D. Cellulose nanocrystals vs. cellulose nanofibrils: a comparative study on their microstructures and effects as polymer reinforcing agents. *ACS applied materials & interfaces*. 2013;5:2999-3009.
9. Vitta S, Thiruvengadam V. Multifunctional bacterial cellulose and nanoparticle-embedded composites. *Curr Sci*. 2012;102:1398-405.
10. Esa F, Tasirin S, Rahman N. Overview of bacterial cellulose production and application. *Agric Agric Sci Procedia*. 2014;2:113-9.
11. Mohite B, Patil S. A novel biomaterial: bacterial cellulose and its new era applications. *Biotechnol Appl Biochem*. 2014;61:101-10.
12. Cai Z, Kim J. Bacterial cellulose/poly(ethylene glycol) composite: characterization and first evaluation of biocompatibility. *Cellulose*. 2009;17:83-91.
13. Moon R, Martini A, Nairn J, Simonsen J, Youngblood J. Cellulose nanomaterials review: structure, properties and nanocomposites. *Chem Soc Rev*. 2011;40(7):3941-94.
14. Iguchi M, Yamanaka S, Budhiono A. Bacterial cellulose - a masterpiece of nature's arts. *J Mater Sci*. 2000;35:261-70.

15. Pinto R, Neves M, Neto C, Trindade T. Composites of cellulose and metal nanoparticles. *Intech*. 2012:1-26.
16. Brown A. On an acetic ferment which form cellulose. *J Chem Soc London*. 1886;49:432-9.
17. Kramer F, Klemm D, Schumann D, Heßler N, Wesarg F, Fried W, et al. Nanocellulose Polymer Composites as Innovative Pool for (Bio)Material Development. *Macromol Symp*. 2006;244:136-48.
18. Ross P, Mayer R, Benziman M. Cellulose biosynthesis and function in bacteria. *Microbiol Rev*. 1991;55:35-58.
19. Hestrin S, Schramm M. Synthesis of cellulose by *Acetobacter xylinum*. 1954;345-351.
20. Schramm M, Hestrin S. Factors affecting production of cellulose at the air/liquid interface of a culture of *Acetobacter xylinum*. *J gen Microbiol*. 1954;11:123-9.
21. Trovatti E, Serafim L, Freire C, Silvestre A, Neto C. *Gluconacetobacter sacchari*: An efficient bacterial cellulose cell-factory. *Carbohydr Polym*. 2011;86:1417-20.
22. Hobzova R, Duskova-Smrckova M, Michalek J, Karpushkin E, Gatenholm P. Methacrylate hydrogels reinforced with bacterial cellulose. *Polym Int*. 2012;61:1193-201.
23. Leitão A, Silva J, Dourado F, Gama M. Production and characterization of a new bacterial cellulose/poly(vinyl alcohol) nanocomposite. *Materials*. 2013;6:1956-66.
24. Vandamme E, Baets S, Vanbaelen V, Joris K, Wulf P. Improved production of bacterial cellulose and its application potential. *Polym Degrad Stab*. 1998;59:93-9.
25. Donini I, Salvi D, Fukumoto F, Lustri W, Barud H, Marchetto R, et al. Biossíntese e recentes avanços na produção de celulose bacteriana. *Ecl Quím* 2010;35:165-78.
26. Delmer D, Amor Y. Cellulose biosynthesis. *The Plant cell*. 1995;7:987-1000.
27. Pokalwar S, Mishra M, Manwar A. Production of Cellulose by *Gluconacetobacter* sp. *Recent Res Sci Technol*. 2010;2:14-9.
28. Sadhu S, Maiti T. Cellulase Production by Bacteria: A Review. *Br Microbiol Res J*. 2013;3:235-58.
29. Krystynowicz A, Czaja W, Wiktorowska-Jezierska A, Goncalves-Miskiewicz M, Turkiewicz M, Bielecki S. Factors affecting the yield and properties of bacterial cellulose. *J Ind Microbiol Biotechnol*. 2002;29:189-95.
30. Keshk S, Sameshima K. Evaluation of different carbon sources for bacterial cellulose production. *Afr J Biotechnol*. 2005;4 478-82.

31. Jung H, Lee O, Jeong J, Jeon Y, Park K, Kim H, et al. Production and characterization of cellulose by *Acetobacter sp.* V6 using a cost-effective molasses-corn steep liquor medium. *Appl Biochem Biotechnol.* 2010;162:486-97.
32. Mikkelsen D, Flanagan B, Dykes G, Gidley M. Influence of different carbon sources on bacterial cellulose production by *Gluconacetobacter xylinus* strain ATCC 53524. *J Appl Microbiol.* 2009;107:576-83.
33. Mohammadkazemi F, Azin M, Ashori A. Production of bacterial cellulose using different carbon sources and culture media. *Carbohydr Polym.* 2015;117:518-23.
34. Oikawa T, Morino T, Ameyama M. Production of cellulose from D-Arabitol by *Acetobacter xylinum* KU-1. *Biosci Biotech Biochem.* 1995;59:1564-5.
35. Oikawa T, Ohtori T, Ameyama M. Production of cellulose from D-Mannitol by *Acetobacter xylinum* KU-1. *Biosci Biotech Biochem.* 1995;59:331-2.
36. Qiu K, Netravali A. A Review of Fabrication and Applications of Bacterial Cellulose Based Nanocomposites. *Polym Rev.* 2014;54:598-626.
37. Knauth P, Schoonman J. Nanocomposites: ionic conducting materials and structural spectroscopies. Tuller HL, editor 2008.
38. Castro C, Cordeiro N, Faria M, Zuluaga R, Putaux J, Filpponen I, et al. *In-situ* glyoxalization during biosynthesis of bacterial cellulose. *Carbohydr Polym.* 2015;126:32-9.
39. Castro C, Vesterinen A, Zuluaga R, Caro G, Filpponen I, Rojas O, et al. *In situ* production of nanocomposites of poly(vinyl alcohol) and cellulose nanofibrils from *Gluconacetobacter* bacteria: effect of chemical crosslinking. *Cellulose.* 2014;21:1745-56.
40. Figueiredo A, Figueiredo A, Alonso-Varona A, Fernandes S, Palomares T, Rubio-Azpeitia E, et al. Biocompatible bacterial cellulose-poly(2-hydroxyethyl methacrylate) nanocomposite films. *BioMed research international.* 2013;2013:1-14.
41. Phisalaphong M, Jatupaiboon N. Biosynthesis and characterization of bacteria cellulose–chitosan film. *Carbohydr Polym.* 2008;74:482-8.
42. Saibuatong O-A, Phisalaphong M. Novo aloe vera–bacterial cellulose composite film from biosynthesis. *Carbohydr Polym.* 2010;79:455-60.
43. Figueiredo A, Figueiredo A, Silva N, Barros-Timmons A, Almeida A, Silvestre A, et al. Antimicrobial bacterial cellulose nanocomposites prepared by in situ polymerization of 2-aminoethyl methacrylate. *Carbohydr Polym.* 2015;123:443-53.

44. Granel C, Dubois P, Jérôme R, Teyssie P. Controlled radical polymerization of methacrylic monomers in the presence of a bis(ortho-chelated) arylnickel(II) complex and different activated alkyl halides. *Macromolecules*. 1996;29:8576-82.
45. Lu G, Wu D, Fu R. Studies on the synthesis and antibacterial activities of polymeric quaternary ammonium salts from dimethylaminoethyl methacrylate. *React Funct Polym*. 2007;67:355-66.
46. Devi R, Maji T, Banerjee A. Studies on dimensional stability and thermal properties of rubber wood chemically modified with styrene and glycidyl methacrylate. *J Appl Polym Sci*. 2004;93(4):1938-45.
47. Labbé A, Brocas A, Ibarboure E, Ishizone T, Hirao A, Deffieux A, et al. Selective Ring-Opening Polymerization of Glycidyl Methacrylate: Toward the Synthesis of Cross-Linked (Co)polyethers with Thermoresponsive Properties. *Macromolecules*. 2011;44:6356-64.
48. Anirudhan T, Rejeena S. Thorium(IV) Removal and Recovery from Aqueous Solutions using Tannin-Modified Poly(glycidylmethacrylate)-Grafted Zirconium oxide Densified Cellulose. *Ind Eng Chem Res*. 2011;50:13288-98.
49. Anirudhan T, Rejeena S. Poly(acrylic acid)-modified poly(glycidylmethacrylate)-grafted nanocellulose as matrices for the adsorption of lysozyme from aqueous solutions. *Chem Eng J*. 2012;187:150-9.
50. Anirudhan T, Senan P. Adsorptive potential of sulfonated poly(glycidylmethacrylate)-grafted cellulose for separation of lysozyme from aqueous phase: Mass transfer analysis, kinetic and equilibrium profiles. *Colloids Surf, A*. 2011;377:156-66.
51. Lainé C, Bounor-Legaré V, Monnet C, Cassagnau P. Free radical polymerization of glycidyl methacrylate in plasticized poly(vinyl chloride). *Eur Polym J*. 2008;44:3177-90.
52. Chauhan G, Guleria L, Sharma R. Synthesis, characterization and metal ion sorption studies of graft copolymers of cellulose with glycidyl methacrylate and some comonomers. *Cellulose*. 2005;12:97-110.
53. Ma M, Li F, Chen F, Cheng S, Zhuo R. Poly(ethylene glycol)-*block*-poly(glycidyl methacrylate) with oligoamine side chains as efficient gene vectors. *Macromol Biosci*. 2010;10:183-91.
54. Altintas E, Denizli A. Monosize poly(glycidyl methacrylate) beads for dye-affinity purification of lysozyme. *Int J Biol Macromol*. 2006;38:99-106.

55. Anirudhan T, Nima J, Divya P. Adsorption of chromium(VI) from aqueous solutions by glycidylmethacrylate-grafted-densified cellulose with quaternary ammonium groups. *Appl Surf Sci.* 2013;279:441-9.
56. Anirudhan T, Nima J, Sandeep S, Ratheesh V. Development of an amino functionalized glycidylmethacrylate-grafted-titanium dioxide densified cellulose for the adsorptive removal of arsenic(V) from aqueous solutions. *Chem Eng J.* 2012;209:362-71.
57. Anirudhan T, Rejeena S, Tharun A. Preparation, characterization and adsorption behavior of tannin-modified poly(glycidylmethacrylate)-grafted zirconium oxide-densified cellulose for the selective separation of bovine serum albumin. *Colloids Surf, B.* 2012;93:49-58.
58. Bayramoğlu G, Arıca M. Ethylenediamine grafted poly(glycidylmethacrylate-co-methylmethacrylate) adsorbent for removal of chromate anions. *Sep Purif Technol.* 2005;45:192-9.
59. Cañamero P, Fuente J, Madruga E, Fernández-García M. Atom Transfer Radical Polymerization of Glycidyl Methacrylate: A Functional Monomer. *Macromol Chem Phys.* 2004;205:2221-8.
60. Benaglia M, Alberti A, Giorgini L, Magnoni F, Tozzi S. Poly(glycidyl methacrylate): a highly versatile polymeric building block for post-polymerization modifications. *Polym Chem.* 2013;4:124-32.
61. Brown A, Khan N, Steinbock L, Huck W. Synthesis of oligo(ethylene glycol) methacrylate polymer brushes. *Eur Polym J.* 2005;41:1757-65.
62. Louguet S, Verret V, Bedouet L, Servais E, Pascale F, Wassef M, et al. Poly(ethylene glycol) methacrylate hydrolyzable microspheres for transient vascular embolization. *Acta Biomater.* 2014;10:1194-205.
63. Lee W, Lin W. Preparation and gel properties of poly[hydroxyethylmethacrylate-co-poly(ethylene glycol) methacrylate] copolymeric hydrogels by photopolymerization. *J Polym Res.* 2002;9:23-9.
64. Qiu Y, Klee D, Pluster W, Severich B, Hocker H. Surface modification of polyurethane by plasma-induced graft polymerization of poly(ethylene glycol) methacrylate. *J Appl Polym Sci.* 1996;61:2373-82.

65. Uguzdogan E, Denkbaz E, Ozturk E, Tuncel S, Kabasakal O. Preparation and characterization of polyethyleneglycolmethacrylate (PEGMA)-co-vinylimidazole (VI) microspheres to use in heavy metal removal. *J Hazard Mater.* 2009;162:1073-80.
66. Duran A, Soylak M, Tuncel S. Poly(vinyl pyridine-poly ethylene glycol methacrylate-ethylene glycol dimethacrylate) beads for heavy metal removal. *J Hazard Mater.* 2008;155:114-20.
67. Foulger S, Jiang P, Amanda C, Smith D, Ballato J. Mechanochromic Response of Poly(ethylene glycol) Methacrylate Hydrogel Encapsulated Crystalline Colloidal Arrays. *Langmuir.* 2001;17:6023-6.
68. Kurosumi A, Sasaki C, Yamashita Y, Nakamura Y. Utilization of various fruit juices as carbon source for production of bacterial cellulose by *Acetobacter xylinum* NBRC 13693. *Carbohydr Polym.* 2009;76:333-5.
69. Abeer M, Mohd Amin M, Martin C. A review of bacterial cellulose-based drug delivery systems: their biochemistry, current approaches and future prospects. *J Pharm Sci.* 2014;66:1047-61.
70. Gomes F, Silva N, Trovatti E, Serafim L, Duarte M, Silvestre A, et al. Production of bacterial cellulose by *Gluconacetobacter sacchari* using dry olive mill residue. *Biomass Bioenergy.* 2013;55:205-11.
71. Zulfiqar S, Zulfiqar M, Nawaz M. Thermal degradation of poly(glycidylmethacrylate). *Polym Degrad Stab.* 1990;30 195-203.
72. Martínez-Sanz M, Abdelwahab M, Lopez-Rubio A, Lagaron J, Chiellini E, Williams T, et al. Incorporation of poly(glycidylmethacrylate) grafted bacterial cellulose nanowhiskers in poly(lactic acid) nanocomposites: Improved barrier and mechanical properties. *Eur Polym J.* 2013;49:2062-72.
73. Lv J, Fang S, Chen L. Preparation and characterization of affinity polymer basic microspheres by soap-free emulsion polymerization. *Chin J Polym Sci.* 2009;27:101-8.
74. Hunter T, Price G. Glycidyl methacrylate and *N*-vinylpyrrolidinone copolymers: synthesis and nuclear magnetic resonance characterization. *Polymer.* 1994;35:3530-4.
75. Nanjundan S, Unnithan C, Selvamalar C, Penlidis A. Homopolymer of 4-benzoylphenyl methacrylate and its copolymers with glycidyl methacrylate: synthesis, characterization, monomer reactivity ratios and application as adhesives. *React Funct Polym.* 2005;62:11-24.

76. Vijayanand P, Kato S, Satokawa S, Kojima T. Copolymerization of 4-biphenyl methacrylate with glycidyl methacrylate: Synthesis, characterization, thermal properties and determination of monomer reactivity ratios. *Polym Bull.* 2007;58:861-72.
77. Mahdavinia G, Pourjavadi A, Hosseinzadeh H, Zhuriaan M. Modified chitosan 4. Superabsorbent hydrogels from poly(acrylic acid-co-acrylamide) grafted chitosan with salt- and pH-responsiveness properties. *Eur Polym J.* 2004;40:1399-407.
78. Silioc C, Maleki A, Zhu K, Kjøniksen A, Nystrom B. Effect of hydrophobic modification on rheological and swelling features during chemical gelation of aqueous polysaccharides. *Biomacromolecules.* 2007;8:719-28.
79. Gea S, Reynolds C, Roohpour N, Wirjosentono B, Soykeabkaew N, Bilotti E, et al. Investigation into the structural, morphological, mechanical and thermal behaviour of bacterial cellulose after a two-step purification process. *Bioresour Technol.* 2011;102:9105-10.
80. Reis A, Fajardo A, Schuquel I, Guilherme M, Vidotti G, Rubira A, et al. Reaction of glycidyl methacrylate at the hydroxyl and carboxylic groups of poly(vinyl alcohol) and poly(acrylic acid): Is this reaction mechanism still unclear? *J Org Chem* 2009;74:3750-7.
81. Cordeiro N, Gouveia C, Moraes A, Amico S. Natural fibers characterization by inverse gas chromatography. *Carbohydr Polym.* 2011;84:110-7.
82. Kádár K, Százdi L, Fekete E, Pukánszky B. Surface characteristics of layered silicates: Influence on the properties of clay/polymer nanocomposites. *Langmuir.* 2006;22:7848-54.
83. Gutmann V. The donor acceptor approach to molecular interactions 1978.
84. Kita R, Svec F, Fréchet J. Hydrophilic polymer supports for solid-phase synthesis: preparation of poly(ethylene glycol) methacrylate polymer beads using “classical” suspension polymerization in aqueous medium and their application in the solid-phase synthesis of hydantoins. *J Comb Chem.* 2001;3:564-71.
85. Chang Y, Shih Y, Ruaan R, Higuchi A, Chen W, Lai J. Preparation of poly(vinylidene fluoride) microfiltration membrane with uniform surface-copolymerized poly(ethylene glycol) methacrylate and improvement of blood compatibility. *J Membr Sci.* 2008;309:165-74.
86. Hu W, Chen S, Yang J, Li Z, Wang H. Functionalized bacterial cellulose derivatives and nanocomposites. *Carbohydr Polym.* 2014;101:1043-60.

87. Aşkin A, Yazıcı D. A study of the surface analysis of some water-soluble polymers by inverse gas chromatography. *Surf Interface Anal.* 2008;40:1237-41.
88. Belgacem M, Czeremuszkin G, Sapieha S. Surface by XPS characterization and inverse gas of cellulose fibres chromatography. *Cellulose.* 1995;2:145-7.
89. Cordeiro N, Ashori A, Hamzeh Y, Faria M. Effects of hot water pre-extraction on surface properties of bagasse soda pulp. *Mater Sci Eng, C.* 2013;33:613-7.
90. Voelkel A, Strzemiescka B, Adamska K, Milczewska K. Inverse gas chromatography as a source of physiochemical data. *J Chromatogr A.* 2009;1216:1551-66.
91. Fowkes M, Mostafa M. Acid-Base Interactions in Polymer Adsorption. *Ind Eng Chem Prod Res Dev.* 1978;17:3-7.
92. Rani P, Ramanaiah S, Reddy K. Lewis acid-base properties of cellulose acetate butyrate by inverse gas chromatography. *Surf Interface Anal.* 2011;43(3):683-8.
93. Thielmann F. Introduction into the characterisation of porous materials by inverse gas chromatography. *J Chromatogr A.* 2004;1037:115-23.
94. Ashori A, Cordeiro N, Faria M, Hamzeh Y. Effect of chitosan and cationic starch on the surface chemistry properties of bagasse paper. *Int J Biol Macromol.* 2013;58:343-8.
95. Yang G, Zhai H. Synthesis and properties of glycidylmethacrylate grafted eucalyptus fibers. *Cellul Chem Technol.* 2012;46:243-8.
96. Sing K, Everett D, Haul R, Moscou L, Pierotti R, Rouquerol J, et al. Reporting physisorption data for gas/solid systems with special reference to the determination of surface area and porosity. *Pure & App Chem.* 1985;57:603-19.

## APPENDIX

---

## Appendix I

### Theoretical background

#### 1. Inverse gas chromatography

Physical chemical properties of the surface nanocomposites can be determined by IGC. This technique is simple, fast and sensitive, giving great accuracy of the results. Unlike GC, in IGC the nonvolatile material to be investigated is immobilized in a chromatographic column (stationary phase) and through passage of molecules probe with known properties, it is obtained the characteristic of the solid, at infinite dilution (Figure 48). Thermodynamic parameters such as surface energy, acid-basic character, enthalpy, entropy, adsorption isotherm, adsorption potential, heterogeneity and kinetic parameters such as diffusion, permeability and solubility can be determined through this technique <sup>(92, 93)</sup>.

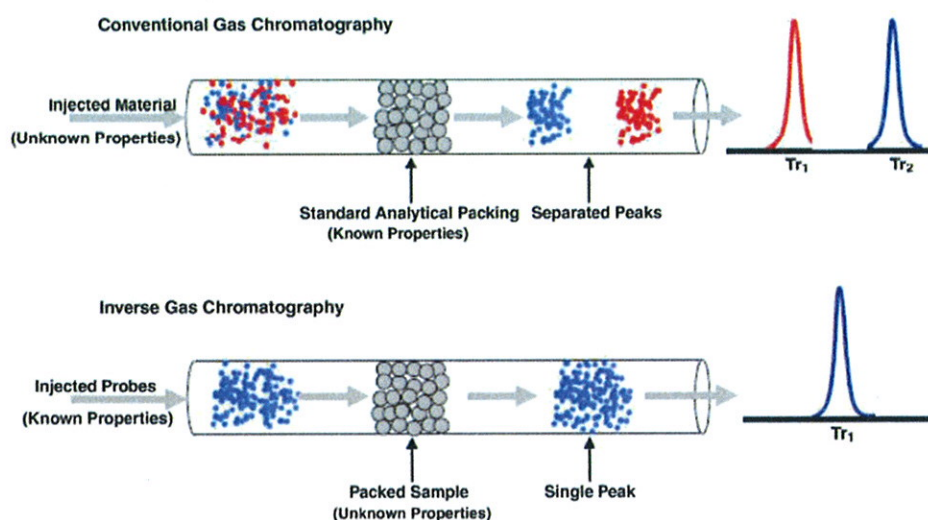


Figure 48. Schematic representation of GC and IGC measurements (91).

### 1.1. Surface energy component

The surface energy of a solid,  $\gamma_s$ , characterize the active energy in the surface of the solid and can be given as the sum of the dispersive component,  $\gamma_s^d$ , which describe all the van der Waals forces interactions and specific component,  $\gamma_s^{sp}$ , which express acid-base character<sup>(92)</sup>.

$$\gamma_s = \gamma_s^d + \gamma_s^{sp} \quad (\text{Equation 6})$$

The retention time obtained from the interaction between the probe molecules and the surface of the solid allows us to obtain the volume of probe molecules used, that is directly related to the energy of adsorption<sup>(94)</sup>,  $\Delta G_{ads}$ :

$$\Delta G_{ads} = RT \ln V_N + K \quad (\text{Equation 7})$$

where  $R$  is the gas constant,  $K$  is a constant depending on the chosen reference state,  $T$  is the column temperature and  $V_N$  is the net retention volume. According Fowkes *et al*,  $\Delta G_{ads}$  is related to the energy of adhesion,  $W_A$ , by the equation:

$$RT \ln V_N = 2N_A(\gamma_s^d)^{1/2} a(\gamma_L^d)^{1/2} + K \quad (\text{Equation 8})$$

where  $\gamma_L^d$  is the dispersive component of the surface energy of the probe molecule,  $a$  is the area occupied by probe molecule and  $N$  is the Avogadro's number.  $\gamma_s^d$  can be calculated from the slope of the obtained line made a plot of  $\Delta G_{ads}$  versus  $a(\gamma_L^d)^{1/2}$  of the series of  $n$ -alkanes.

### 1.2. Acid base character

Knowledge of the surface materials acid or basic character is important to understand their interaction with polar molecules. The polar molecules and solid interactions involve:

dispersive,  $\Delta G_{ads}^d$ , and specific,  $\Delta G_{ads}^{sp}$ , interactions <sup>(96)</sup>. The specific energy of adsorption  $\Delta G_{ads}$  is determined by the equation:

$$\Delta G_{ads} = \Delta G_{ads}^d + \Delta G_{ads}^{sp} \quad (\text{Equation 9})$$

$\Delta G_{ads}^{sp}$  can be determined by the following relation <sup>(96)</sup>:

$$\Delta G_{ads}^{sp} = RT \ln V_N - RT \ln V_{N(ref)} \quad (\text{Equation 10})$$

where  $V_N$  is the net retention volume for the polar probe and  $V_{N(ref)}$  is the net retention volume established by the *n*-alkane reference line for the same polar probe. From  $\Delta G_{ads}$  it's possible to determine the surface enthalpy of adsorption,  $\Delta H_{ads}$  and surface entropy of adsorption,  $\Delta S_{ads}$  through the following relation <sup>(96)</sup>:

$$\frac{\Delta G_{ads}}{T} = \frac{\Delta H_{ads}}{T} - \Delta S_{ads} \quad (\text{Equation 11})$$

$\Delta H_{ads}^{sp}$  and  $\Delta S_{ads}^{sp}$  can be established using the  $\Delta G_{ads}^{sp}$  in the previous equation.  $\Delta G_{ads}^{sp}$  can be used to quantify the Lewis acidity and basicity of the non-volatile material with the following equation <sup>(96)</sup>:

$$\frac{\Delta H_{ads}^{sp}}{AN^*} = \frac{DN}{AN^*} \times K_A + K_B \quad (\text{Equation 12})$$

where  $AN^*$  and  $DN$  are Gutmann's <sup>(83)</sup> modified acceptor and donor numbers, respectively;  $K_A$  is a Lewis acidity constant and  $K_B$  is a Lewis basicity constant.

### 1.3. Isotherm measurements

Using a wide variety of probe molecules at different temperatures, it's obtained the adsorption isotherm by the BET equation <sup>(89)</sup>:

$$\frac{p}{n(p^{\circ}-p)} = \frac{1}{n_m c} + \frac{c-1}{n_m c} \times \frac{p}{p^{\circ}} \quad (\text{Equation 13})$$

where  $n_m$  is the monolayer capacity;  $n$  the amount adsorbed;  $p$  the partial pressure;  $p^{\circ}$  the saturation pressure and  $c$  is related with the heat of sorption. Knowing the monolayer capacity and the cross area,  $a_m$ , of a probe molecule, the surface area,  $S_{BET}$ , can be calculated by the following equation <sup>(89)</sup>:

$$S_{BET} = a_m n_m N_A \quad (\text{Equation 14})$$

where  $N_A$  is the Avogadro constant.

Through the adsorption isotherm, the heterogeneity of the surface can be deduced from the adsorption potential,  $A$  by the following equation:

$$A = RT_S \ln \left( \frac{p^{\circ}}{p} \right) \quad (\text{Equation 15})$$